DEVELOPMENT OF IMPROVED METHODS FOR LATTICE AND CORE PHYSICS SIMULATIONS OF THERMAL REACTORS

By

SHERLY RAY

Enrolment No: PHYS01201304034

BHABHA ATOMIC RESEARCH CENTER, MUMBAI

A thesis submitted to the

Board of Studies in Physical Sciences

In partial fulfilment of requirements for the Degree of

DOCTOR OF PHILOSOPHY

of

HOMI BHABHA NATIONAL INSTITUTE

June, 2020

Homi Bhabha National Institute

Recommendations of the Viva Voce Committee

As members of the Viva Voce Committee, we certify that we have read the dissertation prepared by **SHERLY RAY** entitled "**DEVELOPMENT OF IMPROVED METHODS FOR LATTICE AND CORE PHYSICS SIMULATIONS OF THERMAL REACTORS**" and recommend that it may be accepted as fulfilling the thesis requirement for the award of Degree of Doctor of Philosophy.

Chairman –Prof. Amar Sinha

Attended through Video Conference (consented by e-mail) Date: 26/06/2020

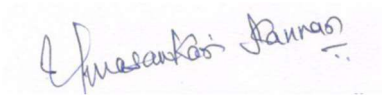

Guide / Convener – Prof. Umasankari Kannan Date: 26/06/2020

Examiner – Prof. Suneet Singh

Attended through Video Conference (consented by e-mail) Date: 26/06/2020

Member 1 – Prof. K. P. Singh

Attended through Video Conference (consented by e-mail) Date: 26/06/2020

Member 2 – Prof. K. Devan

Attended through Video Conference (consented by e-mail) Date: 26/06/2020

Invitee – Prof. S. B. Degweker

Attended through Video Conference (consented by e-mail) Date: 26/06/2020

Final approval and acceptance of this thesis is contingent upon the candidate's submission of the final copies of the thesis to HBNI.

I/We hereby certify that I/we have read this thesis prepared under my/our direction and recommend that it may be accepted as fulfilling the thesis requirement.

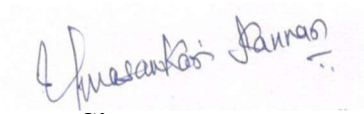

Date:26/06/2020
Place: Mumbai

Signature
Co-guide (if any)

Signature
Guide

STATEMENT BY AUTHOR

This dissertation has been submitted in partial fulfilment of requirements for an advanced degree at Homi Bhabha National Institute (HBNI) and is deposited in the Library to be made available to borrowers under rules of the HBNI.

Brief quotations from this dissertation are allowable without special permission, provided that accurate acknowledgement of source is made. Requests for permission for extended quotation or reproduction of this manuscript in whole or in part may be granted by the Competent Authority of HBNI when in his or her judgment the proposed use of the material is in the interests of scholarship. In all other instances, however, permission must be obtained from the author.

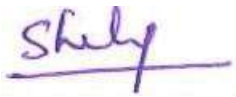

(Sherly Ray)

DECLARATION

I, hereby declare that the investigation presented in the thesis has been carried out by me. The work is original and has not been submitted earlier as a whole or in part for a degree / diploma at this or any other Institution / University.

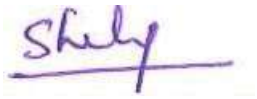

(Sherly Ray)

List of publications arising from the thesis

Journal

1. Sherly Ray, S. B. Degweker, Rashmi Rai, and K. P. Singh, 'A Collision Probability and MOC-Based Lattice and Burnup Code for Analysis of LWR Fuel Assemblies'. Nuclear Science and Engineering, volume 184 (473–494), December 2016. http://dx.doi.org/10.13182/NSE15-127.
2. Sherly Ray, S.B. Degweker, Umasankari Kannan, 'A hybrid method for reactor core simulations employing finite difference and polynomial expansion with improved treatment of transverse leakage'. Annals of Nuclear Energy 131 (2019) 102–111. https://doi.org/10.1016/j.anucene.2019.03.028.
3. Sherly Ray, S.B. Degweker, Umasankari Kannan, 'New homogenised axial diffusion coefficients from lattice calculations'. Annals of Nuclear Energy, 137(2020) 107029. https://doi.org/10.1016/j.anucene.2019.107029.
4. Sherly Ray, S.B. Degweker, Umasankari Kannan, 'Few-Group Diffusion Theory Parameters from Lattice Calculations using Leakage Corrected Collision Probabilities'. Annals of Nuclear Energy, 145 (2020) 107492. https://doi.org/10.1016/j.anucene.2020.107492.

Conference/Symposium

1. Sherly Ray and S. B. Degweker, 'Development of an Assembly Level Lattice Code Using Method of Characteristics,' Proc. DAE-BRNS Symposium on Advances in Reactor Physics: Simulation Techniques & Analysis Methodologies (ARP 2013), Mumbai, India, October 23–25, 2013.

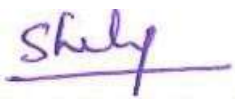

(Sherly Ray)

ACKNOWLEDGEMENTS

My thanks to God Almighty for the blessings and the strength showered on me to complete this work successfully.

I would like to express my sincere thanks and deepest gratitude to my present Ph. D. guide Prof. Umasankari Kannan (RPDD, BARC) and former guide Prof. S. B. Degweker (Retired, Mathematical Physics & Reactor Theory section, BARC) for their support and encouragement during the course of this work. The invaluable guidance and constant encouragement by Prof. S. B. Degweker have made this research and thesis work successful and presentable in this form. His passion and devotion to the work motivated me to work harder.

Sincere gratitude is extended to Prof. Amar Sinha, Prof. K. Devan, Dr. K. P. Singh, Dr. P. D. Krishnani and Dr. Anurag Gupta for their willingness to serve on my doctoral committee and for the useful advice. I would also like to thank Mrs. Rashmi Rai (Mathematical Physics & Reactor Theory section, BARC), Dr. L. Thilagam, SRI-AERB, Kalpakkam and Shri. Gaurav Agarwal of FPS&S Group, NPCIL for the help they have extended. I wish to thank Shri A. S. Pradhan, Head FPS&S group, NPCIL for the encouragement and support extended during the entire period of the research work. I thank all the researchers whose work I have consulted and cited for the thesis.

I am highly grateful to the authorities of Nuclear Power Corporation of India Limited, Bhabha Atomic Research Centre and HBNI, Mumbai for providing a very conducive atmosphere for carrying out this research work.

(Sherly Ray)

CONTENTS

SUMMARY

Accurate estimation of neutron flux distribution and the criticality status of the reactor is required during design and operation of nuclear reactors. The flux distribution is governed by the neutron transport equation (NTE) and can be obtained by performing full core calculations in fine energy groups using transport theory or by continuous energy Monte Carlo method. Though these methods are already being attempted, for routine analysis it appears to be impractical due to the complexity and heterogeneity of the advanced reactors. Thus, the required solution is usually obtained by applying some approximations and simplifying assumptions through a two-step process. The first step is the lattice calculations wherein the two-dimensional NTE is solved for obtaining the detailed flux (space and energy) distribution within a representative region called the lattice cell. This is followed by lattice homogenization that provides the few group homogenized cross sections and diffusion coefficients which forms the input for the second step of the calculation. In the second step, few group neutron diffusion equations are solved to obtain the three-dimensional flux/power distribution in the reactor core.

In the research work presented in the thesis, the development of new methods for the reactor physics analysis of LWRs, for both lattice and core levels, is described. The BOXER3 code was developed as a multi-group transport theory based lattice and burnup code for simulating the fuel assemblies of LWRs. The code has the capability to solve NTE with three methods viz: Collision Probability (CP) method, combination of CP and interface current method and the method of characteristics (MOC). The solution by MOC enables the treatment of anisotropic scattering. The availability of three options for obtaining the transport solution combined with other features like a new method for normalizing the CPs, solution of burnup equations with the predictor-corrector method, calculation of pin-dependent Dancoff factors, inclusion of leakage corrected CPs to obtain the leakage corrected fine-group flux distribution instead of infinite medium distribution and a new formula for obtaining the axial diffusion

coefficient, makes the code an advanced tool for lattice calculations of LWRs. The code can provide few group cross sections and diffusion coefficients as a function of burnup from lattice calculations at the level of LWR fuel assembly (FA). All these features/ improvements for the lattice level computation are verified by analysing various benchmark problems using BOXER3 code and it is found that they yield better results.

Towards the development in the second step, a new method that uses a combination of the finite difference (FD) along X and Y directions and the polynomial expansion method (PEM) along Z-direction is developed. Though there have been a few studies on the use of combined FD and PEM for core calculations, the treatment of transverse leakage by a fourth order polynomial instead of the usual quadratic expansion represents an improvement. Another new feature is the relaxation of the assumption of uniform material properties in a mesh. The treatment of the effect of the non-uniformity (due to burnup, temperature of fuel and coolant) on cross sections and diffusion coefficient within a mesh along the axis, together with the use of a fourth order polynomial expansion for flux (along the fuel length) and the transverse leakage in the diffusion theory code, permits the use of very few axial divisions and is therefore economical in detailed pin by pin core calculations. A code called FDPEM based on the new method has been developed. The benchmark studies carried out using the code FDPEM on LWR core calculations show good agreement in K-effective and power distributions between results by FDPEM and reference results and substantial savings in computer time over the more elaborate FD method. The code can therefore be used to obtain the pin power distribution of the LWR core efficiently without compromising on the accuracy.

The developments discussed in the thesis have been directly applied to square pitch heterogeneous LWR lattices and cores. They represent an important advancement in the methods for lattice and core level calculations of such reactors.

LIST OF FIGURES

LIST OF TABLES

CHAPTER 1

INTRODUCTION

1.1 Nuclear Power and Reactor Types

Since its discovery in 1938, nuclear fission is considered as an important means of nuclear energy generation. Today, most of the nuclear reactors operating world-wide are based on the phenomena of nuclear fission. Nuclear fission is a process in which nucleus of an atom splits into smaller/lighter nuclei. It also produces few (about 2-3) neutrons having an average energy of about 2 MeV and releases a large amount of energy (about 200 MeV per fission). This energy is much higher in comparison with energy produced in chemical reaction (a few eV per reaction). As an example, the complete burning of 1 kg of coal yields about 8 kWhr, whereas fission of 1 kg of U^{235} yields about $2*10^7$ kWhr of heat. Fission process is of two types: spontaneous fission and neutron induced fission. Since spontaneous fission is a rather slow process, nuclear reactors are based on neutron induced fission. The neutrons released during fission can cause further fissions in the fuel and a chain reaction can be maintained.

Uranium is the naturally occurring element that can undergo fission and is commonly used as the nuclear fuel. More specifically, natural uranium mainly consists of two isotopes viz. U^{238} (about 99.3 %) and U^{235} (about 0.7%). U^{235} can undergo fission with neutrons of all energies and is called the fissile isotope. U^{238} on the other hand is called fissionable because it is having a fission threshold energy of about 1.0 MeV. While the energy of the fission neutrons is high enough to cause further fissions in U^{238}, the neutrons rapidly lose their energy in inelastic collisions below the threshold and hence U^{238} cannot sustain a chain reaction. It is the U^{235} that sustains the fission chain reaction in a nuclear reactor. Other important nuclides which cause fission when bombarded with low energy neutrons are Pu^{239}, U^{233} etc. Pu^{239} is produced by interaction of a neutron with U^{238} nucleus followed by two beta decays. U^{233} is also produced in a similar manner from Th^{232}.

At neutron energies around 0.025 eV (referred to as thermal energies i.e. energies comparable to the kinetic energy of the motion of atoms and molecules due to their thermal motion) the neutron induced fission cross section of U^{235} is about 200 times the neutron capture cross section in U^{238} and hence the probability of a neutron causing fission is high in spite of the rather small fraction of the isotope U^{235} in natural uranium. This fact makes it possible to sustain a fission chain reaction in natural uranium provided the neutron energies are in the thermal range. Such reactors in which majority of the fissions are caused by thermal neutrons are called thermal reactors. Since the energy of the neutrons produced in fission is about 2 MeV, the neutrons must be slowed down to thermal energies. This is carried out in a reactor by collisions with light nuclei such as hydrogen or deuterium and is called moderation. Commonly used moderators are light water, heavy water, graphite and beryllium etc. as they have copious quantities of light nuclei [1]. These materials have the additional property that they have small neutron capture cross sections. During the slowing down process however, the neutrons pass through an energy range called the resonance range. In this range, the neutron capture cross sections of U^{238} becomes very large at the resonances of this nuclide and many neutrons may get lost as a result of capture in U^{238}. With carefully calculated amounts of fuel and moderator materials as well as their optimum geometrical arrangement it is possible to sustain fission chain reactions in natural uranium using heavy water or graphite moderators. Sometimes it becomes necessary (as in the case of light water moderated reactors) to increase the U^{235} in the uranium to 2-3% by a process called enrichment. Since the working of first nuclear reactor built by Fermi in 1942 in Chicago, the technology has developed continuously leading to many advanced and complex reactor systems that are currently operating.

All reactors are however not thermal reactors. Nuclear reactors can be broadly classified based on the energy of the neutrons causing fission as fast and thermal reactors. In thermal reactors, majority of the fissions are caused by neutrons of low energy (of few eV) called

thermal neutrons. The thermal neutrons are in thermal equilibrium with the medium, usually the moderator, where neutrons born as fast neutrons from fission are slowed down to lower energy range. In fast reactors, the chain reaction is maintained by high energy neutrons (of few keV) called fast neutrons. Thus, in fast reactor there is no moderator. To increase the probability of fission at such energies, it is necessary to increase the fissile content to 10-20 %. Fast reactors have certain advantages over thermal reactors as they can produce more fissile atoms (Pu^{239} or U^{233}) by the process mentioned above than they consume. Such reactors (called breeder reactors) are under development in various countries and they form an important component of India's nuclear energy program [2]. The majority of the nuclear reactors operating worldwide are thermal reactor types.

Thermal reactors can be further classified based on the material used as coolant/moderator as light water reactors (LWRs) and heavy water reactors (HWRs). In LWRs, light water serves as both coolant and moderator and in HWRs heavy water acts as both moderator and coolant. LWRs can be further divided into two categories as boiling water reactors (BWRs) and pressurized water reactors (PWRs). In BWRs coolant/moderator will be in the boiling condition and in PWRs it is kept pressurized using pumps. In HWRs the high temperature coolant is kept pressurized and the moderator which is completely isolated from coolant is maintained as a low temperature low pressure system. The type of reactors are called pressurized heavy water reactors (PHWRs).

Out of the total 22 nuclear power reactors operating in India, 18 are PHWRs, 2 are BWRs which were originally installed in collaboration with GE, USA and 2 are PWRs of Russian VVER design. The first PHWR units at Rajasthan (RAPS – 1&2) are based on Canadian design. Subsequent to this, 14 small-sized PHWRs of 220 MWe capacity were indigenously designed and are operating successfully, incorporating major changes in design based on the operating experience and R&D activities to achieve the present standardized design. In

addition, two medium-sized PHWRs of 540 MWe capacity are also operating. The successful operation of the small and medium sized PHWRs led to the design of 700 MWe PHWRs. Four 700 MWe PHWRs are almost in the final stages of construction. In PHWR category, India is planning to add about a dozen 700 MWe PHWRs to its power generating capacity. In addition to the existing PWRs (Russian VVER type), India is planning to acquire other types of PWRs through international collaboration [3] to add to the total installed capacity of electricity generation.

1.2 Nuclear Reactor Design and the Role of the Reactor Physicist

The design of a nuclear reactor is very involved task and the objective is to achieve safe and economically efficient operation of the plant, minimizing the occurrence of accidents and ensuring that their consequences can be reliably mitigated. Adherence to the various safety requirements needs to be demonstrated even at the design stage itself through detailed analysis.

The principle of producing power is same for all types of reactors, viz., maintaining a self-sustaining chain reaction. The neutrons that are produced from fission undergo various types of interactions such as elastic and inelastic scattering, radiative capture (n, α), (n, 2n) or fission with fuel, coolant, moderator and structural materials. As a result of these interactions, additional neutrons may be produced as in fission or (n, 2n) reactions or they may be removed as in radiative capture or (n, α) reactions. Neutrons can be also removed by leakage out of the reactor. The reactor is in a stable self-sustaining condition if rate of neutron production and removal from these processes are the same. An important parameter in this regard is the effective multiplication factor which is the ratio of number of neutrons in one generation to that in the previous generation. The neutron chain reaction is self-sustained if the effective multiplication factor is unity and the reactor is said to be critical. Any deviation in the value of multiplication factor from unity will lead to a change in the power output. Thus, maintaining reactor critical and knowing the status of the core is very important. The neutron balance in a

nuclear reactor is thus a dynamic process and there are various processes which contribute to the changes in the neutron population. To maintain the reactor critical, mechanisms such as fueling, use of reactivity control devices etc. are used. In addition, there are intrinsic properties of the reactor system called reactivity feedback effects that affect the effective multiplication factor. These feedback effects come into play due to changes in temperature and density of various materials present. The design of the system should be such that these feedback effects should not lead to an uncontrolled increase in multiplication factor. The reactivity feedback effects play a very important role in reactor operation and safety.

The distribution of neutrons within the reactor is described by the neutron transport equation. Once the neutron flux distribution within the core is known, various quantities of interest like neutron multiplication factor, fuel pin (usually fuel is arranged in the form of small cylinders called fuel pins) power, fuel burnup etc. can be easily obtained.

Nuclear energy in a reactor appears in the form of heat that needs to be removed. The heat removal system is decided during the design stage itself considering the design power output and the intended neutron flux/power distribution. The neutron flux distribution within the reactor at all times should be such that the power produced from the fuel can be safely removed without causing any overheating and consequent damage of the fuel and other components and is within the heat removal capacity of the system. This translates into keeping the parameters like linear heat rate (LHR), the power produced per unit length of the fuel pin, and the fuel and coolant temperatures within the specified limits during operation. These parameters can be obtained once the neutron flux distribution is known.

Control rods which are made of neutron absorbing material are inserted or withdrawn from the core to control the rate of neutron interaction and to cause a change in the neutron multiplication factor. The ‘worth’ or effectiveness of these rods is quantified in terms of the relative change in the effective multiplication caused due to insertion or removal of these rods.

Evaluation of the worth of the control rods, as changes in the worth may occur due to changes in the material composition with reactor operation and with changes in the flux distribution, is a requirement of the design and operation.

The fission products formed during fission and subsequent decay also accumulates and is having an effect on neutron multiplication. Some of these products are having high cross-section for neutron absorption and act as poison. Thus, provision must be made in the design itself to take care of the reactivity effect associated with such fission products during operation and shut down. As the fissile content gets depleted due to fission and fission products accumulates with operation, refueling is required to replenish the irradiated fuel with new fuel. The refueling frequency and amount of fuel to be replaced must be worked out such that both economic and safety aspects are satisfied.

Safety analysis is performed to assess the variation of various parameters like LHR, fuel enthalpy, multiplication factor, temperature of fuel, coolant etc. during the transients, be it caused by any change in power or due to malfunctioning of some devices like tripping of pump, withdrawal of control rods etc. and to check the effectiveness of the control/shutdown systems. Whenever there is an increase in the power, the temperature of the various components like fuel, coolant and moderator etc. will increase. This in turn can cause further change in the flux /power depending on the reactivity feedback associated with these components. Thus, a negative temperature feedback is always preferred to dampen the escalation of the transient in a safe manner.

The reactor physics study covers aspects of the reactor design related to maintaining criticality or the neutron balance, optimization of neutron flux distribution to safely and economically operate the reactor at design rated power. The study also includes the following: estimation of the effectiveness (worth) of control rods/elements, calculation of reactivity coefficients that play an important role in safety, the study of fuel burnup and the effect of

accumulation of fission products and the need as well as the principles of refueling operations, transient and safety analysis.

1.3 Methods and Tools Employed in Reactor Physics Analysis

The tools used by the reactor physicist for analysis of reactors are computer codes and nuclear data (mainly nuclear reaction cross sections) libraries. The basic physical principle governing the behavior of neutrons in a reactor is the neutron transport equation that is a statement of neutron balance in a small volume of space [4]. The codes are based on numerical methods for solving the transport equation (or one of its approximate forms, the diffusion equation) using the data from the cross section libraries. An alternative method is based on a statistical approach to solving neutron transport problems [5]. These methods are briefly described in the following paragraphs.

1.3.1 The Neutron Transport Equation

The basic equation governing the neutron distribution in the reactor is the neutron transport equation (NTE). Neutrons can interact with matter in different ways like scattering, radiative capture, fission etc. in addition to its leakage from the system. The neutron cross section, the probability of interaction of neutrons with various materials, is a function of neutron energy. Any change in the temperature of some material in the system will lead to a change in density of the material as well as a change in the energy distribution of the neutrons and hence the interaction probability.

The neutron transport equation is a statement of neutron balance and can be written as

Rate of change of neutron density $\frac{\partial N(r,\Omega,E,t)}{\partial t}$ = Rate of production – Rate of removal

Rate of production = (In-scattering rate + fission rate + source rate)

Rate of removal = (Net leakage rate + collision rate) in $dV\, d\Omega\, dE$ about ($\boldsymbol{r}$, $\boldsymbol{\Omega}$, E) at time t

$$\frac{\partial N(r,\Omega,E,t)}{\partial t} = \int dE' \int \Sigma_s(r,\Omega',E' \to \Omega,E)\psi(r,\Omega',E',t)d\Omega' +$$

$$\frac{\chi(E)}{4\pi}\int dE' \int \upsilon\Sigma_f(r,E')\psi(r,\Omega',E',t)d\Omega' + Q(r,\Omega,E,t) - \quad (1.1)$$

$$\{\Omega.\nabla\psi(r,\Omega,E,t) + \Sigma_t(r,E)\psi(r,\Omega,E,t)\}$$

$N(r,\Omega,E,t)$ is the number of neutrons at *r* with direction Ω and energy *E* at time *t* per unit volume, per unit solid angle and per unit energy. $\Psi(r,\Omega,E,t)$ is the angular neutron flux and is related to $N(r,\Omega,E,t)$ as:

$$\psi(r,\Omega,E,t) = vN(r,\Omega,E,t)$$

where, v is the neutron velocity. The scalar flux is obtained as the integral of the angular flux over all directions.

$$\Phi(r,E,t) = \int_{4\pi} \psi(r,\Omega,E,t)d\Omega$$

Combining the source terms together, Eq. (1.1) takes the form

$$\frac{1}{v}\frac{\partial\psi(r,\Omega,E,t)}{\partial t} + \Omega.\nabla\psi + \Sigma_t\psi = q(r,\Omega,E,t) \quad (1.2)$$

For the steady state reactor analysis, the time- independent (steady state) transport equation as shown in Eq. (1.3) is solved.

$$\Omega.\nabla\Psi + \Sigma_t\Psi = q(r,\Omega,E) \quad (1.3)$$

$q(r,\Omega,E)$ is the total rate at which neutrons appear at r,Ω,E due to both collisions and extraneous sources if any.

$$q(r,\Omega,E) = \int dE' \int \Sigma_s(r,\Omega',E' \to \Omega,E)\Psi(r,\Omega',E')d\Omega' +$$

$$\frac{\chi(E)}{4\pi}\int dE' \int \upsilon\Sigma_f(r,E')\Psi(r,\Omega',E')d\Omega' + Q(r,\Omega,E) \quad (1.3a)$$

This is the general form of the neutron transport equation in integro-differential form. Here,

$Q(r, \Omega, E)$ - external neutron source,

$\chi(E)$ - fission spectrum,

υ - average number of neutrons produced in fission,

$\Sigma_s(r, \Omega', E' \rightarrow \Omega, E)$ – macroscopic scattering cross section at r from energy E' to E and direction from Ω' to Ω,

$\Sigma_f(r, E')$- macroscopic fission cross section at r with energy E'.

The macroscopic cross section Σ_x for reaction x is the product of number density of nucleus under consideration and its microscopic cross section for reaction x, σ_x. ie.,

$\Sigma_x(E) = n * \sigma_x(E)$, n is the number density of the nuclei.

The microscopic cross sections σ required for solving neutron transport problems are sourced from cross section data libraries that have been prepared for this purpose.

By modifying the fission source in Eq. (1.3) by a constant factor $\frac{1}{k}$ and setting the external neutron source $Q(r, \Omega, E)$ equal to zero, the criticality eigen-value form of the transport equation is obtained as

$$\Omega.\nabla\Psi + \Sigma_t\Psi = \int dE' \int \Sigma_s(r, \Omega', E' \rightarrow \Omega, E)\Psi(r, \Omega', E')d\Omega' + \frac{\chi(E)}{4\pi k} \int dE' \int \upsilon\Sigma_f(r, E')\Psi(r, \Omega', E')d\Omega' \quad (1.4)$$

Eq. (1.4) is solved to get the flux and the eigenvalue. The largest eigen-value of Eq. (1.4) is called the criticality eigen-value of the system and the corresponding Ψ is called the eigen-function or fundamental mode.

If the neutron production due to fission balances the neutron loss due to both capture and leakage, a non-zero steady state neutron flux exists. The introduction of k in the above manner makes it possible to achieve this balance by adjusting the fission source by the eigen-value k. If k is less than one, the system is sub-critical and if k is greater than one, system is super-

critical. If $k = 1$, the loss due to capture plus leakage balances the source due to fission and the system is said to be critical.

In the reactor calculation, above form of transport equation is solved for obtaining both eigen-value and neutron flux. Another form, the integral form, of the steady state transport equation for the neutron flux is

$$\Phi(r,\Omega,E) \quad = \quad \int_0^{\infty} exp\left[-\int_0^{s'} \Sigma_t(r-s''\Omega,E)ds''\right] q(r-s'\Omega,\Omega,E)ds' \qquad (1.5)$$

and states that the flux at r is made up of neutrons which appear in the direction Ω and energy E, at all other possible directions $r - s'\Omega$, multiplied by the attenuation factor by which the flux is reduced while going to $s = 0$.

Even in steady state condition, the neutron flux is a function of position, angle and energy variables. The complexity of the geometry and material heterogeneities within the reactor makes it difficult to obtain the exact solution for the neutron transport equation. The complicated variation of cross sections with neutron energy also add to the complexity of the problem. Except for simple geometries where analytical solutions are obtained, numerical methods are applied to obtain the solution of the transport equation. To solve the transport equation numerically, the variables energy, position and angle needs to be discretized. Various numerical methods have been developed to get the solution of the transport equations.

To treat the energy dependence, multi group approach of the transport equation is widely adopted. In this approach, the entire energy range relevant to fission reaction ie., up to 20 MeV is divided into many intervals (groups) and it is assumed that the cross sections are constant within each energy group and are obtained by weighted averaging of the variation over the energy range of the group. Integration over energy is replaced by the summation over groups.

With this approximation, the steady state neutron transport equation is transformed into a finite system of integro-differential equations, each giving the neutron flux within a particular group.

$$\Omega.\nabla\Phi_g + \Sigma_t\Phi_g \quad = \quad q_g(r,\Omega), \qquad\qquad g = 1, G \tag{1.6}$$

The common methods used for the solution of the transport equation are the Spherical harmonics method or Pn method and the Discrete ordinates or *Sn* method for solving the integro-differential transport equation, the Collision probability (CP) method and its variants that solve the integral transport equation, and the Method of Characteristics (MOC).

For getting the local flux variations in small systems of the size of a pin cell, Collision probability (CP) methods are applied. In the intermediate sized system, like fuel assembly, low-order discrete ordinate method (Sn) is applied. In recent times the collision probability method (and its variants such as interface current method) are also being used for assembly level problems. The method of characteristics is also used for assembly level problems. For problems involving large sized domains such as whole calculations, the diffusion equation that is an approximate form of the transport equation is used with few group homogenized cross sections obtained from lattice calculations. Whole core calculations without homogenization by the method of characteristics are being attempted. The Pn and Sn methods are briefly described in the following paragraphs while detailed treatment of the collision probability and related methods as well as MOC for lattice calculations and the methods for solving the diffusion equation that form the subject of the thesis are discussed in detail in the next chapter.

In the Spherical Harmonics method, the angular flux is expanded in terms of spherical harmonics (Legendre polynomials for one-dimensional plane geometry) and the expansion is substituted in the transport equation. A system of (infinite) coupled linear ordinary differential equations is obtained for the coefficients of the expansion by making use of the orthogonality and recurrence relations of the expansion functions. The expansion is truncated after a finite

number ($N+1$) of terms to get a finite system of equations. The Pn method is of theoretical interest in so far as it leads to the diffusion equation if the method is truncated at n = 1. The method was fairly popular in the early days of nuclear reactor theory but has been replaced by the Sn method, which is more suitable for digital computation.

The Sn method is the most popular method for obtaining solutions to the integro-differential transport equation. The angular distribution of the neutron flux is evaluated in a number of discrete directions. The spatial variables are treated by introducing a discrete mesh and replacing the derivatives by their finite difference equivalents / forms. Thus, with a multi-group treatment of the energy dependence all the variables of the NTE are treated as discrete. The source term is evaluated by replacing the scattering integral by a weighted sum as in a discrete quadrature formula. The method can treat anisotropic scattering and is suitable for large sized domains. Besides reactor cores, the method is also used to solve shielding problems.

1.3.2 The Monte Carlo Method

The Monte Carlo method is a numerical procedure based on statistical theory. In neutron transport problems, the applicability of Monte Carlo techniques arises from the fact that the neutron cross section is interpreted as the probability of interaction per unit distance travelled by a neutron [4]. In Monte Carlo method a set of neutron histories is generated by following individual neutrons through successive collisions. The first step in a neutron history is to select a source neutron location, direction and energy. The next step is to find where the first collision occurs. Once the location of the first collision has been determined, random numbers are used to find the outcome of the first collision, location of the second collision and so on. This procedure is continued until the neutron history is terminated by leakage from the system or by absorption. Quantities of interest such as reaction rates are obtained by counting (tallying) various events during a history and averaging over a large number of histories.

The locations of actual collisions and the outcome of each collisions are determined from the range of possibilities by sampling numbers from the probability distributions for these events. The sampling is carried out by transforming the numbers obtained from random number generators (programs designed to produce uniformly distributed random numbers in the interval 0 to 1) to the probability distribution of the event under consideration.

The MC method is particularly useful in exactly treating the complex geometries and cross section variation with energy where other methods encounter difficulties. There can be uncertainties in the solution due to limitation in the finite number of neutrons considered. Besides increasing the number of histories used, various procedures called variance reduction techniques have been developed for reducing the uncertainty. Monte Carlo methods are particularly good for obtaining parameters like the K-effective. However, obtaining detailed fine flux or power distributions is more difficult due to very large computing times required.

1.4 Lattice and Core Calculations and the Organisation of the Thesis

The transport equation is very detailed and involves many variables like position, energy and angular dependence. Moreover, the distribution of materials in the reactor and the variation of cross sections with energy are very complicated. Thus, obtaining a complete solution of transport equation for the nuclear reactor is very tedious and time consuming. Likewise, even though the Monte Carlo method treats complicated geometries and cross section variation with energy exactly, it is computationally expensive for obtaining detailed power distribution in the reactor.

Hence, traditionally a two-step approach is applied to obtain the required solution. The first step consists of a lattice calculation to obtain the fine and detailed neutron flux distribution, in both space and energy, within a small representative region of the reactor called the lattice cell. A lattice cell typically consists of a fuel assembly, associated moderator and coolant. Since

the probability of neutron interaction depends on the energy of the neutron, these calculations are usually performed using the transport equation with a large number (typically about a hundred) of energy groups (referred to as fine group calculations). The detailed flux distribution obtained in the lattice cell calculations is used to obtain few group homogenized cross sections for the next stage of the calculations. The second step is the core calculation wherein it is assumed that the reactor consists of the homogeneous lattice cells and the diffusion equation – that is an approximate form of the transport equation - in few groups (typically 2-4) is solved to obtain the core flux distribution.

The thesis presents new theoretical developments and their practical implementation for improving existing methods / codes at both the lattice and the core levels of the two step calculations.

The thesis describes the development and verification of a lattice and burnup code for solving the multi-group neutron transport equation by the collision probability method and the MOC. The code has the capability to treat anisotropic scattering and computes pin-wise Dancoff factor. It can perform calculations in fine groups using the WIMS 69 or172 [6] group libraries [7]. The code has a number of novel features as described below:

(a) a new method for normalizing the collision probabilities:

The estimated collision probabilities have to be such that the sum of all the probabilities starting from a region / surface should add up-to one. However due to the quadrature related errors (particularly over the area) the sum does not add up exactly to unity. Many schemes for normalization of the probabilities so that they add up to unity have been proposed in the past and are currently in use in collision probability codes. However, these schemes have drawbacks such as giving negative values of collision probabilities or requiring additional computational requirement. A different approach, which is more satisfactory from a physical

point of view, is applied to normalize the collision probabilities. The approach does not require any additional computation. The scheme is described in detail in Chapter3.

(b) the use of leakage corrected collision probabilities for obtaining the neutron spectrum and spatial distribution:

The lattice calculations are carried out for an infinite medium consisting of a periodic array of lattice cells. But actual reactors are finite in all three dimensions and the leakage from the reactor changes the flux distribution and spectrum within a lattice cell. To account for both spatial and spectral effects, the leakage correction is carried out, with the help of the leakage corrected collision probabilities, during the lattice calculation of the heterogeneous medium and not after the lattice calculation followed by homogenisation (as is done for example in the P1 and B1 methods, that account for only the spectrum change due to leakage but not the spatial change in the lattice flux distribution). This aspect is discussed in detail in Chapter 4.

(c) a new method for obtaining homogenized axial diffusion coefficients:

New formulae have been derived and implemented in the code for obtaining the homogenised axial diffusion coefficients in terms of the flux distribution available from a two-dimensional lattice calculation and collision probability like integrals. The diffusion coefficients thus obtained give more accurate results in the core calculations. The details are given in Chapter 4.

Theoretical validation/verification of the code by analysis of several benchmarks has been carried out to verify the above-mentioned features.

The thesis also describes the development of a few group diffusion theory code for performing detailed pin by pin core calculations by employing a new hybrid method based on finite difference in X-Y direction and a fourth order polynomial expansion method along Z-direction, in which the treatment of transverse leakage is also accurate up to the fourth order. The mesh size along transverse direction is of the order of a pin cell but the use of the

polynomial expansion along the z-axis permits the use of much longer meshes in this direction. There have been attempts to use a similar approach (referred to as 'hybrid finite difference and nodal methods') to pin by pin core calculations. The basic difference in these methods and the proposed method is in the treatment of transverse leakage. In the proposed method, transverse leakage is expressed as fourth order function where as it is represented as a quadratic function even though flux is expanded in fourth order in the 'hybrid finite difference and nodal methods' .This exact treatment of transverse leakage permits the use of long meshes in the z direction thereby mitigating the enhanced demands on memory and computing requirements that arise due to the more detailed treatment in the x-y directions. The code is verified by analysis of benchmark problems [8]. The details are given in Chapter 5.

Chapter 2 presents a review of neutron transport and diffusion theory methods for lattice and core calculations and a survey of the literature on the subject. Chapter 3 discusses the development of a Collision Probability and MOC based lattice code for Analysis of LWR Fuel Assemblies. Chapter 4 contains a discussion on leakage corrected collision probabilities that may be used to obtain the lattice flux distribution in a finite lattice. Homogenised Axial diffusion coefficients are also obtained using this new methodology. Chapter 5 gives a discussion on the development of computer code based on a combination of finite difference and polynomial expansion methods for pin by pin core calculations. Chapter 6 presents the summary of the work, conclusions and scope for future work.

CHAPTER 2

REVIEW OF NEUTRON TRANSPORT AND DIFFUSION THEORY METHODS FOR LATTICE AND CORE CALCULATIONS

2.1 Introduction

To increase the electricity generation capacity, Indian nuclear power program is planning to acquire LWRs of advanced generation III reactors like AP1000, EPR etc. with international collaboration in addition to the fleet mode of 12 numbers of indigenously developed 700 MWe PHWRs. These LWRs are very complex and incorporates many advanced safety systems. It is required to develop advanced computational capabilities to cater to the design and operational related analysis requirement of these reactors. Considering the rather complicated variation of cross sections with energy and distribution of materials in modern reactors, obtaining a complete solution of transport equation for the nuclear reactor is very tedious and time consuming. Similarly, while the exact Monte Carlo methods can easily give the effective multiplication factor (K- effective) of a reactor core, obtaining detailed power distributions as a function of burnup is also a herculean task. While there have been attempts to use these direct methods for whole core calculations [9, 10, 11], clearly, they cannot be used for routine day to day calculations and these continue to be performed by the traditional two step methods that form the subject of this thesis.

Traditionally, the reactor physics calculations are performed in two- steps: first lattice level and then core level calculations. In the first step, detailed transport calculation is performed on a representative cell called lattice cell. Calculations are performed in fine energy groups and geometry is modelled more elaborately, taking all heterogeneities into account. Once the fine group spatial neutron flux distribution is obtained for the lattice cell, next procedure is to generate the few-group lattice parameters which are required as input to the

second step core calculation. Homogenized few group cross sections of the lattice cell are generated by flux volume weighting for spatial homogenization and energy group condensation. In the second step, core calculations are performed by solving the diffusion equation for the entire core in three dimensions. It is assumed that the core consists of the homogenized lattice cells. Usually, finite difference method or nodal methods are applied to solve the diffusion equation. The methods and codes used for both lattice and core level computations are described in the following sections.

2.2 Lattice Level Computational Methods and Codes

Lattice calculations are performed to obtain the neutron flux as a function of space and energy by solving the multi-group neutron transport equation (NTE) in a representative region of the reactor. Homogenised few group parameters as a function of burnup are also obtained as output. One of the basic inputs required for lattice calculations is the microscopic reaction cross sections and other nuclear data such as modes of decay, lifetimes, branching ratios etc. of various nuclides present in the reactor. A brief description about the source of nuclear data and the forms in which it is stored is presented in the following sub-section.

2.2.1 Nuclear Data

Nuclear reaction cross section data comes from nuclear physics experiments and the data is made available by theoretical interpolation / correlations at all energies where experimental data is not available. The nuclear data is stored in evaluated nuclear data files (ENDF) such as JEFF, ENDF/B and JENDL etc. in the form of these theoretical nuclear physics parameters / interpolation functions and cannot be used directly in lattice physics codes. Rather the data is processed by very complicated processing programs such as NJOY [12], PREPRO [13] etc. to ultimately generate the multi-group cross section data that can be used by lattice physics codes.

These processing codes, that are used to generate the group averaged cross sections or the point wise cross sections for use in neutronic calculations, perform major functions like

resonance reconstructions, Doppler broadening, treatment of cross sections in the unresolved energy region, multi-group averaging etc. With the resonance reconstruction module, point-wise cross section data is reconstructed (so that simple linear interpolation of data between two energy points gives the required accuracy) from the original ENDF data that involve complicated nuclear theoretical methods for data reconstruction. The point-wise cross sections are generated considering the nucleus to be at rest. At higher temperatures, Doppler broadening takes place at resonance energies. Hence there is a change in cross-section in resonance energy region. To account for this, the point wise data in the resonance energy range are further processed into Doppler broadened cross sections. In the thermal energy range, the thermal motion and chemical binding of the nuclide should be accounted for. The group averaged cross sections are generated from the point-wise cross section data using suitable neutron spectrum as weighting function.

2.2.1.1 Multi-group Cross Section Libraries: WIMS Library

The choice of energy groups is very important as the number of energy groups will have a significant effect on the lattice calculations in both accuracy and computational time. When number of energy groups are large the accuracy will be better but the computational need will be more. For typical light water reactor, few hundred energy groups are adopted in the cross section library used for the lattice calculation. The most widely used cross section library in India is WIMS 69, 172 groups [14]. In WIMS library, data is divided into three energy ranges: fast, resonance and thermal. In 69 / 172 group library, there are 14 / 45 groups in fast (energy from 10 / 20 MeV to 9.118 keV), 13 / 47 groups in resonance (energy from 9.118 keV to 4 eV) and 42 / 80 groups in thermal range (below 4 eV).

The basic multi-group cross sections used for the lattice calculations are read from the processed multi group cross section data libraries such as WIMS library. However, these are not directly suitable for use in transport theory calculation and some further processing is

necessary. Most lattice codes carry out this processing before using the cross sections in multi-group transport theory calculations. This involves the reformatting from the condensed scattering matrix format to the full matrix format, interpolation of thermal cross-section data for various temperatures, calculation of the background cross section and interpolation from the resonance integral tables for this background cross section and temperature.

Since the resonance treatment is one of the important aspects of the multi-group nuclear data generation from ENDF, the details of the treatment in the WIMS formalism is briefly described below.

2.2.1.2 Resonance Treatment

The effective multi-group cross section that are to be used in the lattice calculation is defined as

$$\sigma_g(r) = \frac{\int_{E_g}^{E_{g-1}} dE\ \sigma(E)\ \phi(r,E)}{\int_{E_g}^{E_{g-1}} dE\ \phi(r,E)} \tag{2.1}$$

When there is resonance material, there is a drastic variation in the cross section and flux around the resonance energy range due to resonance absorption. One of the main issues in lattice physics calculations is the resonance self-shielding calculation. The resonances cause energy and spatial self- shielding effects, with spatial self-shielding effects more pronounced in heterogeneous systems. For the accurate estimation of these self-shielding effects in resonance materials, resonance treatment of the cross sections is performed and multi-group effective cross-sections are generated.

In ultrafine group approach [15, 16] neutron flux distribution is obtained by solving the slowing down equation with a large number of fine energy groups. The use of this approach is limited to simple pin cell problems due to huge computational requirements and is not commonly used in lattice codes. The commonly used approaches for resonance treatment in lattice calculations are the sub-group method and equivalence theory. Resonance treatment

methods are discussed for an infinite homogeneous medium and their extension to practical heterogeneous lattice calculations.

The most widely used approach to resonance self-shielding effects in the lattice calculation is the equivalence theory, in which an equivalent relationship is derived between homogeneous and heterogeneous system through back ground cross section [14, 17]. The effect of heterogeneity is considered through the use of escape cross section from the fuel. The escape cross section in heterogeneous medium replaces the cross section of the moderator outside the fuel. The effective cross section in homogeneous and heterogeneous medium will be same if they have same background cross section. In the neutron cross section library, the effective resonance integrals/cross sections obtained are tabulated as a function of back ground cross section and temperature for homogeneous systems. In equivalence theory approach, background cross section for resonance regions of the heterogeneous system are evaluated as described below. Once the back ground cross sections are known, the appropriate effective resonance integrals or cross sections can be generated by interpolation from the RI tables.

i) Calculations in the resonance region: the infinite homogeneous medium

In the case of the infinite homogeneous medium that is a mixture of light moderator nuclides and the heavy resonant absorber nuclides, the neutron transport equation is simply an integral equation in the energy variable describing neutron slowing down and absorption. Analytical solution can be obtained under a number of approximations that are quite accurate in practical situations. These are narrow resonance (NR) approximation, wide resonance (WR) approximation and intermediate resonance (IR) approximation.

In the narrow resonance approximation, it is assumed that the resonance width of the resonant nuclide is narrow compared to the slowing down width of nuclides present. As the neutron energy loss per scattering collision is much greater than the width of the resonance, the contribution to slowing down density from resonance region is neglected. Outside the

resonance range, the scattering cross section is constant and is taken as potential scattering cross section [18]. Thus, in the case of a homogeneous mixture of a resonant and other non-resonant nuclide, the solution for the flux can be written as [19]

$$\phi(E) \quad = \quad \frac{\left(\sigma_{p,r} + \sigma_0\right)}{\left(\sigma_{t,r}(E) + \sigma_0\right)} \ \frac{1}{E} \tag{2.2}$$

σ_0 is the back ground cross section defined as

$$\sigma_0 \quad = \quad \frac{\sum_{k \neq r} N_k \sigma_{p,k}}{N_r} \tag{2.3}$$

$\sigma_{p,r}$ is the potential scattering cross section of the resonant nuclide *r* and $\sigma_{t,r}(E)$ is the total cross section of the resonant nuclide *r*.

The assumptions made in this method - that there is no overlap of resonances, non-resonant nuclides have constant scattering cross section which are dominated by potential scattering, the slowing down of neutrons is by elastic scattering, dependence of neutron flux in the non-resonant part is as *1/E* - may result in simplifying the energy dependence of the neutron flux, but there can be error due to this. NR approximation holds good for resonances at higher energies but not close to thermal energies.

In the wide resonance or wide resonance infinite (mass) absorber (WRIM or WRIA) approximation, it is assumed that the energy loss per collision with the heavy resonant isotope is negligible compared to the width of the resonance. Thus, all scattering is self-scattering and the slowing down density is the scattering rate. The solution for the flux in WR approximation [19, 20] can be written as

$$\phi(E) \quad = \quad \frac{\sigma_0}{\left(\sigma_{t,r}(E) - \sigma_{s,r}(E) + \sigma_0\right)} \ \frac{1}{E} \tag{2.4}$$

$\sigma_{s,r}(E)$ is the scattering cross section of the resonant nuclide *r.* For arriving Eq. (2.4), NR approximation is applied to non-resonant nuclides and WR approximation is applied to resonant nuclide.

The difference in the NR and WR approximation is in their treatment of scattering cross section of the resonant nuclide. In NR approximation, the scattering cross section of the resonant nuclide is accounted, but in WR approximation it is completely ignored. The WR approximation is applicable to the very low-lying broad resonances.

The NR and WR represent two extreme situations and hence in the IR approximation, these two approximate solutions are combined through Goldstein-Cohen IR parameter [21] and flux is written as:

$$\phi(E) \quad = \quad \frac{\left(\lambda\sigma_{p,r} + \sigma_0\right)}{\left(\sigma_{a,r}(E) + \lambda\sigma_{p,r} + \sigma_0\right)} \frac{1}{E} \tag{2.5}$$

$$\sigma_{a,r}(E) = \sigma_{t,r}(E) - \sigma_{s,r}(E)$$

λ is the IR parameter. $\lambda = 1$ corresponds to NR approximation, $\lambda = 0$ corresponds to WR approximation. Consequently, the IR approximation gives the energy dependence for flux at resonances of all energies with suitably computed values of λ for each of the nuclides involved. This is the approximation used in the WIMS library [14] treatment of resonances. Once the flux is known as a function of energy, the resonance integrals and group cross sections are easily calculated. Due to Doppler broadening of the resonances, the cross sections, flux and hence the resonance integrals are temperature dependent. The WIMS library includes tables of resonance integrals as a function of temperature and the background cross section and hence may be obtained for any homogenous mixture of heavy resonance absorbing nuclides and other light mainly scattering nuclides.

ii) Self-shielding in the case of heterogeneous system: equivalence theory

To estimate the resonance self-shielding effect, the energy dependence of the neutron flux in the heterogeneous system is obtained from the neutron slowing down equation. For the

case of a single fuel rod in a large moderator region, the neutron slowing down equation is written as

$$\Sigma_{t,f}(E)\,\phi_f(E)\,V_f = P_{f\to f}(E)\,V_f \int_0^\infty dE'\,\Sigma_{s,f}(E'\to E)\,\phi_f(E') + P_{m\to f}(E)\,V_m \int_0^\infty dE'\,\Sigma_{s,m}(E'\to E)\,\phi_m(E') \tag{2.6}$$

$\Sigma_{t,f}(E)$ - Total macroscopic cross section of fuel

$\Sigma_{s,f}(E'\to E)$ – Scattering cross section of fuel

$\Sigma_{s,m}(E'\to E)$ – Scattering cross section of moderator

$\phi_f(E)$ – Flux in fuel

$\phi_m(E)$- Flux in moderator

V_f – Volume of fuel

V_m – Volume of moderator

$P_{f\to f}(E)$ - Probability that neutron in fuel will undergo collision in fuel

$P_{m\to f}(E)$ - Probability that neutron in moderator will undergo collision in fuel

The RHS gives the contribution due to the slowing down of neutrons. If the slowing down is mainly by elastic scattering and applying the NR approximation to the moderator integral (this is valid for all resonances) the above equation becomes [22]:

$$\Sigma_{t,f}(E)\,\phi_f(E)\,V_f = \frac{1}{E}\left[P_{f\to f}(E)\,V_f\,\Sigma_{p,f} + P_{m\to f}(E)\,V_m\,\Sigma_{p,m}\right] \tag{2.7}$$

$\Sigma_{p,f}$ and $\Sigma_{p,m}$ are macroscopic potential scattering cross section of fuel and moderator respectively. Applying reciprocity and normalization of the collision probability, Eq. (2.7) can be written in terms of only the escape probability from the fuel as follows:

$$\phi_f(E) = \frac{1}{E}\left[\left(1-P_{f\to m}(E)\right)\frac{\Sigma_{p,f}}{\Sigma_{t,f}} + P_{f\to m}(E)\right] \tag{2.8}$$

For an isolated system which is under consideration, the fuel to moderator collision probability $P_{f\to m}$ is equivalent to the escape probability from fuel and can be approximated by Wigner's rational approximation as [23]

$$P_e(E) = \frac{1}{\Sigma_{t,f}(E)\bar{l} + 1}$$

Here $\bar{l}$ is the average chord length. With this, the equation becomes

$$\phi_f(E) \quad = \quad \frac{1}{E}\,\frac{\left(\sigma_{p,r} + \sigma_{0,f} + \Sigma_e/N_r\right)}{\left(\sigma_{t,r} + \sigma_{0,f} + \Sigma_e/N_r\right)} \tag{2.9}$$

The escape cross section is defined as $\Sigma_e = \frac{1}{\bar{l}}$. Comparing Eqns. (2.2) and (2.9) it can be seen that the energy dependence of the neutron flux can be approximated in a similar form either by σ_0 or $(\sigma_{0,f} + \frac{\Sigma_e}{N_r})$. This is Wigner's equivalence theorem between heterogeneous and homogeneous systems. With NR approximation, the background cross section for a homogeneous system is given by Eq. (2.3) and for a heterogeneous system it is

$$\sigma_0 \quad = \quad \frac{\sum_{k\neq r} N_k \sigma_{p,k}}{N_r} + \Sigma_e/N_r \tag{2.10}$$

The effect of heterogeneity on energy dependence of the neutron flux is represented by escape cross section.

For an array of fuel pins as in the case of a fuel assembly, the escape cross section of the isolated fuel pin will change due to shadowing effect as some neutrons may escape from one fuel pin and may suffer their next collision in the neighboring fuel pin instead of in moderator [22]. This is taken care by the use of Dancoff factor *D* applied to the escape cross section [18, 24, 25]. In the case of a lattice system where many fuel rods are present, the number of neutrons entering a fuel region decreases, as some of the neutrons in the moderator region is absorbed into other fuel rods. To consider this shadowing effect, Dancoff correction is applied as follows:

$$P_{f\to m}(E) \quad = \quad \frac{(1-C)P_e(E)}{1-\left[1-\Sigma_{t,f}(E)\bar{l}P_e(E)\right]C} \tag{2.11}$$

Here C is the Dancoff correction factor (D = 1- C) and represents the degree of shadowing by other fuel rods. The escape probability with the Dancoff correction is in the rational approximation form and hence the equivalence theorem applies to this situation also. Another correction factor suggested by Bell [26] takes care of some of the deviation of the escape probability for real fuel lumps in the form of rods, slabs or cylinders from the rational approximation. With the Bell correction, the escape probability is written as

$$P_e(E) \quad = \quad \frac{a_B\Sigma_e}{\Sigma_{t,f}(E)+ a_B\Sigma_e} \tag{2.12}$$

a_B is the Bell factor. In the case of a lattice system, the self-shielding effect is larger than in an isolated system and the background cross section is smaller than in an isolated system. The background cross section is given by

$$\sigma_0 \quad = \quad \frac{\sum_{k\neq r} N_k\sigma_{p,k}}{N_r} + \frac{(1-\mathrm{C})\ a_B}{[1+C(\ a_B-1)]}\ \frac{\Sigma_e}{N_r} \tag{2.13}$$

Once these background cross sections are calculated the corresponding resonance integrals can be obtained by interpolating from the table of resonance integrals. The resonance integrals thus obtained can be converted to multi-group effective cross section as [27]:

$$\sigma_{g,x} \quad = \quad \frac{I_{g,x}(\sigma_o,T)}{1-I_{g,a}(\sigma_o,T)/(\sigma_{p,r}+\sigma_0)} \tag{2.14}$$

Here $\sigma_{g,x}$ is the group effective cross section for reaction type x, $I_{g,x}(\sigma_o,T)$ is the resonance integral of reaction type x for background cross section σ_0 and temperature T, $I_{g,a}(\sigma_o,T)$ is the resonance integral of absorption reaction for background cross section σ_0 and temperature T, $\sigma_{p,r}$ is the potential scattering cross section of the resonant nuclide.

With this the multi-group cross sections are in a form that is suitable for solving the multi-group neutron transport equation for the representative lattice cell.

2.2.2 Methods and Codes to Solve the Multi-group Transport equations

Once the multi-group cross sections of the various materials are obtained in all energy groups, the lattice code solves the neutron transport equation to obtain the fine group neutron flux distribution across the lattice. Some of the commonly used methods for this purpose are briefly described in this sub-section. In general, the neutron transport equation can be solved analytically only for highly idealized cases [4]. Hence, numerical approximations are made in order to apply the equation in reactor engineering application. The methods for the numerical solution of NTE can be divided into deterministic and stochastic (Monte Carlo) methods. The deterministic methods can be further categorized as integral and integro-differential transport approach. In integral transport approach, the method is derived from integral form of NTE in which the angular dependence of the neutron flux is eliminated by integrating over all angular variables. This technique can be applied in heterogeneous complicated geometries. But with this, only isotropic scattering can be treated accurately.

The common methods used for the solution of the transport equation are the Discrete Ordinates or S_N method [28, 5] for solving the integro-differential form of the transport equation, the Collision Probability (CP) method [4] and its variants that solve the integral transport equation, and the Method of Characteristics (MOC) [29].

In earlier days the representative region used to be a ‘pin cell’ consisting of a single fuel rod and associated moderator with reflective boundary conditions. eg: THERMOS [30], MURLI [31]. Since seventies and early eighties, computer codes were developed for performing the lattice calculations at the fuel assembly level directly. eg: CLUP-77 [32], THERMOGENE [33, 34]. A brief description of the common methods for solution of neutron transport equation at the lattice level is given in the following section.

2.2.2.1 S_N method

This method is the most popular method for obtaining solutions to the integro-differential transport equation. This method was originally developed in the field of cosmic radiation [35] and was introduced to perform reactor calculation by [36]. In this method, the integration along angular variable is replaced by using a quadrature formula with a finite set of N angular directions and associated weights. This will lead to a finite number of coupled differential equations. Thus, the one-speed transport equation in plane geometry for isotropic scattering

$$\mu \frac{\partial \Phi(\mathrm{x}, \mu)}{\partial x} + \Sigma_t(x)\Phi(x, \mu) = q(x, \mu) \tag{2.15}$$

becomes

$$\mu_i \frac{\partial \Phi(\mathrm{x}, \mu_i)}{\partial x} + \Sigma_t(x)\Phi(x, \mu_i) = \sum_{j=1}^{N} w_j \, \Phi\left(x, \mu_j\right) \tag{2.15a}$$

in terms of the set of discrete direction cosine μ_i and associated weight w_i. For treating the spatial derivative, the spatial domain is divided into cells or meshes such that material properties are uniform within each cell. The common method adopted to treat the spatial derivative is by finite-difference. Integrating the above equation w. r. t. x over the k^{th} mesh yield

$$\mu_i\left[\Phi\left(x_{k+1/2}, \mu_i\right) - \Phi(x_{k-1/2}, \mu_i)\right] + \Delta x_k \Sigma_t(x_k)\Phi(x_k, \mu_i) = \Delta x_k \sum_{j=1}^{N} w_j \Phi\left(x_k, \mu_j\right) \tag{2.16}$$

where $\Phi(x_k, \mu_i)$ stands for the average flux in the k^{th} cell while $\Phi\left(x_{k+1/2}, \mu_i\right)$ and $\Phi\left(x_{k-1/2}, \mu_i\right)$ stand for the angular fluxes at the right and left boundaries and Δx_k is the cell width. This equation is an exact statement of neutron balance, but the equations do not form a closed set. In the diamond-differencing, closure is obtained by introducing the assumption that

$$\left[\Phi\left(x_{k+1/2}, \mu_i\right) + \Phi(x_{k-1/2}, \mu_i)\right] = 2\,\Phi(x_k, \mu_i) \tag{2.16a}$$

In two and three dimensions also, the same assumption is made connecting the boundary angular fluxes in any dimension to the average cell flux.

Because of the multi-group treatment of the energy dependence and use of discrete space mesh for spatial dependence, all the variables of the NTE are treated as discrete. The solution of the energy dependent problem corresponds to solving a set of coupled one-speed linear system of equations for each group and is carried out iteratively. The diamond difference scheme gives good accuracy but may result in negative fluxes for large sized meshes and flux fix up procedures have been evolved to take care of the problem [37, 38].

The scalar flux may be obtained as

$$\phi(x) = \int_{-1}^{1} \Phi(x,\mu)d\mu = \sum_{i=1}^{N} w_i \, \Phi(x,\mu_i) \tag{2.17}$$

The accuracy of the solution of NTE by S_N method depends largely on the choice of the quadrature set, ie. the set of direction cosine and associated weights. The limited number of discrete directions can lead to ray-effect [39] giving unphysical oscillations in the flux. This effect is more profound when there are highly angular dependent sources or when the source is highly localized. By increasing the number of directions, this effect can be reduced [39], but results in higher computational cost in terms of memory requirement and time. Other methods have been proposed to mitigate ray effects. Carlson and Lathrop suggested the methods like the use of specialized quadrature set that are invariant under discrete rotations as well as introducing coupling terms into the representation of the divergence operator [40, 41] to partially mitigate the ray effect. Methods based on first collision approximation of the source is also studied [42]. Another suggested approach is to expand the angular flux in terms of the spherical harmonics [43, 5], wherein the angular dependence is treated with continuous polynomial functions. Applicability of the method is limited due to expensive computational requirement. The problems containing strong absorbers require higher order quadrature set to

reduce the ray effect. Various techniques have been proposed to arrive at the specialized quadrature set. Carslon developed the equal weight quadrature set which gives positive weights for any order [44]. The uniform positive weight quadrature set derived by [45] are proved to give more accurate results. Other recent development includes quadrature set based on Legendre and Chebyshev polynomials [46].

Spatial differencing scheme was developed in 1969 by Lathrop [47] for 2-D Cartesian geometry. In 1973, the S_N method was generalized to triangular meshes by [48]. The S_N method was employed to treat the irregular meshes of quadrilateral type in X-Y and R-Z geometry by [49].

Many computer codes based on S_N methods have been developed. Some of the codes are: DTF-IV [50], ANISN [51], DOT [52], TWOTRAN [53], THREETARN [54], TRIDENT [55] which is a triangular mesh S_N code, NEWT by ORNL [56] is based on polygonal geometries. The geometry that is treated in most of these computer codes is based on spatial grids formed by cell with linear boundaries. For circular or curved geometries, approximations of curve need to be applied to consider the re-entrant boundaries. For treating the curved boundaries like fuel pins, the meshes or cells needs to be very fine with linear/planar boundary. Recently, spatial scheme based on simplified step characteristics (SSC) and multiple balance (MB) discrete ordinate methods [57] were derived for treating the curved regions without any approximation [58].

2.2.2.2 Collision Probability (CP) Method

One of the most widely used method for the solution of integral transport equation is collision probability (CP) method. CP method results from spatial discretization of integral transport equation in multi group form, assuming isotropic particle sources. Considering the multi-group treatment for energy discretization, the steady state form of Eq. (1.2) for energy group *g* takes the form as [4]:

$$\psi_g(r,\Omega) \quad = \quad \int_0^{\infty} exp\left[-\tau_g(s)\right] q(r - s\Omega, \Omega) ds \tag{2.18}$$

where $\tau_g(s) = \int_0^s \Sigma_g(r - s'\Omega) ds'$, is the optical path length. For isotropic scattering, the above equation can be written in terms of only the scalar flux $\phi_g(\mathbf{r})$ as

$$\phi_g(\mathbf{r}) \quad = \quad \int \frac{\exp\left[-\tau_g(\mathbf{r},\mathbf{r}')\right]}{4\pi|\mathbf{r}-\mathbf{r}'|^2} Q_g(\mathbf{r}') d^3r' \tag{2.19}$$

where,

$$\phi_g(\mathbf{r}) \quad = \quad \int_0^{4\pi} \psi_g(r,\Omega) d\Omega \tag{2.19a}$$

and

$$\mathrm{Q}_g(r) = \quad \int_0^{4\pi} \mathrm{q}_g(r,\Omega) d\Omega \tag{2.19b}$$

In CP method, the system under consideration is divided into a number of small regions. Integrating Eq. (2.19) over the volume of a region *j (*assuming that the flux (source) is constant in each of the regions) and multiplying both sides by the cross section of region *j* ($\Sigma_{j,g}$), it can be written in the form:

$$V_j \, \Sigma_{j,g} \phi_{j,g} = \quad \sum_i Q_{i,g} \, V_i \, P_{ij,g} \tag{2.20}$$

where $\phi_{j,g}$ is the average flux in the region *j*, $Q_{i,g}$ is the source density in region *i* and $P_{ij,g}$ is the probability that a neutron of energy group *g* born in any region *i* to collide in region *j* of the system and is given by

$$P_{ij,g} \quad = \quad \frac{\Sigma_{j,g}}{V_i} \int \int \frac{\exp\left[-\tau_g(\mathbf{r},\mathbf{r}')\right]}{4\pi|\mathbf{r}-\mathbf{r}'|^2} \, d^3r \, d^3r' \tag{2.20a}$$

where, the integration is limited to volumes of regions *i* and *j*. Thus, in the CP method, every region is connected to all other regions through the collision probabilities. The calculation of

these probabilities is one of the main tasks in CP method, while iterative solution of the CP form of the transport equation is the other.

The above expression for the collision probabilities implies a six-dimensional integration. Many of these integrations can be carried out analytically for example due to symmetries and the rest have to be carried out numerically. For the case of one-dimensional plane geometry all the integrations can be carried out analytically and the collision probabilities can be written in terms of the (E3) exponential integral functions [5]. The calculation of CPs for one-dimensional cylindrical geometry, general two-dimensional geometry [uniform in the z direction (along the length of the fuel rods), as in pin cell and general lattice calculations] and three-dimensional geometry require numerical integration. In the case of cylindrical and general two-dimensional geometries, the CP estimation involves the Bickley-Naylor $Ki_3(x)$ functions [59] given by

$$Ki_3(x) = \int_0^{\pi/2} \sin^2\theta \exp\left(-x/\sin\theta\right)$$

Numerical integration requires detailed tracking of the neutron paths through the geometry. The details are described in Chapter 3.

For a system with N number of meshes / volumes, N^2 collision probabilities need to be calculated and stored. This leads to a limitation in applying the method to large complicated geometries where number of meshes/volumes may be large. Dedicated routines for tracking and integrations of CPs are developed for different geometries. Some early examples of such programs are two-dimensional codes like CLUCOP [60], PROCOPE [61, 62], CLUP77 [32], WIMS'E' [63].

With the flat flux approximation, a solution close to the exact solution can be obtained if the number of regions/zones are increased. However, this can be time consuming and computationally expensive as the number of CPs to be calculated varies as N^2. To improve the

efficiency of CP method for the systems in which there can be strong flux gradient, two approaches have been developed to treat such situation. One is to use more than one expansion function per zone, so that local flux gradients can be taken into account [28] and the second is to use a combination of CP method and interface current (j ±) method, where in the optically large region is subdivided into cells that can be treated with the CP method, and couple the solutions via interface currents. Interface currents can be used to link the solutions in cells of optically large media. In this method, the contribution to collision density in a region due to neutrons that originated elsewhere in the system is expressed through neutrons entering from the bounding surfaces of that region. The simplest assumption for the angular distribution of these neutrons entering the region through the surface is that it is uniform over the 2π solid angle. This is referred to as the cosine current approximation [64, 5]. With this it is possible to calculate the probabilities that these neutrons will collide in the region or escape from some other surface and write the neutron balance equation involving in-currents, out-currents and the region fluxes.

The computer code CLIMAX [65] which was developed in 1980s for PHWR lattice simulation treats the cluster by ring homogenization procedure, and then uses the interface currents approach to get the flux distribution. However, heterogeneity effects in fast and resonance energy ranges are obtained through explicit cluster geometry treatment by collision probabilities. Codes based on a combination of CP coupling over a small set of regions forming a macro region and coupling the macro regions through interface currents have also been developed. An example is LWRWIMS where within the regions of a pin cell, CP coupling is used and interface currents couple various neighbouring pin cells [66]. A similar approach is adopted in the three-dimensional super cell codes BOXER3 [67] and SHETAN [68].

Rather than assume a uniform angular distribution of neutrons at the surface, more complicated angular distributions may be used. An expansion in a basis set of angular functions

may also be carried out. CLUB [69,70,71,72] which is developed for the lattice of PHWR cluster uses the CP method for treating the heterogeneities within the fuel rings and these rings are coupled to each other by interface currents. The two-dimensional fuel assembly lattice cell codes such as APOLLO [64, 73] and DRAGON [74] incorporates this method with double P0/P1 Legendre expansions of angular flux. The computer code VISWAM [75] incorporates this method for treating the hexagonal lattices. The CP method is used within individual lattices and different lattices are connected using interface current with double P2 expansion for the angular flux at lattice cell boundaries. These codes use the "block method" of solving the integral transport equation that couples meshes within a block by collision probabilities and adjacent blocks by interface currents. This method combines the advantages of the conventional collision probability method and the interface current technique.

2.2.2.3 Method of Characteristics (MOC)

The method of characteristics (MOC) first proposed by [29] is based on the integro-differential form of the neutron transport equation. The transport equation is solved analytically along characteristic directions within a computational volume. The streaming term that appears in NTE can be written as

$$\Omega.\nabla\Phi = \frac{d\Phi(\mathrm{r},\mathrm{E},\Omega)}{ds} \tag{2.21}$$

The characteristic form of the neutron transport equation is derived from its integro-differential form as:

$$\frac{d\Phi(\mathrm{r},\mathrm{E},\Omega)}{ds} + \Sigma_t(r,E)\Phi(\mathrm{r},\mathrm{E},\Omega) = \mathrm{Q}(\mathrm{r},\mathrm{E},\Omega) \tag{2.22}$$

where s is the track along which neutrons is traveling in the direction Ω . For a one-dimensional slab geometry, considering the scattering and source is isotropic, the above eqn. becomes

$$\frac{d\Phi}{ds} + \Sigma_{tr}\Phi = \frac{q}{4\pi} \tag{2.22a}$$

Here q is the isotropic scalar source and Σ_{tr} is the transport cross section. The solution to this equation can be obtained by integrating the above equation, as:

$$\Phi(\mathrm{s}) = \Phi(0)\, e^{-\Sigma_{tr}s} + \frac{q}{4\pi\Sigma_{tr}}(1 - e^{-\Sigma_{tr}s}) \tag{2.23}$$

where, $\Phi(0)$ is the known angular flux at s=0 and is given from the boundary conditions. The above solution is written employing the step characteristic method developed by [39] in which source q and macroscopic total cross section are assumed to be constant within a cell. In each direction, there will be many parallel tracks. More than one track can pass through a mesh/region in a particular direction. The scalar flux for a given mesh is obtained by integrating the angular flux along all tracks that cross the mesh and integrating over all directions.

The method is applied to spatial domains with regions having piecewise uniform nuclear properties. The scalar flux within a region (mesh) is obtained by collecting all average angular fluxes in terms of entering angular flux and source inside the region. It combines the best advantages of the collision probability (CP) and discrete ordinate (S_N) method. It has great advantages compared to the collision probability method, because it is applicable for large problems. It can use the same tracking information as that of CP method. In the case of CP method, it is required to generate full square matrices of order equal to number of regions (N^2, N = number of regions / meshes). Because of this, if the system is large, CP method cannot be applied. Other limitation of CP method is that it is limited to isotropic sources. MOC is superior to CP in the sense that both the above limitations are not there with MOC.

In comparison with S_N methods, MOC is capable to model the real geometry of the fuel lattices without any homogenization. MOC, like S_N method, solves the neutron transport equation in selected discrete directions in each group. But it follows the neutron path through the problem region, thus using the exact solution of the transport equation in its characteristics

form. Since streaming term of the neutron transport equation is treated exactly in MOC compared to the finite-difference approximation in S_N method, MOC is a superior computational method for streaming calculations in deep-penetration shielding problems. To account for the spatial dependence of the angular flux, many parallel tracks passing through the problem region can be used in each selected direction. Any geometry can be treated in MOC if adequate ray tracing routines are available. Another advantage is that it can treat anisotropic scattering. The accuracy of the solution depends on the number of selected directions and the track spacing.

The MOC is generally classified into two categories based on the treatment of angular flux at cell surface; first category considers angular flux at only finite number of points on the cell surface and in the second, angular flux is expanded over the cell surface. In the first category, a finite number of characteristic lines are chosen for each direction. The angular fluxes at the points at which the characteristics intersect with the cell surface for each direction is calculated [76]. With the assumption of constant source within the cell, the flux is computed in terms of incoming flux and source. In the second category of MOC, which are based on the use of expansions for the angular flux over the cell surface, the flux is approximated as:

$$\psi^k(r,\Omega) = \sum_j \psi_j^k(\Omega) f_j^k(\mathrm{r}) \tag{2.24}$$

where, $f_j^k(\mathrm{r})$ are the expansion functions and $\psi_j^k(\Omega)$ are the expansion coefficients. This gives the angular flux on an exiting surface, $\psi^k(r,\Omega)$, in terms of known flux on the entering surface and known source. The unknown expansion coefficients can be determined by collocation method [77, 78] and projection method [79].

Many applications of the method of characteristics were developed starting from the 1980s. Thus, for instance, the method was introduced in the code CACTUS [76, 80] module and became the standard transport module of WIMS [81]. MCCG3D [82], CASMO-4 [83, 84],

CRX [85], DRAGON-V3 [86], CASMO-5 [87] are some of the other codes based on the MOC. Recently [88, 89] have developed a MOC based code that has the option of linear source variation option in addition to the usual flat source approximation.

2.2.3 Treatment of Burnup

As the composition of the material within the fuel region of the lattice changes due to irradiation, the number density of fissile, and fertile nuclides in the fuel materials changes. Additionally, fission products are generated as a result of fuel burnup. As the fuel composition changes, the macroscopic cross sections which is the input to solve the transport equations also changes. This changes the neutron flux distribution within the lattice cell. The change in nuclide density with burnup is governed by the Bateman equations [90]. The burnup problem is solved by introducing a number of relatively large (typically days or tens of days) burnup steps. The lattice code solves the burnup equations (Bateman equations) to obtain the number density of various nuclides present during the burnup step. The effective cross sections of each of the nuclides required to solve these equations are assumed to be constant during a burnup step and are obtained by averaging over the energy of the neutrons using the flux spectrum obtained from the lattice code at the beginning of the burnup step. With the new fuel composition available at the end of the burnup step (beginning of the next burnup step), the flux distribution and effective cross sections are obtained again for the next burnup step. These are again used for solving the Bateman equations for the following burnup step. This procedure gives the nuclide density, and flux distribution as a function of burnup. This describes the standard predictor-only method commonly used for solving burnup problems.

Other improved schemes like predictor-corrected method [91] and projected predictor-corrector method [92] are also used in the treatment of burnup. In the predictor only method, the number densities are obtained by using the flux at the beginning of the burnup step and assumes that it remains constant during the integration (burnup) step. However, this assumption

may lead to some error. In the predictor-corrector method, two transport calculations are required per burnup step and the average of two number densities is used as the correct number density for the burnup step. In this scheme, obtain number density $N^{predictor}$ by assuming the flux is same as at the beginning and perform transport calculation using $N^{predictor}$ and obtain the flux, use this flux to obtain the $N^{corrector}$, use the average of $N^{predictor}$ and $N^{corrector}$ as the correct number density for the burnup step and perform one more transport calculation to obtain the flux. Even with predictor- corrector method, the time (burnup) step used may be of the order of 1.0 GWd/teU in the case of a fuel assembly/pin containing Gd, requiring many steps to simulate its depletion [7]. To overcome the error in the number density in such cases due to underestimation at predictor and corrector level, projected predicted corrector method is implemented in codes like AEGIS [93]. The Kawamura-Leonard-Yamamoto (KLY) algorithm and the Yamamoto's quasi-analytic (YQA) algorithm [94] are also used to speed up the calculation (by reducing the number of neutronic calculation). These methods permit the use of coarse time step for burnup without compromising on the desired accuracy.

2.2.4 Homogenisation Methods

The lattice code generates the volume homogenized few group cross sections (diffusion theory parameters) using the fine energy group detailed spatial flux distribution by volume homogenization and group condensation as a function of burnup. The homogenized few group diffusion theory parameters are used in the second step core calculations. It is important that the few group diffusion theory parameters are carefully evaluated. Information generated at the lattice level by multi-group transport theory should be compressed into few group homogenised diffusion theory parameters for each pin cell in such a way that important properties such as reaction rates, and leakage rates or currents from various pin cells or cell surfaces are correctly predicted by the diffusion theory solution.

The lattice calculations are performed considering the heterogeneities present in the lattice cell and in fine energy groups applying reflective boundary condition. The flux volume homogenisation of the cross sections is carried out using the detailed flux distribution thus obtained. To account for the leakage due to finiteness, normally, P1 calculation [18] is performed with a given buckling and obtain the leakage corrected spectrum using the volume homogenised fine group cross sections. With the spatially homogenised fine group cross sections and for a given buckling B, the following equations are solved to obtain the flux and current in the P1 method:

$$\begin{aligned} \Sigma_{t,g}\phi_g \pm iB\, J_g &= \chi_g + \sum_{g'} \Sigma_{0,s\, g'-g}\, \phi_{g'} \\ 3\Sigma_{t,g}\, J_g \pm iB\, \phi_g &= 3\sum_{g'} \Sigma_{1,s\, g'-g} J_{g'} \end{aligned} \tag{2.25a}$$

$\Sigma_{0,s\, g'-g}$ and $\Sigma_{1,s\, g'-g}$ are the spatially homogenised P0 and P1 scattering cross sections and χ_g is the fission spectrum. The fine group diffusion coefficient is obtained as:

$$D_g = \frac{iJ_g}{B\, \phi_g} \tag{2.25b}$$

Using the leakage corrected spectrum, homogenised few group cross sections and diffusion coefficients are obtained by group condensation. The B-1 buckling method is an alternative to the P1 method [95] for estimating the diffusion coefficient. In B1 method, Eq. (25a) gets modified as:

$$\begin{aligned} \Sigma_{t,g}\phi_g \pm iB\, J_g &= \chi_g + \sum_{g'} \Sigma_{0,s\, g'-g}\, \phi_{g'} \\ 3\, a_g(\mathrm{B})\, \Sigma_{t,g}\, J_g \pm iB\, \phi_g &= 3\sum_{g'} \Sigma_{1,s\, g'-g} J_{g'} \end{aligned} \tag{2.25c}$$

where,

$$a_g(B) = \frac{1}{3}x^2\left(\frac{\arctan(x)}{x - \arctan(x)}\right) \qquad \text{if} \quad x^2 = \left(\frac{B}{\Sigma_{t,g}}\right)^2 > 0$$

$$a_g(B) = \frac{1}{3}x^2\left(\frac{\ln\left(\frac{1+x}{1-x}\right)}{\ln\left(\frac{1+x}{1-x}\right) - 2\mathrm{x}}\right) \qquad \text{if} \quad x^2 = -\left(\frac{B}{\Sigma_{t,g}}\right)^2 > 0$$

Several other methods have been proposed to obtain the homogenised diffusion coefficient in the past beginning with the classic works of Benoist [96,97], Deniz [98,99], Gelbard [100], Kohler [101] and Larsen [102]. Basically, they try to define the average diffusion coefficient and cross sections, for the case of a regular lattice with a superimposed buckling (to account for the finiteness of the lattice), such that reaction rates and leakage rates are preserved. The focus has shifted from defining average diffusion coefficients to using flux discontinuity factors (FDF) at the interfaces [103]. The generalized equivalence theory (GET) [104] and black box homogenization (BBH) [105] techniques are the two commonly used approaches for obtaining the FDF. An interesting relation between the use of the Benoist diffusion coefficient and the flux discontinuity factors approach has been pointed out by [106]. An alternative approach to the homogenisation problem referred to as super-homogenisation (SPH) uses a corrective factor for each macro region that multiplies the flux volume weighted cross sections and diffusion coefficient to preserve reaction and leakage rates [107, 108].

In the case of light water reactors, most of the earlier work in this subject was devoted to obtaining homogenised diffusion theory parameters (including flux discontinuity factors) for use in the nodal methods (i.e. for large scale homogenisation over fuel assembly sized regions). With greater interest in pin by pin diffusion theory, there have been successful attempts to obtain homogenised diffusion theory parameters and sub-region wise (for example pin by pin) flux discontinuity factors for such problems [108, 109].

In the axial direction, material discontinuities are few and far between and no axial homogenisation is necessary. Consequently, there are no flux discontinuity factors in this direction. However, it is necessary to obtain the best value of the axial diffusion coefficient (upon transverse homogenisation) that would correctly predict the leakages in the axial direction. Benoist's work [96, 97] in this direction addresses the problem of obtaining the diffusion coefficient for a lattice cell and forms the basis of obtaining the axial homogenised diffusion coefficient in various lattice codes such as WIMS [14]. Due to the more complicated structure of modern LWRs, a more general approach is necessary. Poveschenko and Laletin [110, 111] have carried out some interesting work in this direction. Their approach and notation are rather complicated and the final expressions for the collision probability like integrals involve transformed coordinates rather than the physical path lengths in various regions along a neutron track. Moreover, their results are limited to the case of isotropic scattering and infinite lattices. This problem is re-visited in chapter 4 of the thesis where formulae for homogenised axial diffusion coefficients in terms of collision probability like integrals for isotropic and anisotropic scattering, using the simple text book approach for deriving Fick's law is obtained. The necessary corrections on account of the finiteness of the lattice are also obtained.

2.3 Core Level Computational Methods and Codes

For thermal reactor core calculations, mainly few groups (2 - 4 groups) diffusion equation that is an approximate form of the NTE, is solved to get the flux distribution in the reactor. The diffusion equation is obtainable by expanding the angular flux in the NTE in terms of spherical harmonics (P_N) and the expansion is truncated after $\boldsymbol{l}=1$ terms. This is the P_1 approximation. It is shown in text books that the P_1 approximation is equivalent to the diffusion equation in one group theory but in multi-group theory, a number of other approximations have to be invoked [4].

Considerations of criticality require us to solve the k (or lambda) eigen-value problem for multi group neutron diffusion equation. Its solution provides effective multiplication factor and neutron flux distribution. The few group diffusion equation to be solved for core physics analysis can be written as

$$\nabla . D_g(r)\nabla\phi_g(r) + \Sigma_{r,g}(r)\phi_g(r) = \frac{\chi_g}{K_{eff}} \sum_{g'=1}^{G} \nu\Sigma_{f,g'}(r)\phi_{g'}(r) + \sum_{g'\neq g}^{G} \Sigma_{sg',g}(r)\ \phi_{g'}(r) \qquad (2.26)$$

$$\Sigma_{r,g} = \Sigma_{a,g} + \sum_{g'\neq g}^{G} \Sigma_{sg,g'}\ , g' = 1, 2, \ldots. G.$$

The solution of the group-diffusion equations by analytical methods is practical only for essentially one-dimensional situations involving only a few homogeneous regions within which the group diffusion parameters are spatially constant. An example of such solutions is the two-group theory of the reflected reactors discussed in text books of elementary Reactor Physics [112]. For mathematical models of a reactor that are more realistic, numerical schemes must be used. Common methods for solving these equations are finite difference (FD), Finite element (FE) and Nodal Methods. For PHWRs traditionally FD methods are employed where the mesh size can be of the order of lattice pitch. In LWR calculations, usually nodal methods where nodal size can be of fuel assembly pitch are used. FD method for LWR core calculations require very fine meshes of the order of pin cell pitch. Brief descriptions of these methods are presented in the following sections.

2.3.1 Finite Difference Method (FDM)

FDM involves mainly three steps: Dividing the solution region into meshes, approximating the given differential equation by a finite difference equivalent form that relates the dependent variable (flux) at a point in the solution region to its values at the neighboring points and solving the resulting system of linear equations. The boundary conditions appropriate for the problem such as zero flux or zero incoming current are incorporated at the

stage of finite differencing. The discretization in space is carried out to obtain the first term in Eq. (2.26). The other terms are easy to obtain. Spatial discretization is done by dividing the regions where neutron diffusion equations is to be solved (for eg: usually the core and reflector regions) into a number of discrete meshes. It is assumed that each mesh is having constant nuclear properties which are obtained as volume homogenized cross sections and diffusion coefficients from lattice cell calculations. In 1-D geometry, the meshes are line segments, in 2-D Cartesian geometry (X-Y) they are rectangles and in 3-D (X-Y-Z) geometry the meshes are rectangular parallelepipeds.

There are two variants of the FD methods [18]: corner mesh scheme and center-mesh scheme. In the corner mesh scheme flux at the corners of the mesh is considered as the variable for which solution is sought, whereas in center-mesh scheme mesh average flux (approximated as the flux at the center of the mesh) is considered as the variable. The finite difference equations for the center-mesh scheme is obtained by integrating the diffusion equation over the mesh volume that gives a balance equation involving mesh average flux and mesh surface currents. The finite difference equation is obtained by approximating the surface currents in terms of the average fluxes in the two meshes on either side of the surface. The corner-mesh equations are obtained similarly with the integration carried out over a part of each of the meshes surrounding a corner point. In what follows, the process of converting the diffusion equation into a finite difference equation taking center mesh in one-dimensional plane geometry as an example, is briefly described.

Let us consider a 1-D plane geometry for which the diffusion equation is:

$$\frac{d}{dx}D_g(x)\frac{d}{dx}\phi_g(x) + \Sigma_{r,g}(x)\phi_g(x) = \frac{\chi_g}{K_{eff}}\sum_{g'=1}^{G}\nu\Sigma_{f,g'}(x)\phi_{g'}(x) + \sum_{g'\neq g}^{G}\Sigma_{sg',g}(x)\ \phi_{g'}(x) \tag{2.26a}$$

The right side of Eq. (2.26a) is the total source due to fission and scattering from other groups and is denoted as $Q_g(x)$. The meshing scheme employed for finite differencing is shown below in Fig.2.1.

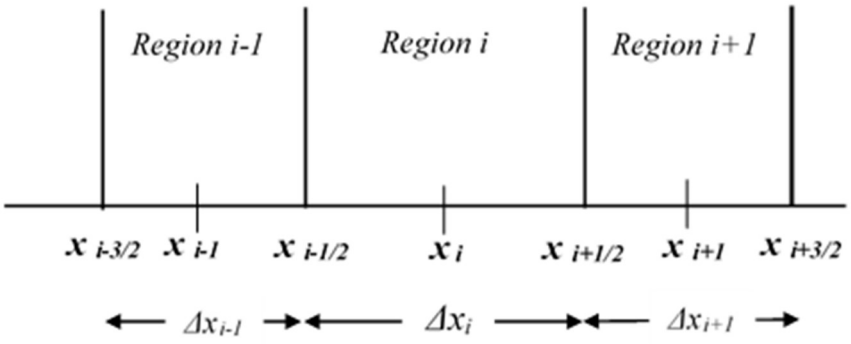

Fig.2.1: Meshing scheme for finite-differencing

In the case of center-mesh FD method the expression is obtained for ϕ_i, ϕ_{i-1}, ϕ_{i+1} etc. In the case of corner-mesh FD method the expression is obtained for $\phi_{i-1/2}$, $\phi_{i+1/2}, \phi_{i+3/2}$ etc. In the center-mesh scheme, integration of the diffusion equation over a mesh gives the following neutron balance equation

$$J_{g,i+1/2} - J_{g,i-1/2} = \Delta x_i \, \Sigma_{r,g,i} \phi_{g,i} - \Delta x_i \, Q_{g,i} \tag{2.27}$$

On approximating the surface currents by the finite difference form

$$J_{g,i+1/2} = -D_g{}^{(i)} \frac{(\phi_{g,i+1/2} - \phi_{g,i})}{2\Delta x_i} = -D_g{}^{(i+1)} \frac{(\phi_{g,i+1} - \phi_{g,i+1/2})}{2\Delta x_{i+1}} \tag{2.28}$$

And a similar equation for $J_{g,i-1/2}$. Using these equations, the boundary values of the fluxes and currents can be eliminated from the balance equation and the final FD equations takes the form:

$$\frac{2D_g{}^{(i+1)}\,D_g{}^{(i)}}{D_g{}^{(i)}\Delta x_{i+1}+D_g{}^{(i+1)}\Delta x_i}(\phi_{g,i+1}-\phi_{g,i})-\frac{2D_g{}^{(i-1)}\,D_g{}^{(i)}}{D_g{}^{(i)}\Delta x_{i-1}+D_g{}^{(i+1)}\Delta x_i}(\phi_{g,i}-\phi_{g,i-1}) \\ =\ \Delta x_i\,\Sigma_{r,g,i}\phi_{g,i}-\Delta x_i\,Q_{g,i} \tag{2.29}$$

Thus in 1-D the flux in mesh *i* is connected with flux in meshes *i-1* and *i*+1. This is for an internal mesh with both left and right neighbor. By applying appropriate boundary conditions, FD equations can be obtained for flux at left and right boundary meshes. These equations are usually called three-point difference equations. The above treatment can be extended to 2-D and 3-D problems. In the case of 2-D, flux in mash *(i, j)* will be connected to four neighboring meshes and the resulting equations are referred as five-point difference equations and in 3-D they are referred as seven-point difference equations, each mesh is connected to six immediate neighbors. In matrix form the above equation takes the form

$$M\Phi=\frac{1}{k}F\Phi\ ,$$

where the elements of column matrix Φ are the unknowns $\phi_1,\phi_2,\ \ldots\ldots\phi_i$.

The matrix M , whose elements represent leakage, capture and scattering, is real, symmetric and its elements have tri-diagonal structure. The equation has a large number of eigenvalues denoted by k_m and corresponding eigen-vectors Φ_m . The matrix M is diagonally dominant and its eigenvalues are real and positive [113]. The largest eigen-value is the K-effective of the fundamental mode. For steady state reactor calculations, the quantity of interest is the flux in the fundamental mode and K-effective. Iterative methods [18] are employed to solve the above set of equations with proper boundary conditions to obtain the mesh-wise fluxes and eigen-value K_{eff}. Power iteration method with inner-outer iteration scheme, inner iteration for flux and outer iteration for eigen-value, is usually employed [113,114]. For each group, source which depends on the flux in all other groups needs to be calculated. Thus, starting with a guess value of flux and eigenvalue one computes the source. Keeping the source fixed in a group, the

inner iteration is carried out for obtaining the group flux. As one proceeds to the next group, scattering source is updated using the latest flux value in the previous groups. The process is continued till all groups have been covered. The k eigenvalue and fission source for the next outer iteration are estimated and brings us to the end of one outer iteration. Outer iterations are repeated till the eigenvalue and flux converge to the desired level of accuracy.

For the inner/flux-iteration, point iterative method like Gauss-Seidel (G-S) method is applied to solve for the flux from $M\Phi = S$. Successive Over relaxation (SOR) method is an improvement in G-S iteration method for faster convergence. When SOR is applied, the flux will be calculated using $\phi'^{,n+1} = \omega\phi^{n+1} + (1-\omega)\phi^{n}$, where n is the iteration index, ω is the over-relaxation parameter [114] and its value lies between 1 and 2. When ω =1, it corresponds to G-S method. Block-iterative method, such as Successive Line Over Relaxation (SLOR) in which fluxes are updated at many points at a time instead of at a single point as in G-S method, are used for faster convergence. Methods like coarse-mesh rebalancing is also applied to achieve faster convergence. For the eigen-value / outer iteration convergence, Two-parameter Chebyshev acceleration scheme is applied [113].

Several computer codes based on the finite difference method have been developed. The computer code PDQ-7 [115, 116] incorporates Chebyshev iterative convergence acceleration scheme for fission source. Computer code VENTURE [117] developed in 1975 employs the SLOR for inner iteration. The computer code DIF3D [118] solves the diffusion equation employing FD method with Chebyshev acceleration scheme for outer iteration and SLOR for inner iteration. Some of the codes developed in India are: the computer code DIMENTRI [119], COMESH [120] based on corner-mesh FD incorporating the acceleration schemes like SLOR for flux and two-parameter Chebyshev acceleration for eigen-value convergence, TAQUIL and TRIVENI [121] which are used for PHWR fuel management is based on center-mesh finite difference scheme with SOR for faster convergence.

2.3.2 Finite Element Method

Though widely used in the engineering field, the application of the finite element method (FEM), to the area of Reactor Physics is limited. In early seventies, the method was successfully applied for few 2-D Benchmark problems [122, 123]. Due to requirement of handling and storage of large matrices and intensive computational scheme, the method did not find wide spread use in 3-D practical reactor problems [124, 125].

In FEM, the problem domain is divided into meshes called elements and flux inside each mesh point is expanded in terms of piecewise polynomials, and consider the expansion coefficients as the primary variables. The unknown expansion coefficients are obtained from continuity conditions along the interface of neighboring elements. In FDM, as discussed in the previous section, the differential operator $\frac{d^2\phi}{dx^2}$ is approximated with a difference quotient. In FEM, ϕ is approximated as a linear combination of simple known functions as [123]

$$\phi(x) = \sum_{i=1}^{I} a_i \, u_i(x)$$

Where $u_i(x)$ satisfy the boundary conditions and a_i are the unknown combining coefficients. With the above representation of flux, the diffusion equation becomes:

$$-D \sum_{i=1}^{I} a_i \frac{d^2 u_i(x)}{dx^2} + \left(\Sigma_a - \frac{\nu \Sigma_f}{\lambda} \right) \sum_{i=1}^{I} a_i \, u_i(x) = Q\,(x) \qquad (2.30)$$

For generating algebraic relations between the unknown a_i, the Galerkin method [126] is widely used and it requires that the above equation be orthogonal to $u_i(x)$. With this requirement, the above equation can be written as:

$$-D\boldsymbol{Fa} + \left(\Sigma_a - \frac{\nu \Sigma_f}{\lambda} \right) \boldsymbol{Ma} = S \qquad (2.30a)$$

where, $F_{ji} = \langle u_j, \frac{d^2 u_i(x)}{dx^2} \rangle$ and $M_{ji} = \langle u_j, u_i \rangle$

The solution is obtained by solving the above equation for a_i and then finding $\phi(x)$.

The advantage of the method is that it can be used for treating the complex geometries. Though it works well for homogeneous systems, in the case of large heterogeneous systems, the number of elements or the number of basic functions has to be increased. This results in large number of equations and unknowns and becomes difficult to solve. For these reasons, 3D FEM is somewhat expensive for routine design computations and is not very popular.

While FEM has been used for reactor fuels modelling for many years and is most often used for fuel performance modelling at the pellet and pin scale, its use for solving neutron diffusion problems has been limited. The codes FEM3D [125], FEM-BABEL [127], FINERC [128] are a few examples of the use of the finite element method for solving multi group diffusion theory equations.

2.3.3 Nodal Expansion Method (NEM)

For solving few-group neutron diffusion equations by finite-difference method for LWRs, large number of mesh points are required to represent the spatial variation of the neutron flux accurately. For LWR analysis, with the development of nodal methods, the computational time has significantly reduced. The nodal methods are referred to as coarse mesh methods. There are two approaches in the nodal method: Analytical nodal method [129] and polynomial nodal method [130,131]. In both the methods, one-dimensional equations obtained by integrating the three-dimensional equation over the two directions transverse to each coordinate axis, are solved. The directions which are integrated out appear as the transverse leakage terms in the 1-D diffusion equation. In polynomial method, the one-dimensional flux is expanded in terms of suitably chosen polynomials. The nodal expansion method [132] is an example of PEM. ANM can be applied to problems where two group calculations yield fairly accurate results. In the case of PEM, this limitation is not there. For this reason, NEM is more popular for reactor analysis.

In the NEM developed by Lawrence [132], the one-dimensional flux is expanded in terms of polynomials up to the fourth order. Thus, there are 5 unknowns as the expansion coefficients. These are obtained from boundary conditions and residual moments. The method is described in detail in Chapter 5.

The concept of using the solution of one-dimensional equation to obtain the multi-dimensional problems originated with the development of two different variants of nodal method viz. Nodal Synthesis method [133] and analytical method [134, 129]. In NSM, the coupling coefficient, which is the ratio of face averaged partial current to node average flux, is used to express the surface current and the resulting diffusion equation becomes like finite-difference equation in node average flux. These coupling coefficients are to be computed during the iterative process for the solution of nodal equations. In the analytical method, Taylor series expansion is used for the expression relating the face averaged current and nodal flux. The computer code QUANDRY is based on the Nodal Analytical method in two-groups [135, 129]. The nodal expansion method, NEM, is an improvement in NSM, in the sense that in NEM the one-dimensional flux is expanded in polynomials thereby eliminating the fine-mesh finite difference calculations in NSM [136]. Though NEM has been initially developed to treat rectangular geometry it has been successfully applied to hexagonal geometry, which is the case of VVER type PWRs, liquid metal fast reactors and gas cooled reactors [137, 132].

Regarding the solution method with NEM, the usual inner-outer iteration scheme is employed to obtain the flux and eigen-value of the problem. For outer iteration, the Chebyshev acceleration techniques which is applied in FD method has been found suitable in Nodal methods also [135]. It has been found from the numerical examples that, for the same accuracy of the results, the computing time taken by NEM is less than that by FD owing to the less number of unknowns to be evaluated in the case of NEM due to its applicability to much coarser mesh than that can be used in FD [132]. In addition, the convergence rate of the inner iteration

depends on spectral radius of the iterative matrix [113]. As the mesh size becomes larger, the spectral radius decreases and the convergence rate increases. Thus, in NEM, the number of unknowns is less as well as these unknowns are computed fewer times than in FD method.

Since its development, nodal method has been adopted for reactor analysis and implemented in several large-scale codes. The FLARE [138] code which was originally developed for BWR core simulation is based on the nodal coupling method where one-group diffusion equation is solved. Some of the computer codes that incorporates NEM for the solution of the few group diffusion equation are IQSBOX [139], SIMULATE-E [140], DIF3D [141], FEMINA [142], QPANDA [131], NODHEX [143], NESTLE [144], DYN3D [145], HEXNEM [146] and IQSHEX [147]

The methods discussed so far are suitable for core simulation considering the fuel assembly as the node. To obtain the pin power distribution within the FA, the pin power reconstruction is applied. It is obtained based on the superposition of the pin power map from the transport solution and the smooth power profile based on the results of nodal solution. The pin power maps are evaluated for each fuel type as a function of burn-up at the time of assembly homogenization at lattice level calculation.

Recently, core calculations using transport theory without homogenization using the method of characteristics or interface current methods are being attempted [9,10] to obtain detailed pin by pin power and burnup distributions. Another approach adopted for obtaining pin power distribution is by 'hybrid FD-Nodal method' [148].

Since the aim of the present work was to develop a computational tool for obtaining the pin power distribution of LWRs, an improved form of the hybrid FD-NEM is developed and the details of the formalism and verification are presented in Chapter 5 of the thesis.

2.4 Summary

The thesis presents new theoretical developments and their practical implementation for improving existing methods / codes at both the lattice and the core levels of the two step calculations. For the lattice level calculations, the computer code developed implements the collision probability method and MOC for the solution of neutron transport equation. The code has the capability to treat anisotropic scattering and computes pin-wise Dancoff factor. It can perform calculations in fine energy-groups using the WIMS 69 or172 group libraries. The code has other features like the use of leakage corrected collision probabilities for obtaining the neutron spectrum and spatial distribution and a new method for obtaining homogenized axial diffusion coefficients. For the core level calculation, the method developed for obtaining the pin wise power distribution is based on the combination of finite difference method in X-Y direction and a fourth order polynomial expansion method along Z-direction, in which the treatment of transverse leakage is also accurate up to the fourth order. The mesh size along transverse direction is of a pin cell but the use of the polynomial expansion along the z-axis permits the use of much longer meshes in this direction.

CHAPTER 3

COLLISION PROBABILITY AND MOC BASED LATTICE CODE FOR ANALYSIS OF LWR FUEL ASSEMBLIES

3.1 Introduction

The computational requirement for obtaining 3-D neutron flux distribution in fine energy groups for practical problems involving power reactor is very large and even with many fold increase in computational capability compared to seventies, for routine reactor calculations a two-step approach is followed for obtaining the required solution. As discussed in chapter 1, the first step involves solving the neutron transport equation for a small representative region called lattice cell in fine energy groups. It is assumed that the lattice cell repeats periodically throughout the reactor. The lattice cell typically consists of fuel, clad, coolant and associated moderator. Since the neutron reaction cross section (probability of neutron interaction) depend strongly on the energy of the neutron, the lattice calculations are performed using the transport equation with a large number (typically about a few hundred) of energy groups (referred to as fine group calculations). In addition to treating complicated geometry and energy dependence of the neutron cross sections, another aspect that needs to be treated at the lattice level relates to the changes in material composition within the lattice cell due to neutron irradiation in the reactor. These burnup effects in turn change the flux distribution within the cell. Lattice calculations yield a detailed flux distribution in space and energy across the lattice cell at various burnup stages (or steps) and forms the subject of the present chapter. The detailed flux distribution thus obtained is used to obtain few group homogenized cross sections and diffusion coefficients as a function of burnup for the second step of the calculations. The second step is the core calculation wherein it is assumed that the reactor consists of the homogeneous lattice cells and the diffusion equation – that is an approximate form of the transport equation - in few

groups (typically 2-4) is solved to obtain the core flux distribution. This aspect is discussed in chapter 5.

As discussed in chapter 2 of the thesis, several numerical methods have been developed to solve the neutron transport equation (NTE) for the complicated geometry that is usually found in modern power reactors. Several computer codes based on these numerical methods are in existence.

In earlier days the representative region/lattice cell used to be a 'pin cell' consisting of a single fuel rod and associated moderator with reflective boundary conditions. Since seventies and early eighties, computer codes were developed for the lattice calculations at the fuel assembly level directly. For treating the complex geometries that are involved in practical lattice cells, the integral transport theory using either the collision probability, the interface current or a combination of these methods was popular. Computer codes like CLUP-77 [32], LWRWIMS [66], THERMOGENE [33, 34], BOXER3 [67] and LWRBOX [149] are based on this method. The method has the added advantage that it can be formulated in terms of only the scalar flux, since the scattering anisotropy plays only a minor role and can be corrected by the use of transport cross sections. Method of Characteristics (MOC) which gained popularity in recent times, even though the method was developed in early 1970s for solving NTE, have many advantages over commonly used methods such as the collision probability, the S_N and the Monte Carlo method. These include its capability (a) to treat complex geometries (b) to handle anisotropic scattering (3) to produce detailed flux and power distribution over the region of solution and (4) to obtain solution in neutronically large sized domains. Several lattice level codes have incorporated the MOC as a method of solving the multi-group transport equation, examples being DRAGON [86], CASMO-4 [84] and CASMO-5 [87] and more recently, by Mazumdar and Degweker [88].

The BOXER3 code [67] was developed during the eighties, in Bhabha Atomic Research Centre (BARC), as a three-dimensional code for the analysis of pressurized heavy water reactor (PHWR) supercell containing fuel, moderator and a reactivity device inserted perpendicular to the fuel. Taking into account the computing resources available then, the code was run in few groups after obtaining condensed group cross sections for various materials from a one-dimensional multi-group calculation. BOXER3 can treat one-dimensional cylindrical pin-cell and slab geometries (as in plate type fuels), two-dimensional problems such as fuel assemblies and three-dimensional problems. The geometry that can be represented consists of cylinders imbedded in a rectangular mesh. The cylinders can be further subdivided into radial circular or annular regions as well as azimuthal divisions up to π /4. The outer most boundary must be a rectangular parallelepiped. Some examples of geometries that are available are shown in Fig.3.1. For both the two and three-dimensional calculations, particularly for large domain problems, there is an option to use a mixed method involving a detailed collision probability treatment within smaller sub domains and coupling these sub domains using interface currents.

This chapter describes the development work carried out in BOXER3 code to make it suitable for lattice level calculations including burnup calculations of LWR fuel assemblies [7]. Coupling of the code to the WIMS 69/172 group library and introduction of burnup has enabled it to perform multi-group calculations using CP methods, and solve the burnup equations and thus be used as a lattice code.

Much of the LWR calculations at BARC was being carried out using a three-stage calculation viz. one-dimensional pin-cell lattice followed by assembly level few group diffusion and full core few group diffusion calculations. For treating the lattice, the computer code RICANT [150] was developed for 2-D rectangular one-zone cell using interface current method. In this, six terms are considered for the expansion of angular flux in terms of Legendre

polynomials. The introduction of code LWRBOX [149] based on a combination of collision probability and interface current method was an improvement.

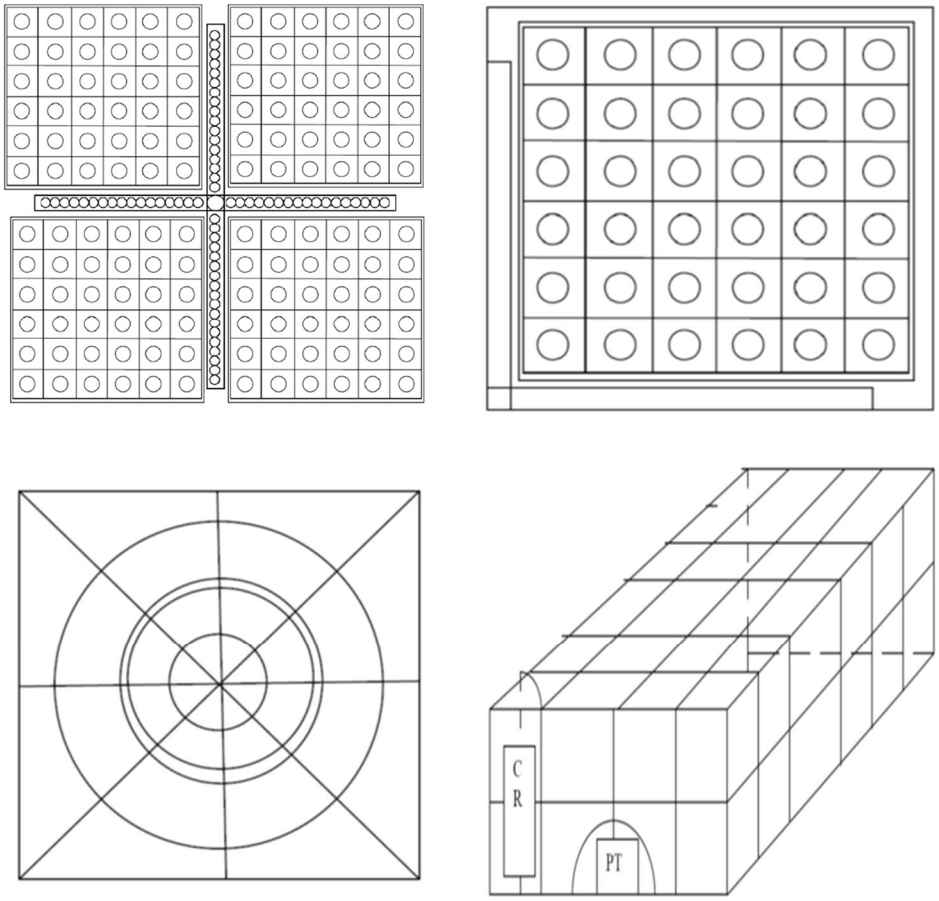

Fig. 3.1: Typical geometries with sub divisions that can be handled by BOXER3

The present work represents a further improvement in lattice calculation methodology. One can use assembly level P_{ij} (that is more accurate) in addition to the option of interface currents between pin-cells. Other improvements include the use of pin-dependent Dancoff factors for resonance treatment, a more straightforward method for normalizing collision probabilities and introduction of a predictor corrector approach to burnup calculations. All these features are described in this chapter.

The introduction of MOC is another important development. It permits the use of anisotropic scattering (the WIMS library has P1 scattering matrices for H, D, C, and O and these can be used). For both collision probability (CP) and MOC methods, the problem domain

needs to be divided into meshes and sufficient number of characteristic lines or rays, along which the transport equation is solved in MOC, are to be traced over the mesh structure. Thus, using the information from the same ray tracing algorithm used for CP method, MOC can be easily implemented in the code.

The outline of the chapter is as follows: The neutron balance equation and the solution method by CP method as in BOXER3 is described in section 3.2. Section 3.3 details computation and normalization method of the collision probabilities. Section 3.4 describes the solution method using MOC for both isotropic and anisotropic scattering. In section 3.5, a brief description about pin-wise Dancoff factor estimation is given. Section 3.6 covers the treatment of burnup. Verification results of BOXER3 code for various benchmark problems are presented in section 3.7. Summary and scope of future study is discussed in section 3.8.

3.2 Neutron Balance Equation and Solution Method by CP Method

BOXER3 solves the integral transport equation using the block method (mixed P_{ij} and $J^{\pm}$ methods). In the block method the equations can be written as follows:

$$\varphi_i^g \Sigma_i^g V_i = \sum_j Q_j^g P_{ji}^g + \sum_m S_m J_m^{g(in)} P_{mi}^g \tag{3.1}$$

$$S_m J_m^{g(out)} = \sum_j Q_j^g P_{jm}^g + \sum_{m'} S_{m'} J_{m'}^{g(in)} P_{m'm}^g \tag{3.2}$$

$$Q_i^g = \sum_h \varphi_i^h V_i \left(\Sigma_{si}^{h \to g} + \frac{\chi^g (\nu \Sigma_{fi}^h)}{k} \right) \tag{3.3}$$

where,

φ_i^g – flux in region *i* in energy group *g*

$J_m^{g(in)}$ – in-current at surface m in group *g*

$J_m^{g(out)}$ – out-current at surface m in group *g*

V_i – volume of region *i*

S_m – area of surface *m*

Σ_i^g – transport cross section in region *i* in group *g*

Q_i^g – scattering and fission sources in region *i* in group *g*

$\Sigma_{si}^{h\to g}$ – transfer cross section from group *h* to group *g* in region *i*

χ^g – fission spectrum

ν – number of neutrons per fission

Σ_{fi}^h – fission cross section in region *i* in group *h*

P_{ji}^g – region *j* to region *i* collision probabilities

P_{mi}^g – surface *m* to region *i* collision probabilities

P_{jm}^g – region *j* to surface *m* collision probabilities

$P_{m'm}^g$ – surface *m'* to surface *m* (escape) probabilities in group *g*.

The left side of Eq. (3.1) is the collision rate in region *i* and group *g* while the right side is the sum of all volume and surface sources in group *g* multiplied by the respective probabilities of such source neutrons to collide in region *i*. The left side of Eq. (3.2) is the total number of neutrons escaping through surface *m* and group *g* while the right side is the sum of all volume and surface sources in group *g* multiplied by the respective probabilities of such source neutrons to escape through the surface *m*. The various probabilities obey the following reciprocity relations:

$$\Sigma_i V_i P_{ij} = \Sigma_j V_j P_{ji}, \quad 4\Sigma_i V_i P_{im} = S_m P_{mi} \quad \text{and} \quad S_m P_{mm'} = S_{m'} P_{m'm}$$

3.2.1 Solution Method

Inner-outer iteration technique is applied for the solution of the above set of equations to obtain the fluxes, currents and the eigenvalue *k*. Each outer iteration commences with the highest energy group and progresses downwards till all groups are covered. For each group the

total source consisting of the sum of in-scatter source and fission source, is computed. The fission source is updated at the beginning of an outer iteration but remains constant during the outer iteration. The in-scatter is updated before commencing inner iterations for a particular group. The inner iterations are used to obtain the converged fluxes and currents corresponding to this total source. The inner iterations are carried out using the following equations derived from Eqs. (3.1 to 3.3) and the reciprocity relations, with the expression for flux and current as:

$$\varphi_i^g = \sum_j \left(\frac{\Sigma_{sj}^{g \to g}}{\Sigma_j^g} \right) P_{ij}^g \varphi_j^g + \sum_m P_{im}^g J_m'^{g(in)} + \wp_{\varphi i}^g \tag{3.1a}$$

$$J_m'^{g(out)} = \sum_j \left(\Sigma_{sj}^{g \to g} / \Sigma_j^g \right) P_{mj}^g \varphi_j^g + \sum_{m'} P_{mm'}^g J_{m'}'^{g(in)} + \wp_{Jm}^g \tag{3.2a}$$

Where $J_m'^g = 4J_m^g$, $\wp_{\varphi i}^g$ and $\wp_{Jm}^g$ are related to the in-scatter and fission source terms.

$$\wp_{\varphi i}^g = \sum_{h \neq g, j} \left(\frac{\Sigma_{sj}^{h \to g} \varphi_j^h}{\Sigma_j^g} \right) P_{ij}^g + \frac{1}{k} \sum_{h,j} \left(\frac{\chi^g \nu \Sigma_{fj}^h \varphi_j^h}{\Sigma_j^g} \right) P_{ij}^g \tag{3.3a}$$

$$\wp_{Jm}^g = \sum_{h \neq g, j} \left(\frac{\Sigma_{sj}^{h \to g} \varphi_j^h}{\Sigma_j^g} \right) P_{mj}^g + \frac{1}{k} \sum_{h,j} \left(\frac{\chi^g \nu \Sigma_{fj}^h \varphi_j^h}{\Sigma_j^g} \right) P_{mj}^g \tag{3.3b}$$

The above form of the equations, Eqs. (3.1a) and (3.2a), for inner iterations is a manifestly convergent form as the iteration matrix has a row sum less than unity for all rows. Consequently, the spectral norm is less than unity, which means that the norm of the error vector will fall monotonically with the number of iterations [151]. A check is performed for convergence of the fluxes and currents, failing which the inner iteration is repeated. If convergence is acceptable, proceed to the next group. When all groups have been covered an outer iteration is complete. The eigen-value *k* is estimated and checked for convergence. If the convergence is inadequate, the outer iteration is repeated, else the computation of flux and eigenvalue is over.

3.3 Computation Method of Collision Probabilities

In order to solve the above set of equations, the collision probabilities (CPs) needs to be calculated using the information from the ray tracing program. These are described in the following sections.

3.3.1 CPs in Three-Dimensional Lattice

The following equations were derived [67] for various probabilities i.e. $P_{ii,}$ P_{ij}, $P_{is,}$ P_{si} and $P_{s1,s2}$ that are required for solution of three-dimensional problems,

$$P_{ii} = \frac{1}{4\pi\Sigma_i V_i}\int dA\, d\boldsymbol{\Omega}\,\{\tau_i - 1 + \exp\,[-\tau_i]\} \tag{3.4}$$

$$P_{ij} = \frac{1}{4\pi\Sigma_i V_i}\int dA\, d\boldsymbol{\Omega}\,\{\exp[-\tau_{ij}] - \exp[-(\tau_{ij}+\tau_i)] - \exp\,[-(\tau_{ij}+\tau_j)] + \exp\,[-(\tau_{ij}+\tau_i+\tau_j)]\} \tag{3.5}$$

$$P_{iS} = \frac{1}{4\pi\Sigma_i V_i}\int dA\, d\boldsymbol{\Omega}\,\{\exp[-\tau_{iS}] - \exp[-(\tau_{iS}+\tau_i)]\} \tag{3.6}$$

$$P_{Si} = \frac{1}{\pi S}\int dA\, d\boldsymbol{\Omega}\,\{\exp[-\tau_{iS}] - \exp[-(\tau_{iS}+\tau_i)]\} \tag{3.7}$$

$$P_{S_1S_2} = \frac{1}{\pi S_1}\int dA\, d\boldsymbol{\Omega}\exp[-\tau_{S_1S_2}] \tag{3.8}$$

where τ_{ij}, τ_i and τ_j are the optical path lengths between *i* and *j*, in *i* and in *j* respectively, τ_{iS} is the optical path length between *i* and *S* and $\tau_{S_1S_2}$ is the optical path length between the surfaces S_1 and S_2.

In the three-dimensional version, the angular integration is performed using weights and directions taken from a fully symmetric Sn quadrature set. For each integration direction, the rectangular parallelepiped (outer boundary of the solution domain) is projected in a plane perpendicular to the direction. In 3-D, the projection of a rectangular parallelepiped is an

'irregular hexagon'. A rectangular mesh is constructed within the hexagon and the neutron trajectories are started from the center of each rectangle with a weight equal to the product of the area of the small rectangle and the angular quadrature weight for that direction. The tracing program generates the intercepts of the ray in each of the meshes starting from an area element of the outer surface of a sub-domain and ending on another such area element. The integrals are computed by multiplying the contribution to a probability by any ray with its weight and adding over all possible rays.

3.3.2 CPs in Two-Dimensional Lattice

In two dimensions, ray tracing is done in a plane perpendicular to the z direction (direction of homogeneity). This is accomplished by setting the direction cosine in z direction to be zero. In this case the 'hexagon' collapses to a rectangle, and since the integration lines are drawn in a plane perpendicular to the z direction, a single mesh is taken in the direction of uniformity. The angular integration over the azimuthal angle is done using uniform angular spacing and constant weights or with Gauss Quadrature. For different azimuthal angles, integration over y is carried out using a uniform quadrature in a direction perpendicular to the direction of the trajectories. In two dimensions the formulae derived by Carlvik [152] involving Bickley functions are used

$$P_{ii} = \frac{1}{2\pi\Sigma_i V_i}\int dy\, d\varphi \,\{\tau_i - Ki_3(0) + Ki_3\,(-\tau_i)\} \tag{3.9}$$

$$P_{ij} = \frac{1}{2\pi\Sigma_i V_i}\int dy\, d\varphi \,\{Ki_3[-\tau_{ij}] - Ki_3[-(\tau_{ij}+\tau_i)] - Ki_3\,[-(\tau_{ij}+\tau_j)] + Ki_3\,[-(\tau_{ij}+\tau_i+\tau_j)]\} \tag{3.10}$$

$$P_{iS} = \frac{1}{2\pi\Sigma_i V_i}\int dy\, d\varphi \,\{Ki_3[-\tau_{iS}] - Ki_3[-(\tau_{iS}+\tau_i)]\} \tag{3.11}$$

$$P_{Si} = \frac{1}{\pi S}\int dy\, d\varphi \,\{Ki_3[-\tau_{iS}] - Ki_3[-(\tau_{iS} + \tau_i)]\} \tag{3.12}$$

$$P_{S_1S_2} = \frac{1}{\pi S_1}\int dy\, d\varphi \, Ki_3\left(-\tau_{S_1S_2}\right) \tag{3.13}$$

One-dimensional problems involving cylindrical geometry (pin cells with cylindricalised outer boundary) are special cases that can be treated with only one direction (since integration over φ is not required).

3.3.3 CPs in One-Dimensional (slab or plate type geometry) Lattice

In slab geometry, numerical integration for computation of collision probabilities is not required. The calculation of various probabilities is done using the following expressions [7]:

$$P_{ii} = 1 - \frac{\frac{1}{2} - E_3(-\tau_i)}{\tau_i} \tag{3.14}$$

$$P_{ij} = \frac{1}{2\tau_i}\{E_3[-\tau_{ij}] - E_3[-(\tau_{ij} + \tau_i)] - E_3\left[-(\tau_{ij} + \tau_j)\right] + E_3\left[-(\tau_{ij} + \tau_i{+}\tau_j)\right]\} \tag{3.15}$$

$$P_{iS} = \frac{1}{2\tau_i}\left[E_3(-\tau_{ij}) - E_3\{-(\tau_{ij} + \tau_i)\}\right] \tag{3.16}$$

$$P_{Si} = 2\left[E_3(-\tau_{ij}) - E_3\{-(\tau_{ij} + \tau_i)\}\right] \tag{3.17}$$

$$P_{S_1S_2} = 2\,E_3(-\tau_{S_1S_2}) \tag{3.18}$$

3.3.4 Normalisation of the Probabilities

The estimated probabilities have to be such that the sum of all the probabilities starting from a region / surface should add up to one. However due to the quadrature related errors (particularly over the area) the sum does not add up exactly to unity. Many schemes for normalization of the probabilities so that they add up to unity have been proposed. In diagonal normalization scheme, which is employed in the code DRAGON, the diagonal elements of the CP matrix are updated using the error. This scheme may result in negative values of diagonal elements if the value itself is small and cannot be applied in the case of problems with voided

zone [153]. In Gelbard normalization scheme [154], correction is applied based on the probabilities in the homogeneous limit. Even though this can be applied to voided zones, it can result in negative probabilities. In the multiplicative normalization scheme [153, 155], the probabilities are updated by multiplying with weighting factors. This method results in an additional computation of the weighting factors. In BOXER3 a different approach, which is more satisfactory from a physical point of view, is applied to normalize the collision probabilities. It can be seen from Eqs. (3.4) to (3.6) that for each ray, the integrand of the expressions for the three probabilities adds up to τ_i.That is

$$
\begin{aligned}
P_{ii} + \sum_{j\neq i} P_{ij} + \sum_{S} P_{iS}
&= \frac{1}{4\pi\Sigma_i V_i}\Bigg[\int dA\, d\boldsymbol{\Omega}\,\{\tau_i - 1 + \exp[-\tau_i]\} \\
&\quad + \sum_{j\neq i}\int dA\, d\boldsymbol{\Omega}\,\{\exp[-\tau_{ij}] - \exp[-(\tau_{ij}+\tau_i)] - \exp[-(\tau_{ij}+\tau_j)] \\
&\quad + \exp[-(\tau_{ij}+\tau_i+\tau_j)]\} \\
&\quad + \sum_{S}\int dA\, d\boldsymbol{\Omega}\,\{\exp[-\tau_{iS}] - \exp[-(\tau_{iS}+\tau_i)]\}\Bigg] \\
&= \frac{1}{4\pi\Sigma_i V_i}\int dA\, d\boldsymbol{\Omega}\Bigg[\{\tau_i - 1 + \exp[-\tau_i]\} \\
&\quad + \sum_{j\neq i}\{\exp[-\tau_{ij}] - \exp[-(\tau_{ij}+\tau_i)] - \exp[-(\tau_{ij}+\tau_j)] \\
&\quad + \exp[-(\tau_{ij}+\tau_i+\tau_j)]\} + \sum_{S}\{\exp[-\tau_{iS}] - \exp[-(\tau_{iS}+\tau_i)]\}\Bigg] \\
&= \frac{1}{4\pi\Sigma_i V_i}\int dA\, d\boldsymbol{\Omega}\,\tau_i
\end{aligned}
$$

Upon carrying out the numerical integration of the expression on the right side for the collision probabilities, the above sum will be given by

$$P_{ii} + \sum_{j \neq i} P_{ij} + \sum_{S} P_{iS} = \frac{V_{i(est)}}{\mathrm{V}_i} \tag{3.19}$$

where $V_{i(est)} = \frac{1}{4\pi} \sum_{k,\Omega} w_\Omega \, (\Delta A)_k \, l_k(i)$ is the numerically estimated volume of the region *i*. The summation over k is limited to the rays that pass through the region *i*. By using $\mathrm{V}_i = \mathrm{V}_{i(est)}$ to divide the collision probabilities of neutrons starting in the region *i,* the right side of Eq. (3.19) is unity. In other words, the probabilities satisfy conservation. Since the estimated volume of each region is well defined, the probabilities also satisfy reciprocity provided the same set of rays is used to calculate P_{ij} and P_{ji}. A similar estimated surface area is used as the divisor in the expressions for the surface probabilities. The transformed form of collision probability equations given by Eqs. (3.1a) and (3.2a) does not explicitly involve region volumes. Thus, the use of the estimated volumes in the calculation of the collision probability equations together with the forms (3.1a) and (3.2a) of the integral transport equation ensures that there is no inconsistency.

3.4 The Method of Characteristics (MOC) for Neutron Transport Equation

The main limitations of the collision probability method for the solution of integral transport equation are that it can be used for optically small regions and the assumption of isotropic scattering. MOC on the other hand can treat complex geometries as well as anisotropic scattering. Since the same geometric options and ray tracing scheme developed in BOXER3 for CP estimation can be used for MOC also, a solution module based on MOC is introduced in BOXER3 code. A brief description of the MOC equations and method of solution is presented in this section.

3.4.1 Isotropic Scattering

The steady state integro-differential form of Boltzmann transport equation in multi group eigenvalue form is written as

$$\boldsymbol{\Omega}.\nabla\psi_g(\boldsymbol{r},\boldsymbol{\Omega}) + \Sigma_{tg}(\boldsymbol{r})\psi_g(\boldsymbol{r},\boldsymbol{\Omega}) = Q_g(\boldsymbol{r},\boldsymbol{\Omega}) \tag{3.20}$$

$\psi_g(\boldsymbol{r},\boldsymbol{\Omega})$ - the angular flux,

$\Sigma_{tg}(\boldsymbol{r})$ - the total macroscopic cross section,

$Q_g(\boldsymbol{r},\boldsymbol{\Omega})$ - the total angular source of neutrons in energy group g at location $\boldsymbol{r}$ in direction $\boldsymbol{\Omega}$ and is written as

$$Q_g(\boldsymbol{r},\boldsymbol{\Omega}) = \sum_{g'}\left(\int \Sigma_{sg'\to g}(\boldsymbol{r},\boldsymbol{\Omega}'\to\boldsymbol{\Omega})\psi_{g'}(\boldsymbol{r},\boldsymbol{\Omega}')d\boldsymbol{\Omega}' + \frac{\chi_g \nu\Sigma_{fg'}(\boldsymbol{r})}{4\pi k}\int \psi_{g'}(\boldsymbol{r},\boldsymbol{\Omega}')d\boldsymbol{\Omega}'\right) \tag{3.21}$$

For the case of isotropic scattering, $\Sigma_{sg'\to\boldsymbol{g}}(\boldsymbol{r},\boldsymbol{\Omega}'\to\boldsymbol{\Omega}) = \Sigma_{sg'\to\boldsymbol{g}}(r)/4\pi$. Hence the scattering and fission sources can be written in terms of the scalar flux (integral of the angular flux).

The solution is sought for a number of discrete directions taken from a suitably chosen quadrature formula. Thus, the integration over angle variable can be written as weighted sum, e.g.

$$\phi_g(\boldsymbol{r}) = \int \psi_g(\boldsymbol{r},\boldsymbol{\Omega})d\boldsymbol{\Omega} = \sum_m w_m\psi_g(\boldsymbol{r},\boldsymbol{\Omega}_m) = \sum_m w_m\psi_{gm} \tag{3.22}$$

$\boldsymbol{\Omega}_m$ are the discrete directions, w_m are the corresponding weights and $\psi_g(\boldsymbol{r},\boldsymbol{\Omega}_m)$ has been abreviated as ψ_{gm}. For spatial discretization, problem domain is divided into meshes with uniform material properties within each mesh. The scattering and fission sources in a mesh (i) can thus be written as

$$Q_{igm}{}^{(scat)} = \sum_{g'}\frac{\Sigma_{s,i,g'\to\boldsymbol{g}}}{4\pi}\phi_{ig'} \tag{3.23a}$$

$$Q_{igm}{}^{(fiss)} = \frac{\chi_g}{4\pi k}\sum_{g'}\nu\Sigma_{f,i,g'}\,\phi_{ig'} \tag{3.23b}$$

To derive the MOC equations the partial derivative in streaming term in Eq. (3.20) is converted into a total derivative along the neutron motion. In the multi group form, the characteristic form of the transport equation is

$$\frac{d\psi_{igm}}{ds_m} + \Sigma_{tig}\psi_{igm} = Q_{igm} \tag{3.24}$$

Here s_m is the distance along a neutron track measured from the point the track enters the mesh i in direction $\mathbf{\Omega}_m$; ψ_{igm} is the angular flux in direction $\mathbf{\Omega}_m$ across mesh i in energy group g. Assuming that the source is constant in a mesh (i), the solution of this equation is

$$\psi_{igm}(s_m) = \psi_{igm}(0)e^{-\Sigma_{tig}s_m} + \frac{Q_{igm}}{\Sigma_{tig}}\left(1 - e^{-\Sigma_{tig}s_m}\right) \tag{3.25}$$

The average angular flux in the mesh for the particular track, $\bar{\psi}_{igm}$, is obtained by integrating Eq. (3.25) over the length of the track in the mesh and dividing by the length of the track, as

$$\bar{\psi}_{igm} = \frac{1}{\Sigma_{tig}}\left(Q_{igm} + \frac{\psi_{igm}(0) - \psi_{igm}(\Delta s)}{\Delta s}\right) \tag{3.26}$$

Since along a given direction, more than one ray can pass through a mesh, average angular flux for the mesh is obtained by averaging over all such rays. Thus, average angular mesh flux is obtained as

$$\bar{\bar{\psi}}_{igm} = \frac{\sum \bar{\psi}_{igm} A_{\mathrm{m}} \Delta s}{\sum A_{\mathrm{m}} \Delta s} \tag{3.27}$$

where the summation extends over the different neutron tracks that cross mesh i in direction Ωm. Δs is the length of each track crossing mesh i and A_{m} is the area of the 'tube' (typically the uniform separation between (the projections of) parallel streaming tracks in the case of two-dimensional problems). The average scalar flux in mesh i in group g is obtained by numerical integration of the average angular flux as:

$$\bar{\bar{\phi}}_{igm} = \sum_m w_m \bar{\bar{\psi}}_{igm} \tag{3.28}$$

The tracks terminate at the domain boundary, which is divided into small surface elements. The outgoing angular flux for each element is obtained by averaging over various tracks that contribute to that element in the given direction. The incoming angular flux for the element is then obtained by equating this outgoing flux to the incoming flux in the reflected direction, in case a reflective boundary condition is used. For a periodic boundary condition, the direction of the incoming flux remains the same, but the surface element is changed to one that is related to the given element by periodicity.

The solution is obtained by employing the usual inner-outer iteration scheme. Outer iteration is for eigen-value and inner iteration is for flux. Each outer iteration commences with the highest energy group and progresses downwards till all groups are covered. For each group the total source, consisting of the sum of two sources viz., due to in scatter and due to fission, is computed. The fission source is updated at the beginning of an outer iteration but remains constant during the outer iteration. The in-scatter is updated before commencing inner iterations for a particular group. The inner iterations are used to obtain the converged fluxes corresponding to this total source. Each inner iteration consists of the following steps. The outgoing angular flux and the average angular flux along the characteristics (for the i^{th} mesh) are computed using Eqs. (3.25) and (3.26) respectively and the mesh averaged angular flux is obtained using Eq. (3.27). Finally, the average scalar flux is updated using Eq. (3.28) which is used to obtain the self-scatter source. A check is performed for convergence of the flux, failing which the inner iteration is repeated. If convergence is acceptable, the solution proceeds to the next group. When all groups have been covered, one outer iteration is complete. The multiplication factor (eigenvalue) is estimated and checked for convergence. If the convergence is inadequate, the outer iteration is repeated, else the computation of flux and eigenvalue is over.

3.4.2 Anisotropic Scattering

Anisotropic scattering is considered by expanding the scattering cross sections in terms of Legendre polynomials and using the addition theorem of spherical harmonics, it can be written as.

$$\Sigma_{sg\prime\to g}(\boldsymbol{\Omega}'\to\boldsymbol{\Omega})=\Sigma_{sg\prime\to g}(\boldsymbol{\Omega}'.\boldsymbol{\Omega})=\sum_{\mathrm{l}=0}^{\mathrm{L}}\frac{2l+1}{4\pi}\Sigma_{lg\prime\to g}\,P_l(\boldsymbol{\Omega}'.\boldsymbol{\Omega})$$

$$=\sum_{l=0}^{L}\frac{2l+1}{4\pi}\Sigma_{lg\prime\to g}\left[P_l(\cos\theta')\,P_l(\cos\theta)\right. \tag{3.29}$$

$$\left.+2\sum_{m=1}^{l}\frac{(l-m)!}{(l+m)!}P_{lm}(\cos\theta')\,P_{lm}(\cos\theta)\,\cos\{m(\varphi-\varphi')\}\right]$$

where, L is the scattering order. In BOXER3, expansion up to the third order is introduced even though the WIMS library contains only P1 transfer matrices for H, D, C, and O. For the case of linearly anisotropic scattering,

$$P_0(\boldsymbol{\Omega}'.\boldsymbol{\Omega})=1\,,\quad P_1(\boldsymbol{\Omega}'.\boldsymbol{\Omega})=\boldsymbol{\Omega}'.\boldsymbol{\Omega}$$

$$\Sigma_{sg\prime\to g}(\boldsymbol{\Omega}'\to\boldsymbol{\Omega})\;=\frac{\Sigma_{0g\prime\to g}}{4\pi}$$

$$+\frac{3\Sigma_{1g\prime\to g}}{4\pi}[\cos\theta\,\cos\theta'+\sin\theta\,\sin\theta'(\cos\varphi\,\cos\varphi'+\sin\varphi\,\sin\varphi')] \tag{3.30}$$

In the above representation, the various coefficients of the cross-section expansion are obtained by multiplying by $P_l(\boldsymbol{\Omega}'.\boldsymbol{\Omega})$ and integrating over Ω. Σ_0 is the total scattering cross section. Since the flux is expected to be symmetrical about $\theta=\pi/2$, the first term in the linearly anisotropic scattering will not contribute. The following three moments have to be calculated which contribute to the scattering source

$$\phi_{ig}=\int\psi(\Omega')d\Omega'=\sum_m w_m\,\psi_{ig}(\theta_m,\varphi_m)=\sum_m w_m\,\psi_{igm} \tag{3.31}$$

$$J_{yig} = \int \sin\theta' \sin\varphi' \, \psi(\Omega') d\Omega' = \sum_m w_m \sin\theta_m \sin\varphi_m \, \psi_{igm} \tag{3.32}$$

$$J_{xig} = \int \sin\theta' \cos\varphi' \, \psi(\Omega') d\Omega' = \sum_m w_m \sin\theta_m \cos\varphi_m \, \psi_{igm} \tag{3.33}$$

The scattering source in any direction (θ_m, φ_m) per unit solid angle is computed using

$$Q_{igm}{}^{(scat)} = \sum_{g'} \left(\frac{\Sigma_{0g' \to g}}{4\pi} \phi_{ig'} + \frac{3\Sigma_{1g' \to g}}{4\pi} \left(\sin\theta_m \sin\varphi_m \, J_{yig'} + \sin\theta_m \cos\varphi_m \, J_{xig'} \right) \right) \tag{3.34}$$

The iteration strategy is modified somewhat to include anisotropic scattering. The mesh averaged angular flux calculated at the end of an inner iteration is used to update the mesh averaged scalar flux and currents using Eqs. (3.31) to (3.33). These are used for calculating the self-scatter source using Eq. (3.34) (with $g' = g$). Similarly for in-scattering source calculations, at the end of all inner iterations in a group, only the three moments ϕ_{ig}, J_{yig} and J_{xig} are stored and the in-scattering source in any other group and any direction is obtained using Eq. (3.34).

3.5 Calculation of the Dancoff Factor

To make BOXER3 code suitable for simulating any type of lattice, it is coupled with 69/172 group WIMS update library [6]. While the library formats are the same for any source of the evaluated data, calculations presented in this thesis are based on the 69 group ENDF/B-VI.8 data. The cross-section data read from the WIMS library needs to be processed and formatted for use in BOXER3. The processing includes reformatting from the condensed scattering matrix format to the full matrix format used in BOXER3, interpolation of thermal cross section data for various temperatures and calculation of the background cross section and interpolation from the resonance integral tables for this background cross section and the given temperature. For heterogeneous systems, estimation of the background cross section requires calculation of the Dancoff factor [4]. The Dancoff factor is the probability that a neutron escaping a fuel surface with a cosine current distribution, reaches another fuel rod without

collision in the moderator. As discussed in chapter 2, Dancoff factor is required for correcting the escape cross section from a single fuel rod and which goes as an input into calculating the scattering cross section per absorber atom for interpolating from the resonance tables given in the cross-section library. This is calculated using the ray tracing facility of BOXER3 to obtain the following integrals.

$$D = \frac{1}{\pi S_1} \int dA \, d\boldsymbol{\Omega} \exp\left[-\tau_{S_1 S_2}\right] \tag{3.35}$$

where, τ is the optical path length between the surface of the fuel rod and that of the pellet of any other fuel rod that is first crossed by an outgoing ray and S_1 is the surface area of the fuel rod. In two dimensions for cylindrical fuel rods, the above integral reduces to the following formula for the Dancoff factor

$$D = \frac{1}{\pi^2 r} \int_0^{2\pi} d\varphi \int Ki_3\,(\tau_p) dy' \tag{3.36}$$

Here τ_p is the projection of τ in a plane perpendicular to the axis of the rod, *r* is the radius of fuel rod and dy is the separation between rays. Pin dependent Dancoff factors are obtained by calculating the above expression separately for each pin by considering all rays that start from the surface of that pin.

3.6 Treatment of Burnup

Due to irradiation in the reactor, the composition of the fuel material changes continuously. For the solution of NTE, number density of each material present in the lattice is an input. To obtain the number density of various nuclide as a function of time, the Bateman equations (burnup equations) $\frac{d\,\bar{x}(t)}{dt} = A\,\bar{x}(t)$ are solved, where $\bar{x}(t)$ is the nuclide concentration vector and *A* the transformation matrix obtained from various reaction cross sections and decay constants of the nuclides. For the solution of the above equation, predictor-corrector method [91] is used. The region of interest is divided into a number of fuel zones,

each zone being typically a single pin or a group of symmetrically placed pins having the same initial composition. The time for which burnup is to be calculated is divided into macro time steps also called burnup steps.

During each of these burnup (macro) steps, the one group cross sections and flux within each burnup zone are assumed to be constant. These zone wise microscopic cross sections for various actinides and fission products in different fuel burnup zones are obtained by averaging over the flux and spectrum distribution in the zone calculated by a transport calculation at the beginning of the macro time step. Likewise, the flux in each burnup zone is obtained by summing over all energy groups and averaging over the meshes in that burnup zone. The zone wise flux is then normalised so as to give the correct total power of the assembly (given as input). The reaction rates per atom are then given by the product of the zone flux and the average cross section of the reaction under consideration.

The other quantities that are required are the decay constant of the various fission products and actinides, tables giving transformation of one nuclide into another by various reactions and fission yields of fission products. These are read from the WIMS burnup library. Finally, all this data is used to form the matrix A which is then fed to an ODE solver based on Gear's backward difference method [156] used for this purpose. Gear's method has the advantage of stability and also gives good accuracy. The integrator chooses a number of micro time steps depending upon the specified accuracy. The burnup equations are solved to give the concentrations of the actinides and fission products at the end of the macro (or burnup) time step as well as at any intermediate steps if so desired. The concentrations at the end of the burnup step (also the concentrations at the beginning of the next time step), are called the predictor concentrations and go as input into the solution of the transport equation for obtaining the cross sections and the normalised flux and are used to calculate the matrix A for the next time step. The process is repeated till all the burnup steps have been completed. It is referred

to as the predictor only method and is adequate for many problems. A significant improvement, particularly for problems involving burnable absorbers, can be obtained by adding a corrector step. In this, the matrix *A* calculated at the end of the burnup time step, using the predicted nuclide concentrations for performing a transport calculation, is used to perform one more burnup integration called the corrector. The nuclide concentrations thus obtained at the end of the burnup step are different from those obtained by the predictor, and the corrected nuclide concentrations are obtained by taking a simple average of the predictor and corrector values. The predictor step for the next burnup step requires another transport calculation using the corrected nuclide concentrations. Thus, two transport calculations are required per burnup step.

3.7 Verification of the Lattice Code

Several benchmark problems were analysed with BOXER3 code to verify the various options that are introduced in the code as discussed in the previous sections. These include verification calculations for the MOC part of the code, for the multi-group code for lattice analysis based on both the methods and test the features such as Dancoff factors, burnup calculations etc. The verification results are summarised in the following sections.

3.7.1 Few Group Benchmarks for Verification of MOC

To check the performance of MOC part, benchmark problems [157] consisting of one homogeneous case and four heterogeneous cases were analysed. The cases are (1) k-infinity calculations of homogeneous benchmarks (2) mono-group eigenvalue problem (3) BWR cell (4) LWR fuel element with burnable poison cell and (5) 4 × 4 BWR problem with gadolinium pins.

K - infinity calculations of homogeneous benchmarks

Infinite multiplication factor K-infinity (K_∞) is calculated for the benchmark problems for infinite medium with isotropic scattering. The benchmark provided the cross section of materials (as given in Table 3.1) and reference K-infinity for all problems. 12 directions with

equal weight are considered for integration along azimuthal angle φ. For polar direction θ integration, six-point Gauss-Legendre quadrature set is used. 200 parallel lines are considered for each direction i.e. for each (θ, φ) pair and convergence criterion of 10^{-6} is applied for both neutron flux and K_∞. Since the medium is infinite, the geometry considered is a square of 6 cm × 6 cm size with reflective boundary condition. The K_∞ values calculated by BOXER3 code is summarized in Table 3.2 along with the reference values and is in good agreement.

Table 3.1: Cross sections for homogeneous benchmark problems

Case	G	χ	ν	Σ_a	$\nu\Sigma_f$	Σ_t	Σ_s1-G	Σ_s2-G	Σ_s3-G	Σ_s4-G	Σ_s5-G	Σ_s6-G
Pua-1-N	1	1.0	3.24	0.101184	0.2643840	0.326400	0.225216					
Pub-1-N	1	1.0	2.84	0.101184	0.2317440	0.326400	0.225216					
Ua-1-IN	1	1.0	2.7	0.078336	0.1762560	0.326400	0.248064					
Ub-1-IN	1	1.0	2.7971	0.078336	0.1825948	0.326400	0.248064					
Ud_2o-1-IN	1	1.0	1.7	0.081942	0.0928676	0.546280	0.464338					
Ue-1-IN	1	1.0	2.5	0.079365	0.1730686	0.407407	0.328042					
PU-2-IN	1	0.575	3.1	0.098400	0.2901600	0.220800	0.079200	0.000				
	2	0.425	2.93	0.099840	0.2503392	0.336000	0.043200	0.23616				
U-2-IN	1	0.575	2.7	0.065760	0.1671840	0.216000	0.078240	0.000				
	2	0.425	2.5	0.082560	0.1728000	0.345600	0.072000	0.26304				
UAl-2-IN	1	1.0	0	0.000222	0.000000	0.26817	0.247516	0.000				
	2	0.0	2.83	0.063850	0.171799	1.27698	0.020432	1.21313				
URR-2-IN	1	1.0	2.5	0.002053	0.002621	0.65696	0.625680	0.000				
	2	0.0	2.5	0.076420	0.126580	2.52025	0.029227	2.44383				
URR-3-IN	1	0.96	3.0	0.012000	0.0180000	0.240000	0.024000	0.000	0.0000			
	2	0.04	2.5	0.100000	0.1500000	0.975000	0.171000	0.6	0.0000			
	3	0.0	2	1.100000	1.8000000	3.100000	0.033000	0.275	2.0000			
URR-6-IN	1	0.48	3.0	0.0120	0.0180	0.2400	0.0240	0.0000	0.000	0.00	0.000	0.0000
	2	0.02	2.5	0.1000	0.1500	0.9750	0.1710	0.6000	0.000	0.00	0.000	0.0000
	3	0.0	2	1.1000	1.8000	3.1000	0.0330	0.2750	2.000	0.00	0.000	0.0000
	4	0.0	2	1.1000	1.8000	3.1000	0.0000	0.0000	0.000	2.00	0.275	0.0330
	5	0.02	2.5	0.1000	0.1500	0.9750	0.0000	0.0000	0.000	0.00	0.600	0.1710
	6	0.48	3	0.0120	0.0180	0.2400	0.0000	0.0000	0.000	0.00	0.000	0.0240

Table 3.2: Results of homogeneous benchmark problem

Case	**Reference** K_∞	**BOXER3–MOC** K_∞
Pua-1-0-IN	2.612903	2.612905
Pub-1-0-IN	2.290323	2.290323
Ua-1-0-IN	2.25	2.25
Ub-1-0-IN	2.330917	2.330919
UD2O-1-0-IN	1.133333	1.133331
Ue-1-0-IN	2.180667	2.180668
PU-2-0-IN	2.683767	2.683769
U-2-0-IN	2.216349	2.21635
UAL-2-0-IN	2.661745	2.661769
URR-2-0-IN	1.631452	1.631459
URR-3-0-IN	1.600000	1.600003
URR-6-0-IN	1.600000	1.600004

Mono-group eigenvalue problem

The geometry of one group isotropic scattering problem which consists of two zones; zone M and zone F is a square of side 20 cm as shown in Fig. 3.2. Within the square, six rectangles of 1cm × 18 cm are placed. These rectangles are of material F and the remaining part of the square is filled with material M. Vacuum boundary condition is applied on the outer boundary. Cross-sections of each material are given in Table 3.3.

Table 3.3: Cross sections for mono-group eigenvalue problem

Material	$\boldsymbol{\Sigma_f}$	$\boldsymbol{\nu\Sigma_f}$	$\boldsymbol{\Sigma_t}$	$\boldsymbol{\Sigma_s}$
M	0.0	0.0	1.0	0.93
F	0.1	0.24	1.5	1.35

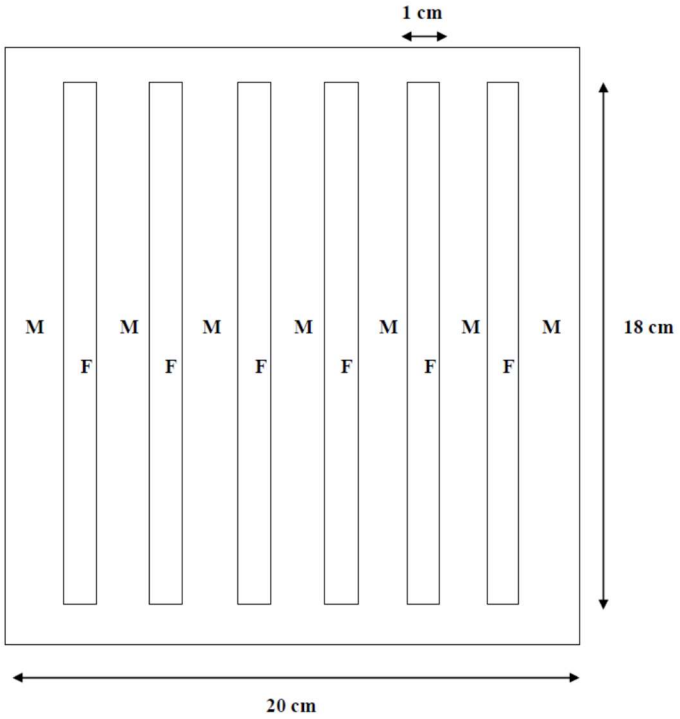

Fig. 3.2: Geometry of mono-group eigenvalue problem

For modeling the geometry in BOXER3, it is divided into rectangular meshes. 24 directions with equal weight are considered for integration along azimuthal angle φ. Six-point Gauss-Legendre quadrature set is used for integration along polar direction. For each direction i.e. for each (θ, φ) pair, 100 parallel lines are considered and convergence criterion of 10^{-6} is applied for both neutron flux and K_{∞}. Comparison of the BOXER3-MOC result with other codes as presented in Table 3.4 shows BOXER3-MOC is as per other codes.

Table 3.4: Comparison of results with other codes

Code	K-effective
P_1	0.776534
SP_3	0.798617
S_{16}	0.806132
TPTRI	0.806123
TEPFEM(P_5)	0.803068
BOXER3- MOC	**0.801470**

BWR cell

The boiling water reactor (BWR) cell is a square with two regions as shown in Fig. 3.3. The outer region dimension is 8.9cm × 8.9cm and the inner square is of 6.4 cm × 6.4 cm.

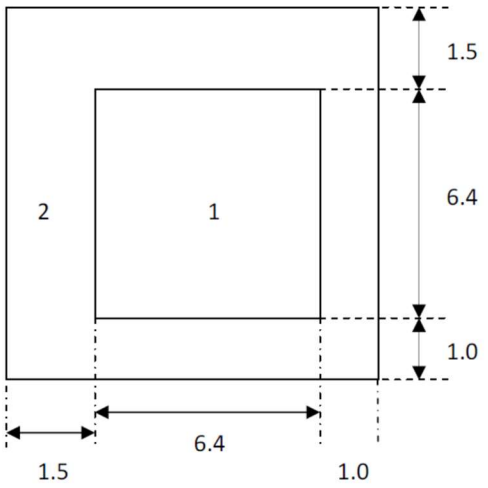

Fig. 3.3. Geometry of BWR cell

The material within the inner square is homogenized fuel and the remaining part of the outer square is light water. Scattering is isotropic and the boundary condition is reflective at all the outer surfaces of the system. Cross sections of both the materials are given in Table 3.5. The fission spectrum is equal to 1.0 in the first group and 0.0 in the second group.

Table 3.5: Two group cross section of BWR cell

Material	**group**	Σ_a	$\nu\Sigma_f$	Σ_t	$\Sigma_{s1\text{-}G}$	$\Sigma_{s\ 2\text{-}G}$
1	1	8.6270E−3	6.2030E−3	1.96647E−1	1.78000E−1	1.08900E−3
	2	6.9570E−2	1.1010E−1	5.96159E−1	1.00200E−2	5.25500E−1
2	1	6.8400E−4	0.0	2.22064E−1	1.99500E−1	1.55800E−3
	2	8.0160E−3	0.0	8.87874E−1	2.18800E−1	8.78300E−1

For integration along azimuthal angle φ, 12 directions with equal weight are considered. Six-point Gauss-Legendre quadrature set is used for polar (θ) direction integration. 200 parallel lines are considered for each direction i.e. for each (θ, φ) pair. The calculated K_∞ value is in

good agreement with the results of SURCU, TEPFEM and TPTRI as can be seen from the Table 3.6.

Table 3.6: Comparison of K-infinity for BWR

Benchmark	K calculated by other codes	K by BOXER3 MOC	K by BOXER3 CP
BWR	1.2127 (SURCU)	1.2127	1.2122
	1.2136 (TEPFEM)		
	1.2128 (TPTRI)		

LWR fuel element with burnable poison cell

This two-energy group problem which contains a poison element, uranium fuel pins and light water, as shown in Fig.3.4. In the inner square there are 16 square cells arranged in 4 by 4 geometry. Out of the 16 cells, 15 are of fuel and one is burnable poison cell. Table 3.7 gives the cross-sections of each material and the fission spectrum is 1.0 and 0.0 in the first and the second energy group respectively. The estimated K-effective is in good agreement with results of other codes as shown in Table 3.8.

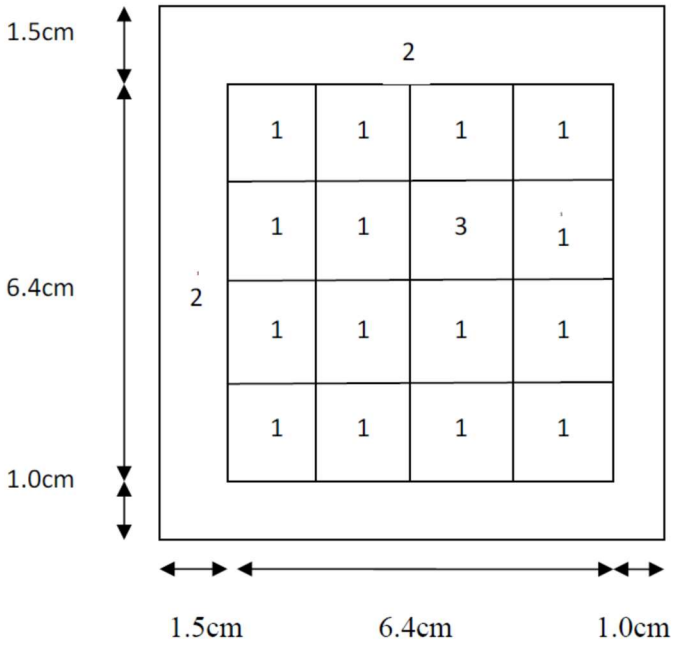

Fig. 3.4. LWR fuel element with burnable poison cell

Table 3.7: Two group cross section of LWR fuel element with burnable poison

Material	group	Σ_a	$\nu\Sigma_f$	Σ_t	$\Sigma_{s1\text{-}G}$	$\Sigma_{s\ 2\text{-}G}$
1	1	9.0E-3	6.2E-3	1.990E-1	1.8E-1	1.0E-3
	2	7.0E-2	1.1E-1	6.010E-1	1.0E-2	5.3E-1
2	1	7.0E-4	0.0	2.227E-1	2.0E-1	2.0E-3
	2	8.0E-3	0.0	8.900E-1	2.2E-2	8.8E-1
3	1	9.0E-3	6.2E-3	1.990E-1	1.8E-1	1.0E-3
	2	3.0	1.1E-1	3.531	1.0E-2	5.3E-1

Table 3.8: Comparison of K-infinity for LWR fuel element with burnable poison

Benchmark	K by other codes	K by BOXER3-MOC	K by BOXER3-CP
LWR problem with burnable poison	0.8805 (SURCU)	0.884846	0.8848
	0.8828 (TPTRI)		

4 × 4 BWR problem with gadolinium pins

The 4 × 4 BWR lattice which contains 14 fuel pins and 2 Gadolinium pins [29] as shown in Fig. 3.5 is modelled in BOXER3. All the pins are cladded with 0.1 cm thick Zircaloy-2. Light water is used as moderator.

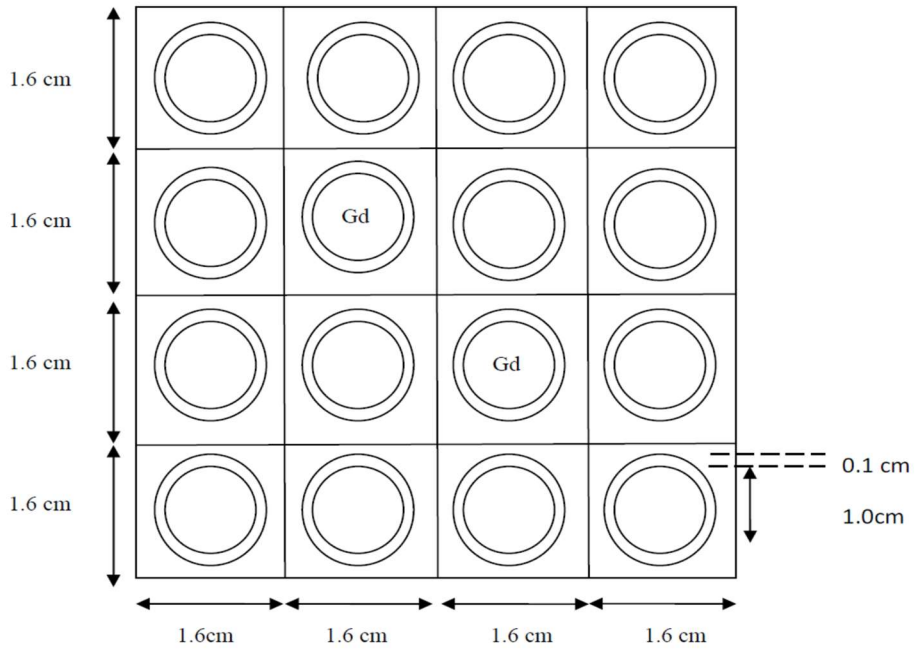

Fig. 3.5: 4×4 BWR problem with gadolinium pins

Cross sections of UO_2, UO_2+Gd_2O_3, Zircaloy-2 and light water are given in Table 3.9. Fission spectrum is 1.0 for the first energy group and 0.0 for the second energy group.

Table 3.9: Cross sections for 4 × 4 BWR problem with gadolinium pins

Material	group	Σ_f	$\nu\Sigma_f$	Σ_t	$\Sigma_{s1\text{-}G}$	$\Sigma_{s\ 2\text{-}G}$
1(Fuel)	1	7.22964E-3	1.86278E-2	3.62022E-1	3.33748E-1	0.0
	2	1.41126E-1	3.44137E-1	5.72155E-1	6.64881E-4	3.80898E-1
2 (Zr)	1	0.0	0.0	2.74144E-1	2.72377E-1	0.0
	2	0.0	0.0	2.80890E-1	1.90838E-4	2.77230E-1
3 (Fuel+Gd)	1	6.97904E-3	1.79336E-2	3.71785E-1	3.38096E-1	0.0
	2	6.47524E-2	1.57929E-1	1.75	6.92807E-4	3.83204E-1
4 (Water)	1	0.0	0.0	6.40711E-1	6.07382E-1	0.0
	2	0.0	0.0	1.69131	3.31316E-2	1.68428

The result of BOXER3 compares well with the results of DRAGON and MOCUM [157] as shown in Table 3.10.

Table 3.10: Comparison of K-infinity for 4 × 4 BWR problem with gadolinium pins

Benchmark	K calculated by other codes	K by BOXER3 MOC	K by BOXER3 CP
4×4 BWR problem with gadolinium pins	0.986561 (DRAGON)	0.9876	0.9872
	0.987785 (MOCUM)		

3.7.2 Verification of BOXER3 as a Lattice Code

To qualify BOXER3 code as a lattice code along with its affiliated neutron cross-section library, verification exercise using benchmark problems of pin-cell and fuel assembly (FA) cell have been performed. The results of some of the cases are presented in the subsequent sections.

Pin cell problems

LWR pin cell [159] with fuel outer radius of 0.40 cm and clad outer radius of 0.45 cm as shown in Fig. 3.6 is considered.

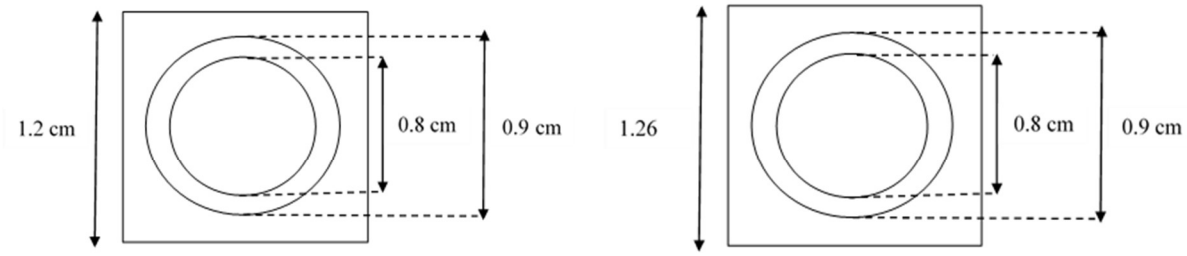

Fig. 3.6: Fuel pin cells of LWR benchmarks

The problem was analysed for both UO_2 fuel as well as $UO_2 – PuO_2$ MOX fuel and for different dimensions of fuel, clad and rod pitch. The benchmark problem details are given in Table 3.11.

Table 3.11: Specifications for Pin Cell Benchmarks

Input	LWR pin cell		VERA
	UO2	MOX	
Pellet radius	0.40 cm	0.40 cm	0.409 cm
Clad inner radius	0.40 cm	0.40 cm	0.418 cm
Clad outer radius	0.45 cm	0.45 cm	0.475 cm
Rod pitch	1.20 cm	1.26 cm	1.26 cm
Pellet material	UO_2	(UO_2+PuO+Am)	UO_2
Clad material	Zr(natural)	Zr(natural)	Zircalloy 4

For UO_2 fuel, K_∞ of the pin cell were estimated for four cases for different temperatures of materials in the cell. In cases 1 and 2, the temperature of various materials is same at 293K, but the water density is different. In cases 3 and 4, water density is same but the fuel temperature is different (550K and 900K). For $UO_2 – PuO_2$ MOX fuel, the K_∞ is estimated for two cases; first at the isothermal temperature of 300K and the second at a higher fuel temperature (560K). In these calculations the fuel pin was sub-divided in 3 regions, the clad in two sub-regions and the moderator in 3 sub-regions. A comparison between the K_∞ obtained

by BOXER3, using collision probability and the MOC, with the reference results for UO_2 and MOX fuels is shown in Tables 3.12 and 3.13 respectively.

Table 3.12: Result for UO_2

Problem	Temperature (K)			Mod. density (g/cc)	K-infinity			Del K	
					BOXER3		reference	K_{CP} - K_{Ref}	K_{MOC} - K_{Ref}
	Mod.	fuel	clad		CP (K_{CP})	MOC (K_{MOC})	K_{Ref}		
CASE1	293	293	293	1.000	1.38711	1.38699	1.38680	0.00031	0.00019
CASE2	293	293	293	0.708	1.33451	1.33505	1.33447	0.00004	0.00058
CASE3	550	900	600	0.708	1.30097	1.30156	1.30221	-0.00124	-0.00065
CASE4	550	550	550	0.708	1.31677	1.31667	1.31660	0.00017	0.00007

Table 3.13: Result for MOX

Problem	Temperature (K)			Mod. Density (g/cc)	K-infinity			Del K	
					BOXER3		reference	K_{CP} - K_{Ref}	K_{MOC} - K_{Ref}
	Mod	fuel	clad		CP (K_{CP})	MOC (K_{MOC})	K_{Ref}		
CASE1	300	300	300	0.709	1.22030	1.21917	1.21971	0.00059	-0.00054
CASE2	300	560	300	0.709	1.20598	1.20476	1.20498	0.00100	-0.00022

The geometrical description of the second set of pin cell problems [160] analysed are given in Table 3.11 (VERA). The fuel enrichment is 3.1%. Calculations were performed at various fuel temperatures (denoted by 1A for 565K, 1B for 600K, 1C for 900K and 1D for 1200K). The fuel and clad radii are 0.41 and 0.475 cm respectively and lattice pitch is 1.26 cm. Comparison between K_∞ obtained using BOXER3 by collision probability and MOC with the reference results (obtained using KENO-VI) are presented in Table 3.14. The good agreement between reference results and the results obtained by BOXER3 is an indication that both the methods implemented in BOXER3 can provide an accurate solution for pin cell problems.

Table 3.14: Calculations for pin cell for VERA Benchmark

Problem	Temperature (K)		Mod. Density (g/cc)	K-infinity			Del K	
				BOXER3		VERA		
	Mod.	Fuel		CP (K_{CP})	MOC (K_{MOC})	K_{VERA}	K_{CP} - K_{VERA}	K_{MOC} - K_{VERA}
1A	565	565	0.743	1.1844	1.1839	1.1833	0.00110	0.00060
1B	600	600	0.661	1.1784	1.1781	1.1785	-0.00010	-0.00040
1C	600	900	0.661	1.1671	1.1689	1.1681	-0.00100	0.00080
1D	600	1200	0.661	1.1571	1.1589	1.1592	-0.00210	-0.00030

Fuel Assembly (FA) calculations: 17×17 PWR Benchmark

For verifying the code capability for FA calculations, another set of problems of the VERA benchmark [160] for 17×17 PWR fuel assemblies is analysed. This 17×17 assembly contains 264 fuel rods, 24 guide tubes and one instrument tube at the center of the lattice as shown in Fig.3.7. For the purpose of the present calculation, all the guide tubes and instrument tubes are considered to be filled with water. This introduces the required inhomogeneity in the lattice for the purpose of verification of the code. $1/8^{th}$ of FA is considered in simulation due to the symmetry in FA.

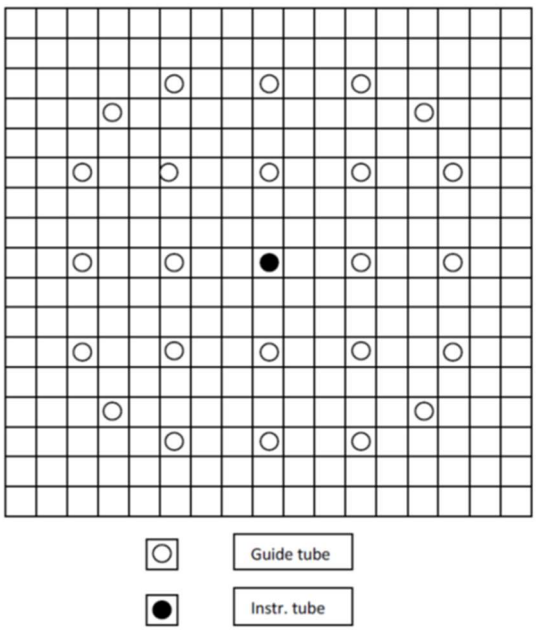

Fig. 3.7: 17×17 PWR fuel assembly

Pin dependent Dancoff factors

For a PWR FA of 17×17, pin dependent [25] Dancoff factors have been obtained using BOXER3 with the formula given in section 3.5. Comparison of Dancoff factors among various pins shows that there are small variations depending upon the number of neighbors and these small variations in the Dancoff factor are in agreement with the reference results as shown in Table 3.15.

Table 3.15: Pin dependent Dancoff factors

0.6945 0.698	0.6657 0.6669	Reference BOXER3						
0.6945 0.6991	0.6657 0.6695	0.6657 0.6640						
---	0.6945 0.6981	0.6945 0.6980	---					
0.6945 0.6952	0.6657 0.6667	0.6658 0.6719	0.6968 0.6984	0.6842 0.6865				
0.6945 0.6942	0.6657 0.6691	0.6657 0.6677	0.6944 0.6953	0.7151 0.7165	---			
----	0.6944 0.6951	0.6947 0.6966	----	0.7130 0.7146	0.6947 0.6974	0.6611 0.6611		
0.6945 0.6955	0.6635 0.6641	0.6636 0.6669	0.6944 0.697	0.6635 0.6666	0.6450 0.6455	0.6451 0.6471	0.6427 0.6482	
0.6428 0.6486	0.6452 0.6492	0.6452 0.647	0.6428 0.645	0.6453 0.6458	0.6428 0.6439	0.6429 0.6469	0.6428 0.645	0.6429 0.6501

K-infinity calculations

For a 17×17 PWR fuel assembly having UO_2 as fuel (3.1 % enrichment) and natural zirconium as cladding at various fuel temperatures (denoted by 2A for 565K, 2B for 600K, 2C for 900K and 2D for 1200K as shown in Table 3.16), calculations are performed. The fuel radii and lattice pitch are the same as for the pin cell problem. 24 discrete directions were used for the φ integration and 100 neutron trajectories (parallel lines) were taken per direction in the cell. Table 3.16 shows a comparison of the K_∞ obtained using BOXER3 by CP as well as MOC with the reference KENO-VI results and are in good agreement with the reference results.

Table 3.16: Results for 17×17 fuel assembly

Problem	Temperature (K)		Mod. Density (g/cc)	K-infinity			Del K	
				BOXER3		VERA	K_{CP} - K_{VERA}	K_{MOC} - K_{VERA}
	Mod.	Fuel		CP (K_{CP})	MOC (K_{MOC})	K_{VERA}		
2A	565	565	0.743	1.1816	1.1821	1.1783	0.00330	0.00380
2B	600	600	0.661	1.1848	1.1851	1.1798	0.00500	0.00530
2C	600	900	0.661	1.1749	1.1752	1.1703	0.00460	0.00490
2D	600	1200	0.661	1.1663	1.1666	1.1621	0.00420	0.00450

3.7.3 Burnup Studies

This study also carried out for both pin-cell and FA levels. The details are presented in the following sections.

Pin- cell benchmarks

For both UO_2 and U-Pu MOX problems the high burnup benchmark cases given in [161,162] were studied. The pin and pellet diameters are 9.52 and 8.24 mm respectively while the pitch is 12.65 mm. Burnup calculations were performed using the predictor corrector option with a burnup step of 5 GWd/Te. A comparison between K_∞ by BOXER3 and a selection of results presented at the benchmark exercise and the average of all the results is shown in figures 3.8a and 3.8b for UO_2 and U-Pu (MOX) pin cells respectively. The selection is based on the assessment of the methodical exactness and the use of similar data sets.

For UO_2 fuel, BOXER3 results agree well with those of other contributors. There is a difference of about 300 pcm between BOXER3 and SHETRAN which increases to 350 pcm at 70 GWd/Te. The average of several benchmarks agrees with BOXER3 result within 200 pcm at zero burnup but the BOXER3 result is about 300 pcm higher at 70 GWd/Te.

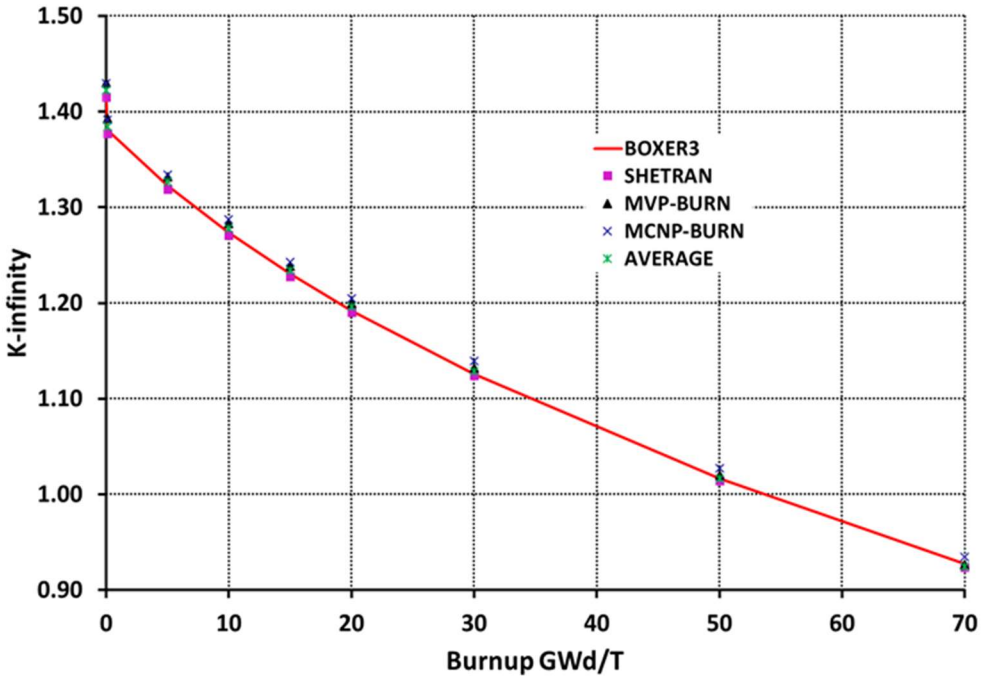

Fig. 3.8a: Comparison of the variation of k infinity with burnup for UO_2 pin cell

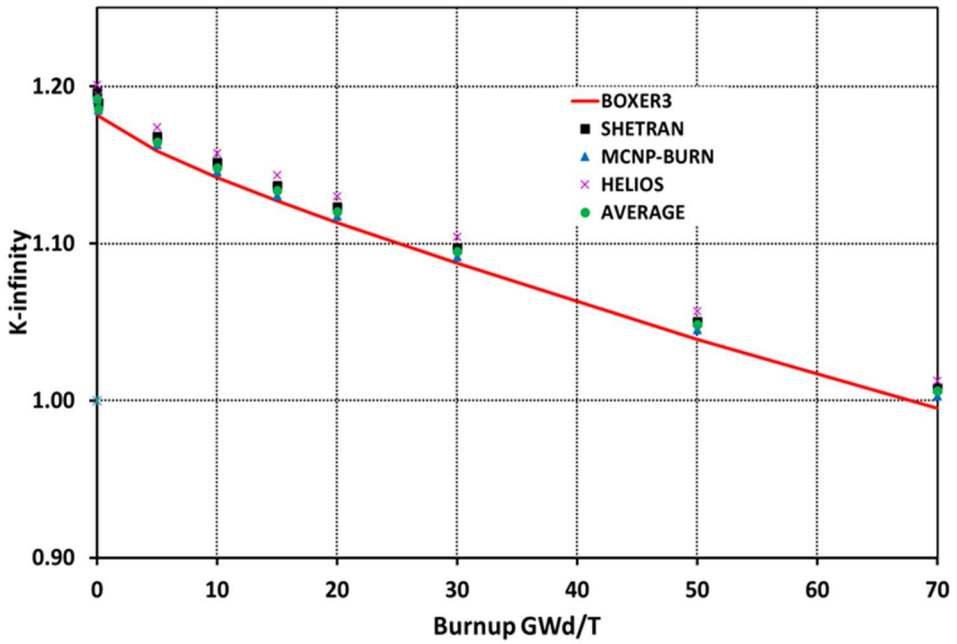

Fig. 3.8b: Comparison of the variation of K-infinity with burnup for U-Pu MOX pin cell

For MOX fuel, the spread in the U-Pu MOX results by various methods is larger than in the UO_2 problem. The BOXER3 results are somewhat lower. There is a difference of about 600 pcm between BOXER3 and SHETRAN at zero burnup which increases to 1300 pcm at 70 GWd/Te. The average of several benchmarks is higher by 300 pcm than the BOXER3 result

at zero burnup and higher by about 1100 pcm at 70 GWd/Te. The BOXER3 results agree better with the Monte Carlo codes but the latter are based on a different library viz. JENDL as against ENDF/B-VI of BOXER3. Considering the difference between various results for the MOX pin cell, the overall agreement between BOXER3 and other results are satisfactory for both fuels.

PWR Fuel Assembly Benchmarks

For this study, the FA considered is same as given in Fig.3.7 and two types of fuels as given in the benchmark [159] are considered: (1) enriched uranium fuel having 6.2 % U^{235} with several pins mixed with Gd burnable absorber (2) the MOX assembly with three types of fuel pins bearing different loadings of Pu in each. The geometric details of the pin cell are the same as described for the pin-cell problem. The two types of fuel assemblies as illustrated in Fig.3. 9 are modelled.

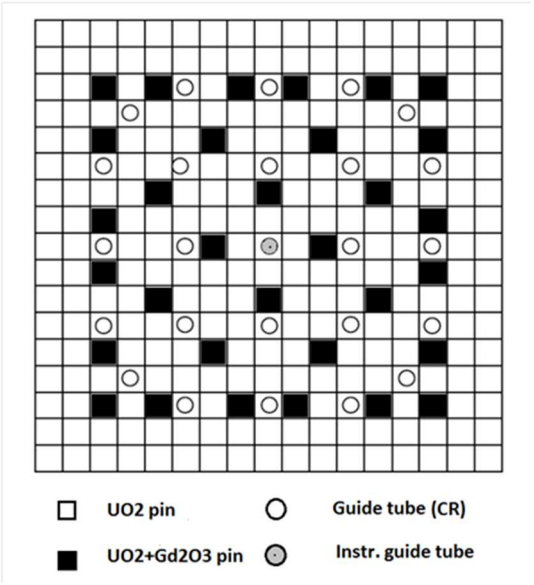

Fig. 3.9a: Fuel assemblies for the PWR (UO_2) burnup benchmarks

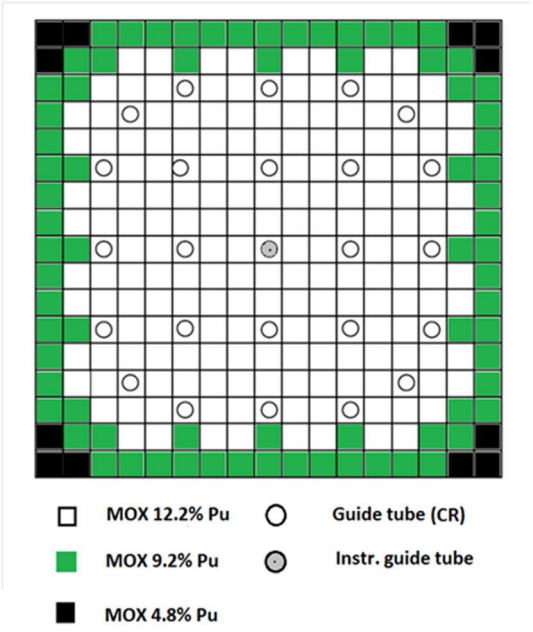

Fig. 3.9b: Fuel assemblies for the PWR (MOX) burnup benchmarks

The high Gd concentration in the uranium assembly, makes the problem particularly challenging. The problem was simulated by using different burnup zones and materials in each

of the four annular division of a Gd containing fuel pin. While all other benchmarks could be simulated using the predictor corrector method with relatively coarse burnup steps of 5 GWd/Te, in this problem, burnup step of 1 GWd/Te in the first 15 GWd/Te and 2.5 GWd/Te in the remaining steps is used. The results are given in Fig.3.10a. BOXER3 results agree much better with both the SHETRAN at the beginning and average results (difference being about 100 pcm). The agreement is by and large satisfactory with SHETRAN and average values (the maximum difference being about 800 pcm near the Gd peak), throughout the burnup period. Problems involving fuel containing burnable Gd absorbers are particularly difficult to treat and require small time steps. This is reflected in the results by various methods. Improvements over the predictor corrector method, such as the projected predictor corrector method [92] and the dual time step method [163] may be useful in mitigating this problem.

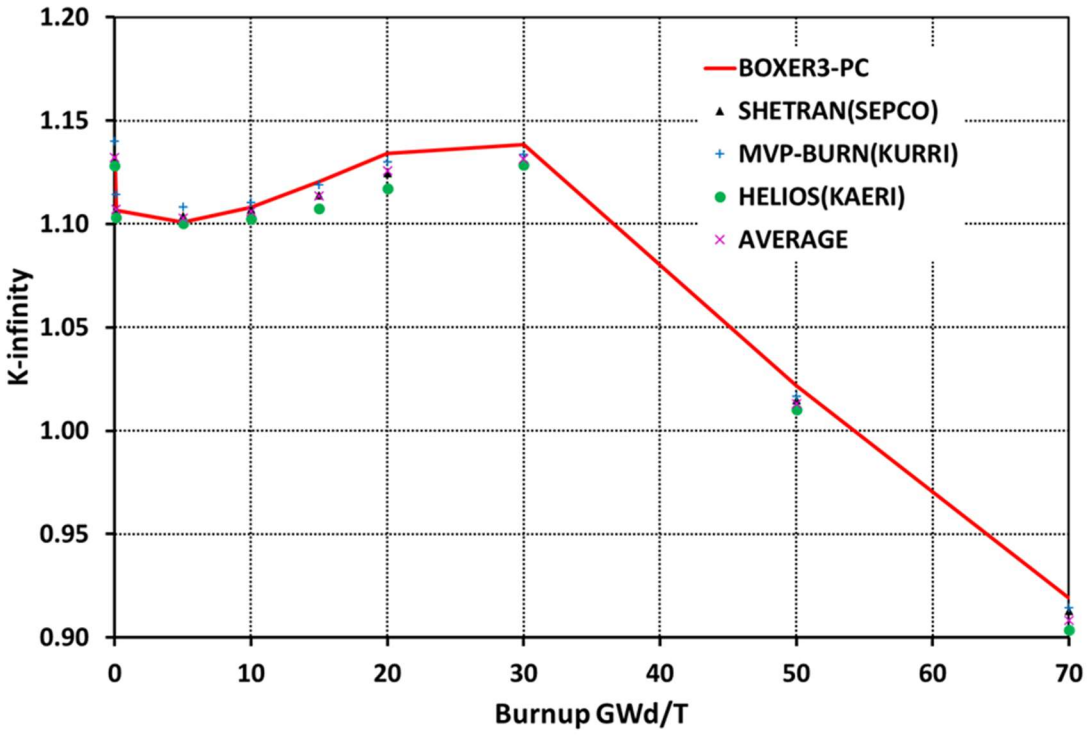

Fig. 3.10a: Comparison of variation of K-infinity with burnup for PWR UO_2 FA with Gd

Fig. 3.10b shows comparisons for the MOX fuel assembly. The MOX assembly burnup results are similar to those of the pin cell burnup, with BOXER3 values being somewhat lower

(400 pcm than the SHETRAN values) in the beginning with the difference increasing to about 650 pcm at 70 GWd/Te. The comparison with the average values is much better, with maximum difference being about 300 pcm. The deviation between BOXER3 results and SHETRAN values is typically lower than that amongst various codes used in the benchmark exercise.

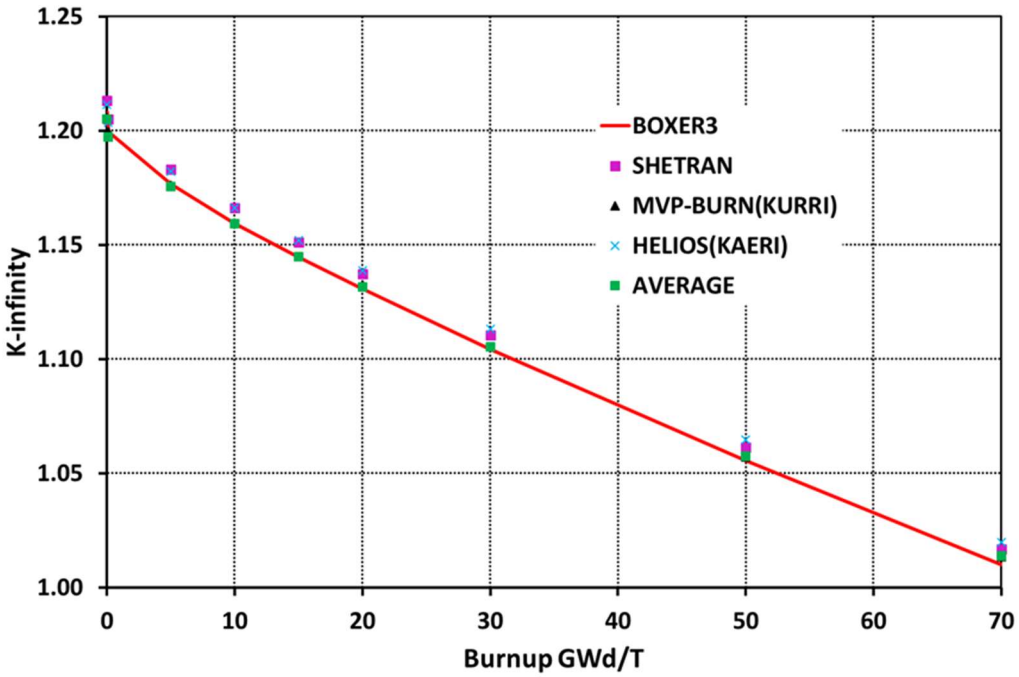

Fig. 3.10b: Comparison of variation of K-infinity with burnup for PWR U-Pu MOX FA

3.8 Summary and Scope for Future Study

The lattice code BOXER3 with various features like solution method by CP and MOC, anisotropic scattering treatment, coupling to multi-group neutron cross section library etc., is usable for square lattices typical of BWR and PWR fuel assemblies. Three methods available for solving the transport equation viz., the exact collision probability method, the mixed collision probability and interface currents method, and the method of characteristics gives the flexibility to choose based on the problem. The treatment of energy variable is through the 69 or 172 group WIMS library together with its equivalence principle based resonance treatment.

The verification study of the code against a number of benchmarks involving UO_2 and U-Pu MOX fuels including burnup with and without Gd pins show generally good agreement with various benchmarks and other codes used for comparison. Thus, the code can be used for (assembly level) LWR lattice calculations including burnup. For UO_2 assemblies, the spread in the benchmarks results by different codes is small. The agreement between BOXER3 results and the benchmark values can be seen to be particularly good for these cases. For U-Pu MOX fuels and assemblies having Gd in some of the pins there is greater spread in the benchmark results analysed by different codes.

Burnup calculations for pin cells and 17×17 PWR assemblies with enriched uranium (UO_2) fuel having Gd bearing pins are particularly difficult requiring very short time steps and it is proposed to incorporate better methods such as the projected predictor corrector (PPC) for these problems. While PPC could be beneficially employed for other burnable isotopes, its need is felt mostly for Gd burnable absorber due to the rather high cross sections of its isotopes (particularly Gd^{155} and Gd^{157}).

CHAPTER 4

NEW HOMOGENISED AXIAL DIFFUSION COEFFICIENTS

4.1 Introduction

As discussed in the previous chapters, the lattice calculation provides a detailed spatial and spectral neutron flux distribution within the representative region called the lattice cell. The flux distribution is used to generate the homogenized few group macroscopic cross sections and diffusion coefficient which forms the main input for the next-step of core calculation. In the traditional procedure that is widely used for this purpose [18, 95], the homogenized cross sections are obtained by a flux volume weighting. This is followed by a P1 / B1 calculation for obtaining the leakage corrected spectrum and the few group reaction cross sections and diffusion coefficients. In addition to this, there is a large body of literature (which was reviewed in Chapter 2) discussing various methods for carrying out this homogenization, so that important features such as reaction rates, surface currents or cell leakage rates are preserved. In these methods, while the few group reaction cross sections are usually obtained by the flux volume weighted homogenization, either the diffusion coefficient is obtained by some other prescription, or flux discontinuity factors are introduced at the surfaces of the lattice cells.

In the axial direction, no axial homogenisation is necessary as the material discontinuities are few and far between and consequently there are no flux discontinuity factors in this direction. However, it is still necessary to have the best value of the axial diffusion coefficient (upon transverse homogenisation) that would correctly predict leakages in the axial direction. Benoist's work [97] in this direction addresses the problem of obtaining the diffusion coefficient for a simple lattice cell and forms the basis of obtaining the axial homogenised diffusion coefficient in various lattice codes such as WIMS [14]. Due to the more complicated structure of modern LWRs, a more general approach is necessary.

The previous chapter discussed the development of the lattice code that provides the detailed space energy flux distribution within a lattice cell. This chapter addresses some aspects of the homogenisation problem. A new method is developed to obtain the axial diffusion coefficient. The chapter gives a description of the method, its implementation in the lattice code BOXER3 and the verification studies carried out.

Poveschenko and Laletin [110,111] have carried out similar work for obtaining axial diffusion coefficients. However, their approach and notation are rather complicated and the final expressions for the collision probability like integrals involve transformed coordinates rather than the physical path lengths in various regions along a neutron track. Moreover, their results are limited to the case of isotropic scattering and infinite medium spectrum.

The derivation of the formula for homogenised axial diffusion coefficients (for isotropic and anisotropic scattering) described in the following section uses the simple text book approach [164] used for deriving Fick's law. The formulae express the diffusion coefficients in terms of the flux distribution available from a two-dimensional lattice calculation and collision probability like integrals. The treatment is extended to the case involving anisotropic scattering. This does not require anisotropic scattering treatment at the level of the lattice calculation for this purpose and hence can be implemented in collision probability based lattice codes. The leakage correction in the flux distribution (spatial and spectrum) through the use of leakage corrected collision probabilities is also obtained. Numerical calculations for typical lattice cells show that the proposed diffusion coefficient is significantly different from the usual one based on the P1 method. Comparisons with Monte Carlo calculations also suggest that the use of the new diffusion coefficient results in better prediction of axial leakage in core calculations.

The outline of the chapter is as follows: The derivation of the formulae for the axial diffusion coefficients [165] for an infinite lattice is given in section 4.2. The method is extended to anisotropic scattering case also and the details are discussed in section 4.3. Effect of leakage

from a finite lattice and derivation of leakage corrected collision probabilities for obtaining the leakage corrected flux distribution, homogenized cross sections and axial diffusion coefficient [166] are presented in section 4.4. The verification of the proposed method and the results of diffusion theory calculations using homogenized diffusion coefficients obtained by the method is given in section 4.5. A summary is given in section 4.6.

4.2 Homogenised Axial Diffusion Coefficient for an Infinite Lattice

The properties of the medium are almost uniform and change only slowly along the axial (z) direction within any pin-cell. Rapid changes of flux and abrupt changes in material properties are few and far between and consequently there is no homogenisation along this direction. To obtain the homogenised diffusion coefficient, we must have the average current and flux gradient in the z direction. Most lattice codes perform two-dimensional calculations at the lattice level and not three-dimensional calculations that would be required for obtaining the currents and flux gradients in the z direction. Due to the near homogeneity of the medium in this direction over long distances, a method similar to that discussed in elementary reactor physics text books [164] for obtaining Fick's law in an infinite homogeneous medium is used to estimate the z-component of the currents from the two-dimensional calculations.

4.2.1 Contribution to Current from Volume Sources

Consider an infinite medium in which nuclear properties do not vary in the z direction. To find the z-component of the few group neutron current at a point in the z = 0 plane which is at the origin in the system of coordinates as shown in Fig. 4.1, consider a small volume element dV at the point (ρ, z, φ) that is at a distance r from the origin and is the source of scattered neutrons. The number of these neutrons that pass through the small area element dA located at the origin and is perpendicular to the z axis is to be estimated. The line joining the elements dV and dA makes an angle θ with the z axis.

The relations between the various coordinates are:

$$r = \frac{\rho}{\sin\theta} \tag{4.1a}$$

$$x = \rho\cos\varphi \tag{4.1b}$$

$$y = \rho\sin\varphi \tag{4.1c}$$

$$z = \rho\cot\theta \tag{4.1d}$$

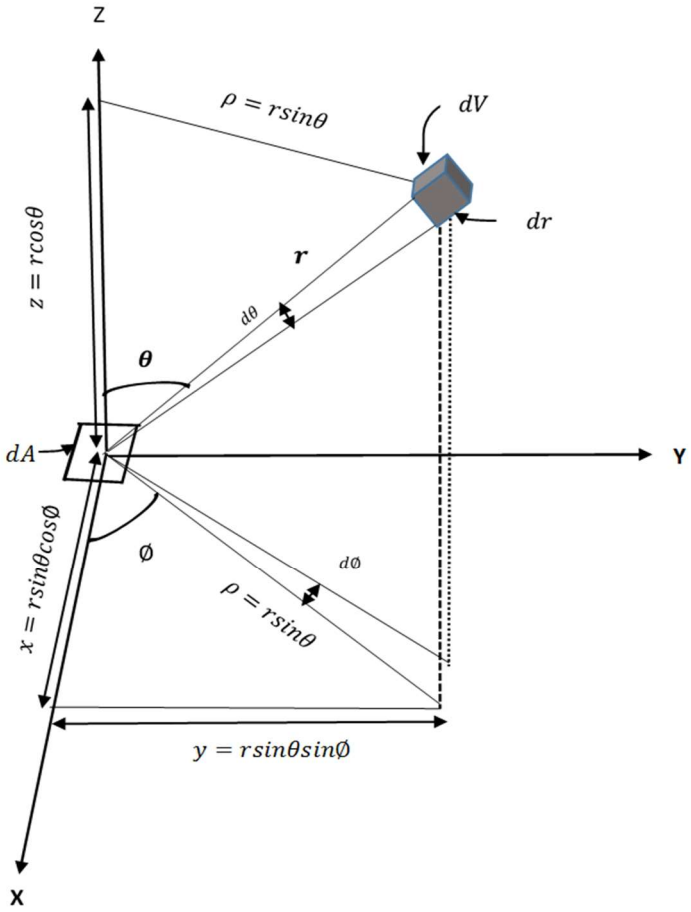

Fig. 4.1: Coordinate system for calculation of the z component of the current

The volume element can be written as:

$$dV = r^2\sin\theta\, dr\, d\theta\, d\varphi = \rho^2\mathrm{cosec}^2\theta\, d\rho\, d\varphi\, d\theta \tag{4.2}$$

while the solid angle subtended by dA at the volume element dV is given by

$$\frac{dA\ cos\theta}{\mathrm{r}^2} = \frac{dA\ \cos\theta\ \sin^2\theta}{\rho^2} \tag{4.3}$$

The required partial current is obtained by multiplying the source density with the volume element, the solid angle subtended by *dA* at *dV*, and the exponential attenuation factor, dividing by 4π and integrating over the volume above the z = 0 plane. The source density is assumed to be factorizable into a function of z and a function of x, y and the energy group.

$$\begin{aligned} J_G{}^- dA &= \sum_{g\in G} \frac{dA}{4\pi} \int_0^{\infty} d\rho \int_0^{2\pi} d\varphi \int_0^{\pi/2} S_g(x,y) f(z)\, exp\left(-\tau_g/sin\theta\right) cos\theta\ d\theta \\ &\approx \sum_{g\in G} \frac{dA}{4\pi} \int_0^{\infty} d\rho \int_0^{2\pi} d\varphi \int_0^{\pi/2} S_g(x,y)\{f(0) + z f_z(0)\}\, exp\left(-\tau_g/sin\theta\right) cos\theta\ d\theta \\ &= \sum_{g\in G} \frac{dA}{4\pi} \int_0^{\infty} d\rho \int_0^{2\pi} d\varphi \int_0^{\pi/2} S_g(x,y)\{f(0) + \rho\ \cot\theta f_z(0)\}\, exp\left(-\tau_g/sin\theta\right) cos\theta\ d\theta \end{aligned} \tag{4.4}$$

τ_g is the projection of the optical path length between the area and volume elements in a plane perpendicular to the z- axis. A similar procedure gives the following expression for $J_G{}^+$

$$\begin{aligned} &J_G{}^+ dA = \\ &-\sum_{g\in G} \frac{dA}{4\pi} \int_0^{\infty} d\rho \int_0^{2\pi} d\varphi \int_{\frac{\pi}{2}}^{\pi} S_g(x,y)\{f(0) + \rho\ \cot\theta f_z(0)\} \exp\left(-\tau_g/sin\theta\right) cos\theta\ d\theta \end{aligned} \tag{4.5}$$

The negative sign arises because the direction of the unit normal to the area element is opposite to the unit normal while calculating $J_G{}^-$. On taking the difference $J_G = J_G{}^+ - J_G{}^-$, the first term in the two expressions are identical and therefore cancels out, while the last term gives

$$\begin{aligned} J_G dA &= -\sum_{g\in G} \frac{f_z(0)}{2\pi} dA \int_0^{\infty} \rho\ d\rho \int_0^{2\pi} d\varphi\ S_g(x,y) \int_0^{\frac{\pi}{2}} \cot\theta \exp\left(-\tau_g/sin\theta\right) cos\theta\ d\theta \\ &= -\sum_{g\in G} \frac{f_z(0)}{2\pi} dA \int_0^{\infty} \rho\ d\rho \int_0^{2\pi} d\varphi\ S_g(x,y)\left[Ki_0(\tau_g) - Ki_2(\tau_g)\right] \end{aligned} \tag{4.6}$$

where the integral over θ has been written in terms of the Bickley functions. Thus, the net current is proportional to the derivative of the source density with respect to z. The above expression gives the net number of neutrons crossing an area dA, whereas what is required is the average current through the pin cell surface perpendicular to the z direction. The average current through an area of a pin cell K is therefore given by integrating over the source and destination coordinates and dividing out by the area of the pin cell A_{pcK}.

$$\bar{J}_{GK} = -\frac{f_z(0)}{2\pi A_{pcK}} \sum_{g\in G} \int_{A_{pcK}} dA \int_0^{\infty} \rho \, d\rho \int_0^{2\pi} d\varphi \, S_g(x,y)\left[Ki_0(\tau_g) - Ki_2(\tau_g)\right] \qquad (4.7)$$

The integrals represent integrations over the area of a cross section of the lattice cell (fuel assembly in this case) and over the area of cross section of a pin cell and can be calculated by the same ray tracking technique used for obtaining the collision probabilities. The ray tracking can be used to calculate both the area integrals together. Since in practice the source is available as a piecewise constant set of functions, and so are the cross sections used in calculating optical path lengths in the region of interest, one should write the above expression as a sum of integrals over each pair (source point and destination point) of meshes.

This is done by integrating over the portions of each ray lying in a source mesh and within the area of the destination mesh of the pin cell, as is done for obtaining expressions for collision probabilities. A direction of emission of the source neutron (represented by an angle φ relative to the x axis of a fixed coordinate system in the X-Y plane) is chosen. For this direction, the integration over the source point area is carried out as for collision probability calculations by introducing a coordinate system (rotated by an angle φ relative to the fixed frame) and by integrating over the rotated cartesian coordinates (x_1, y_1). For integration over the destination points, starting from any source point (Fig. 4.2), imagine a ray drawn parallel to the rotated x axis and two lines around it forming an angle $d\varphi$ between them.

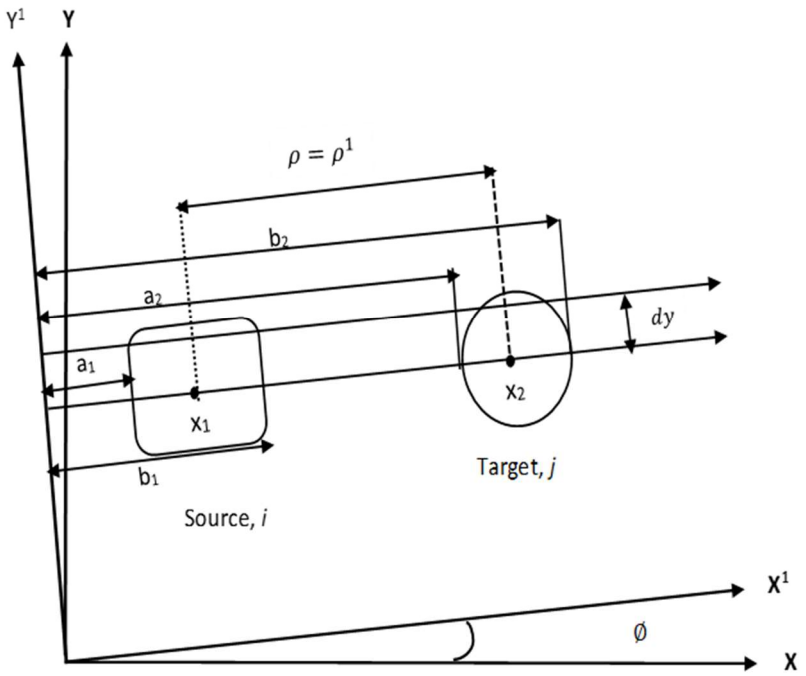

Fig. 4.2: Coordinate system for carrying out the double area integrations. The integration variables x_1 x_2 and y are the Cartesian coordinates of the source (x_1, y) and target (x_2, y) points in the rotated system, while the integration variable φ is the angle of rotation relative to the fixed system.

With reference to Fig. 4.2, the polar coordinates of the destination point, with the emission point as origin and angle φ relative to the fixed frame are:

$(\rho', \varphi) = (x_2 - x_1, \varphi)$, where x_2 is the x-coordinate of the destination point in the rotated frame. Hence, the area element at the destination point can be written as:

$$\rho' d\varphi = (x_2 - x_1) d\varphi \tag{4.8}$$

The equation for the current then becomes:

$$\begin{aligned} \bar{J}_{GK} = -\sum_{i,j\in K, g\in G} \frac{S_{ig} f_z(0)}{2\pi A_{pcK}} \int_0^{2\pi} d\varphi \int dy_1 \int_{a_1}^{b_1} dx_1 \int_{a_2}^{b_2} dx_2 (x_2 \\ - x_1) \left[Ki_0 \left(\tau_{ijg} + \Sigma_{gi}(b_1 - x_1) + \Sigma_{gj}(x_2 - a_2) \right) \right. \\ \left. - Ki_2 \left(\tau_{ijg} + \Sigma_{gi}(b_1 - x_1) + \Sigma_{gj}(x_2 - a_2) \right) \right] \end{aligned} \tag{4.9}$$

where (a_1, b_1) and (a_2, b_2) are the x coordinates of the intersection points of the ray with the source and destination meshes respectively. Now proceed to carry out the integrations over the variables x_2, x_1. Two cases arise viz. when these variables fall in the same mesh ***($i = j$)*** and when they do not ***($i \neq j$).***

4.2.1.1 Contribution to Current from Volume Sources ($i \neq j$)

Direct integration of the above expression over the variables is possible but gives the final expression in terms of (a_1, b_1) and (a_2, b_2) (the x co-ordinates of the intersection points of the ray with the source and destination meshes respectively), as in [110] rather than the physical quantities such as the path lengths in the regions *i* and *j* or the distance between them along the chord. To obtain the results directly in terms of physical quantities rather than coordinates, the integration over the variables x_2, x_1 is carried out by making the substitutions as:

$$\xi_1 = b_1 - x_1 \tag{4.10a}$$

$$\xi_2 = x_2 - a_2 \tag{4.10b}$$

$$x_2 - x_1 = \xi_1 + \xi_2 + a_2 - b_1 \tag{4.10c}$$

These integrals then become

$$I = \int_0^{p_1} d\xi_1 \int_0^{p_2} d\xi_2 (p_{12} + \xi_1 + \xi_2)\left[Ki_0\left(\tau_{ijg} + \Sigma_{gi}\xi_1 + \Sigma_{gj}\xi_2\right) - Ki_2\left(\tau_{ijg} + \Sigma_{gi}\xi_1 + \Sigma_{gj}\xi_2\right)\right] \tag{4.11}$$

where the symbols p_1 and p_2 are for the path lengths through the regions *i* and *j* and p_{12} for the path length in between the regions *i* and *j.* The integration is easily carried out by noting that the integral of a Bickley function is the next higher order Bickley function. On writing $Ki'_n = Ki_n - Ki_{n+2}$ as in [110], the integral becomes

$$
\begin{aligned}
I_{ij} = \frac{p_{12}}{\Sigma_{gi}\Sigma_{gj}}\left[Ki'_2(\tau_{gij}) - Ki'_2(\tau_{gij}+\tau_{gi}) - Ki'_2(\tau_{gij}+\tau_{gj}) + Ki'_2(\tau_{gij}+\tau_{gj}+\tau_{gi})\right] \\
+\left(\frac{1}{\Sigma_{gi}\Sigma_{gj}^2}+\frac{1}{\Sigma_{gj}\Sigma_{gi}^2}\right)\left[Ki'_3(\tau_{gij}) - Ki'_3(\tau_{gij}+\tau_{gi}) - Ki'_3(\tau_{gij}+\tau_{gj})\right. \\
\left. + Ki'_3(\tau_{gij}+\tau_{gj}+\tau_{gi})\right] \\
-\frac{p_2}{\Sigma_{gi}\Sigma_{gj}}\left\{Ki'_2(\tau_{gij}+\tau_{gj}) - Ki'_2(\tau_{gij}+\tau_{gj}+\tau_{gi})\right\} \\
-\frac{p_1}{\Sigma_{gi}\Sigma_{gj}}\left\{Ki'_2(\tau_{gij}+\tau_{gi}) - Ki'_2(\tau_{gij}+\tau_{gj}+\tau_{gi})\right\}
\end{aligned}
\tag{4.12}
$$

4.2.1.2 Contribution to Current from Volume Sources ($i = j$)

For the special case when $i = j$, the integral I_{ii} is somewhat different. On writing

$Ki'_n = Ki_n - Ki_{n+2}$, the integral can be written as

$$
\begin{aligned}
I_{ii} &= \int_{a_1}^{b_1} dx_1 \int_{x_1}^{b_1} dx_2 (x_2 - x_1) Ki'_0\left(\Sigma_{gi}(x_2 - x_1)\right) \\
&= \int_0^{p_1} x(p_1 - x) Ki'_0(\Sigma_{gi}x) = \frac{1}{\Sigma_{gi}}\int_0^{p_1} (p_1 - 2x) Ki'_1(\Sigma_{gi}x) \\
&= \frac{p_1}{\Sigma^2{}_{gi}}\left(\frac{1}{3} + Ki'_2(\tau_{gi})\right) - \frac{2}{\Sigma^3{}_{gi}}\left(\frac{\pi}{16} - Ki'_3(\tau_{gi})\right)
\end{aligned}
\tag{4.13}
$$

The following expression for the average current through the area of a pin cell is obtained.

$$
\bar{J}_{GK} = -\frac{f_z(0)}{A_{pcK}} \sum_{i,j \in Kg \in G} S_{ig}\, T_{ijg} \tag{4.14}
$$

where the quantity T_{ijg} is defined as

$$
T_{ijg} = \frac{1}{2\pi}\int_0^{2\pi} d\varphi \int dy\, I \tag{4.15}
$$

τ_{gi}, τ_{gj} and τ_{gij} are the optical path lengths of the intercepts of the integration rays in the mesh *i, j* (belonging to pin cell *K*) and the portion in between mesh *i* and mesh *j* (belonging to pin

cell *K*). The integration over y and φ has the usual interpretation as in collision probability calculations by the ray tracing method. The source can be written as:

$$S_{ig} = \sum_{h} \left(\Sigma_{h \to g} + \frac{\chi_g \nu \Sigma_{fh}}{k} \right) \phi_{ih} \tag{4.16}$$

The average flux in group G in a pin cell K can be written as:

$$\bar{\phi}_{GK} = \sum_{g \in G} \frac{1}{A_{pcK}} \int_{A_{pcK}} \phi_g(x,y) f(z) = \frac{1}{A_{pcK}} \sum_{i,g \in G} \phi_{ig} A_i f(z) \tag{4.17}$$

and its derivative w. r. to z at z = 0 is:

$$\frac{\partial \bar{\phi}_{GK}}{\partial z} = \frac{1}{A_{pcK}} \sum_{i,g \in G} \phi_{ig} A_i f_z(0) \tag{4.18}$$

The diffusion coefficient in the z direction is obtained as the ratio of the current to the derivative of the flux

$$D_{GK} = -\frac{\bar{J}_{GK}}{\frac{\partial \bar{\phi}_{GK}}{\partial z}} = \left(\sum_{i,g \in G} S_{ig} \, T_{ijg} \right) \left(\sum_{i,g \in G} \phi_{ig} A_i \right)^{-1} \tag{4.19}$$

4.2.2 Contribution to Current from Surface (in-currents) Source

In situations where combination of interface currents coupling at the surfaces of pin cells and collision probabilities coupling of various meshes within a pin cell, integration over the area variables φ and y is limited to the area within the pin cell and the remaining portion must be replaced by integration over the surfaces with the calculated interface currents. The contribution to current from the surface source is proportional to the current multiplied by the surface area and cosine of the angle the surface normal makes with the direction in which the contribution is sought. Consequently, an additional factor of $\sin\theta$ appears in the numerator of Eq. (4.6). Therefore, the Bickley functions appearing in Eq. (4.6) are one order higher.

Secondly since instead of a volume source there is a surface source, the integration over x_1 or ξ_1 is absent in Eq. (4.9). Taking these factors into account the contribution from the x-y surface currents to the average z current $\bar{J}_{GK}$ can be written as,

$$-\sum_{j\in K, g\in G} \frac{J^{in}_{xyg} f_z(0)}{2\pi A_{pcK}} \int_0^{2\pi} d\varphi \int dy_1 \, I_{Sj} \tag{4.20}$$

$$\begin{aligned} I_{Sj} &= \int_{a_2}^{b_2} dx_2 \, x_2 \left[Ki_1\left(\tau_{Sjg} + \Sigma_{gj}(x_2 - a_2)\right) - Ki_3\left(\tau_{Sjg} + \Sigma_{gj}(x_2 - a_2)\right)\right] \\ &= \int_0^{p_2} d\xi_2 \, (p_{S2} + \xi_2) Ki'_1\left(\tau_{Sjg} + \Sigma_{gj}\xi_2\right) \\ &= \frac{p_{S2}}{\Sigma_{gj}}\left[Ki'_2\left(\tau_{Sjg}\right) - Ki'_2\left(\tau_{Sjg} + \tau_{jg}\right)\right] - \frac{p_2}{\Sigma_{gj}} Ki'_2\left(\tau_{Sjg} + \tau_{jg}\right) \\ &\quad + \frac{1}{\Sigma^2_{gj}}\left[\left\{Ki'_3\left(\tau_{Sjg}\right) - Ki'_3\left(\tau_{Sjg} + \tau_{jg}\right)\right\}\right] \end{aligned} \tag{4.21}$$

p_{s2} is the path length between the surface and destination *j*.

4.3 The Case of Anisotropic Scattering

Most lattice codes based on integral transport theory make the assumption that source is isotropic by replacing the total cross section by the transport corrected cross section that is available in all libraries. However, if the anisotropic scattering cross sections (usually limited to linear anisotropy) are available in the library (for example, the WIMS library has linearly anisotropic cross sections for the light elements H, D, C and O) and MOC based codes have the anisotropic option, it should be possible to obtain the diffusion coefficient in such cases as well. This section describes the method to obtain the diffusion coefficient in the case of anisotropic scattering.

In the case of linearly anisotropic scattering the expression for the source [7] is written as:

$$S_g(x,y,\omega,\chi)f(z)$$

$$= \frac{f(z)}{4\pi}\sum_h \left[\left(\frac{\chi_g \nu\Sigma_{fh}}{k} + \Sigma_{0h\to g}\right)\phi_h \right.$$

$$\left. + 3\Sigma_{1h\to g}\left(\sin\omega\cos\chi\, J_{xh} + \sin\omega\sin\chi\, J_{yh} + \cos\omega\, J_{zh}\right)\right] \tag{4.22}$$

where the angles ω and χ are related to θ and φ by $\omega = \pi - \theta$ and $\chi = \pi + \varphi$.

4.3.1 One - group Infinite Homogeneous Medium

To test the method on a simple problem by checking if it gives the correct known result, a one group infinite homogeneous medium case having Σ, Σ_0 and Σ_1 as the total cross section and the isotropic and linearly anisotropic components of the scattering cross section is considered. The scattering source in this case can be written as in Eq. (4.22) using the relations for the angles ω and χ

$$S(x,y,z,\theta,\varphi) = \frac{1}{4\pi}\left[\,\Sigma_0\phi - 3\Sigma_1(\sin\theta\cos\varphi\, J_X + \sin\theta\sin\varphi\, J_Y + \cos\theta\, J_Z)\right]$$

Following the same procedure as in the isotropic scattering case, this form of the source gives the following expression for the partial current

$$J_G^{-} = \frac{1}{4\pi}\int_0^{\infty} dr \int_0^{2\pi} d\varphi \int_0^{\frac{\pi}{2}} d\theta\, \left[\,\Sigma_0\phi - 3\Sigma_1(\sin\theta\cos\varphi\, J_X + \sin\theta\sin\varphi\, J_Y + \cos\theta\, J_Z)\right] \tag{4.23}$$

$$\exp(-\Sigma r)\cos\theta\sin\theta$$

ϕ, J_X, J_Y, and J_Z are functions of (x,y,z). On carrying out an expansion up to terms linear in these variables and writing in terms of the polar variables (r,θ,φ) results

$$
\begin{aligned}
J^- = \quad & \frac{1}{4\pi}\int_0^{\infty} dr \int_0^{2\pi} d\varphi \int_0^{\pi/2} d\theta \left[\Sigma_0 \left(\phi(0) + r\,\sin\theta\,\cos\varphi\,\phi_x(0) + r\,\sin\theta\,\sin\varphi\,\phi_y(0) + r\cos\theta\,\phi_z(0)\right)\right. \\
& -3\Sigma_1\,\sin\theta\cos\varphi\left(J_X(0) + r\sin\theta\cos\varphi\,J_{Xx}(0) + r\sin\theta\sin\varphi\,J_{Xy}(0) + r\cos\theta\,J_{Xz}(0)\right) \\
& -3\Sigma_1\,\sin\theta\sin\varphi\,\left(J_Y(0) + r\sin\theta\cos\varphi\,J_{Yx}(0) + r\sin\theta\sin\varphi\,J_{Yy}(0) + r\cos\theta\,J_{Yz}(0)\right) \\
& \left.-3\Sigma_1\,\cos\theta\,\left(J_Z(0) + r\sin\theta\cos\varphi\,J_{Zx}(0) + r\sin\theta\sin\varphi\,J_{Zy}(0) + r\cos\theta\,J_{Zz}(0)\right)\right]\exp(-\Sigma r)\,\cos\theta\sin\theta
\end{aligned}
\tag{4.24}
$$

where, the lower-case subscripts denote differentiation while the upper-case subscripts denote component of the current. The corresponding expression for J^+ is

$$
\begin{aligned}
J^+ = \quad & \frac{1}{4\pi}\int_0^{\infty} dr \int_0^{2\pi} d\varphi \int_0^{\pi/2} d\theta \left[\Sigma_0 \left(\phi(0) + r\,\sin\theta\,\cos\varphi\,\phi_x(0) + r\,\sin\theta\,\sin\varphi\,\phi_y(0) - r\cos\theta\,\phi_z(0)\right)\right. \\
& -3\Sigma_1\,\sin\theta\cos\varphi\left(J_X(0) + r\sin\theta\cos\varphi\,J_{Xx}(0) + r\sin\theta\sin\varphi\,J_{Xy}(0) - r\cos\theta\,J_{Xz}(0)\right) \\
& -3\Sigma_1\,\sin\theta\sin\varphi\,\left(J_Y(0) + r\sin\theta\cos\varphi\,J_{Yx}(0) + r\sin\theta\sin\varphi\,J_{Yy}(0) - r\cos\theta\,J_{Yz}(0)\right) \\
& \left.+3\Sigma_1\,\cos\theta\,\left(J_Z(0) + r\sin\theta\cos\varphi\,J_{Zx}(0) + r\sin\theta\sin\varphi\,J_{Zy}(0) - r\cos\theta\,J_{Zz}(0)\right)\right]\exp(-\Sigma r)\,\cos\theta\sin\theta
\end{aligned}
\tag{4.25}
$$

The net current at z = 0 is obtained as follows

$$
\begin{aligned}
J_Z(0) &= J^+ - J^- \\
&= -\frac{2}{4\pi}\int_0^{\infty} dr \int_0^{2\pi} d\varphi \int_0^{\frac{\pi}{2}} d\theta \;\left[\,\Sigma_0\, r\cos\theta\,\phi_z(0) - 3\Sigma_1\sin\theta\,\cos\varphi\, r\cos\theta\,J_{Xz}(0)\right. \\
&\qquad - 3\Sigma_1\sin\theta\,\sin\varphi\, r\cos\theta\,J_{Yz}(0) \\
&\qquad - 3\Sigma_1\cos\theta\left(J_Z(0) + r\sin\theta\,\cos\varphi\,J_{Zx}(0)\right. \\
&\qquad \left.\left. + r\sin\theta\,\sin\varphi\,J_{Zy}(0)\right)\right]\exp(-\Sigma r)\,\cos\theta\,\sin\theta
\end{aligned}
\tag{4.26}
$$

The terms involving derivatives of currents do not contribute because of the integration over φ from 0 to 2π of the functions $\cos\varphi$ or $\sin\varphi$. On integrating the remaining terms, the expression for net current is obtained as

$$J_Z(0) = -\frac{2}{4\pi}\int_0^{\infty} dr \int_0^{2\pi} d\varphi \int_0^{\frac{\pi}{2}} d\theta \,[\, \Sigma_0 r\cos\theta\, \phi_z(0) - 3\Sigma_1\cos\theta\, J_Z(0)\,]\exp(-\Sigma r)\cos\theta\,\sin\theta$$

$$= -\frac{\Sigma_0}{3\Sigma^2}\phi_z(0) + \frac{\Sigma_1}{\Sigma}J_Z(0\,) \tag{4.27}$$

$$J_Z(0) = -\frac{\Sigma_0}{3\Sigma(\Sigma - \Sigma_1)}\phi_z(0) = -\frac{c}{3\Sigma(1-c\mu)}\phi_z(0) \tag{4.28}$$

which gives $D = \frac{1}{3\Sigma(1-c\mu)}[1 + \mathrm{o}(1-c)]$.

This is the standard expression for the transport corrected diffusion coefficient in the presence of anisotropic scattering (Eqs. (2.85) and (2.90) of [4]) within an order of $(1-c)$. Thus, the method forms an alternative derivation of the above formula for the diffusion coefficient of a homogeneous medium.

4.3.2 The general case of the two-dimensional lattice

For the general heterogeneous case, if the source is written as a product of the slowly varying function and the two-dimensional source from the lattice calculation as in Eq. (4.22), the expression for the current (Eq. (4.26)) gets modified as follows

$$\begin{aligned} J_Z(0) &= J^+ - J^- \\ &= -\frac{2}{4\pi}\int_0^{\infty} dr \int_0^{2\pi} d\varphi \int_0^{\frac{\pi}{2}} d\theta \;\; [\, \Sigma_0\, r\cos\theta\, f_z(0)\phi - 3\Sigma_1\sin\theta\,\cos\varphi\, r\cos\theta\, J_X f_z(0) \\ &\quad -3\Sigma_1\sin\theta\,\sin\varphi\, r\cos\theta\, J_Y f_z(0) \\ &\quad -3\Sigma_1\cos\theta\left(J_Z(0) + r\sin\theta\,\cos\varphi\, J_Z f_x(0) + r\sin\theta\,\sin\varphi\, J_Z f_y(0)\right)\Big]\exp(-\Sigma r)\cos\theta\,\sin\theta \end{aligned} \tag{4.26a}$$

The terms involving transverse currents i.e. J_X, J_y or derivatives of $f(x,y,z)$ i.e. $f_x(0)$, $f_y(0)$ are much smaller than the other two main terms on the right hand side of eq.(4.26a).

The two terms containing J_Z involve the derivative of the global flux as a factor and are of a smaller magnitude than $J_Z(0)$. The terms involving transverse current components have fluctuating (positive and negative) contribution to the integral along a ray and hence these also give a small contribution. The integration over φ from 0 to 2π (which gives a zero contribution in the homogeneous case due to the cosine or sine factors) and averaging over the pin cell surface (perpendicular to the fuel) of all these terms, makes their contribution negligibly small. After dropping these terms, there are two source contributions to the current in this case viz. the one proportional to the flux (due to fission and the $l = 0$ scattering component) and the one proportional to the current itself due to the $l = 1$ scattering component. On carrying out the averaging over the source and destination meshes, finally obtain (following an identical method as before) the anisotropic equivalent of Eq. (4.14) as

$$J_{Zjg} = f_z(0)\sum_{h,i}\left(\Sigma_{0i,h\to g} + \frac{\chi_g \nu\Sigma_{fi,h}}{k}\right)\phi_{ih}T_{ijg} + \sum_{h,i} 3\Sigma_{1i,h\to g}J_{Zih}T'_{ijg} \qquad (4.29)$$

One point that needs to be noted with regard to the differences in two equations is that since there are two types of source terms with different angular dependence, such that the first has a factor $r\cos\theta = \rho\cot\theta = \rho\cos\theta/\sin\theta$, whereas the second has the factor $\cos\theta$. Hence the collision probability like factors are different. The expressions for T'_{ijg} will be same as that for T_{ijg} given in Eq. (4.15), but with a somewhat different integrand I' that has one order higher Bickley function. Consequently, instead of Eqs. (4.11 to 4.13), the following equations are obtained:

$$I' = \int_0^{p_1} d\xi_1 \int_0^{p_2} d\xi_2 \left[Ki_1\left(\tau_{ijg} + \Sigma_{gi}\xi_1 + \Sigma_{gj}\xi_2\right) - Ki_3\left(\tau_{ijg} + \Sigma_{gi}\xi_1 + \Sigma_{gj}\xi_2\right)\right] \qquad (4.11a)$$

$$I'_{ij} = \frac{1}{\Sigma_{gi}\Sigma_{gj}}\left[Ki'_3(\tau_{gij}) - Ki'_3(\tau_{gij}+\tau_{gi}) - Ki'_3(\tau_{gij}+\tau_{gj}) + Ki'_3(\tau_{gij}+\tau_{gj}+\tau_{gi})\right] \tag{4.12a}$$

$$I'_{ii} = \int_{a_1}^{b_1} dx_1 \int_{x_1}^{b_1} dx_2 Ki'_1\left(\Sigma_{gi}(x_2 - x_1)\right)$$

$$= \frac{1}{\Sigma^2_{gi}}\left[\tau_{gi} Ki'_2(0) - \left(Ki'_3(0) - Ki'_3(\tau_{gi})\right)\right] \tag{4.13a}$$

$$= \frac{1}{\Sigma^2_{gi}}\left[\frac{\tau_{gi}}{3} - \left(\frac{\pi}{16} - Ki'_3(\tau_{gi})\right)\right]$$

As in the simple case of one group infinite homogeneous medium [viz. Eq. (4.27)], the current appears on the left side and the right side of Eq. (4.29). However unlike in the simple case one cannot simply solve for the current as an explicit function of the derivative of the flux [as in Eq. (4.28)]. This is because the current of a mesh in a group implicitly involves currents of other groups and meshes as well and will have to be obtained by an iterative process. Hence, instead of carrying out the group condensation and spatial averaging over a pin cell, the system of equations Eq. (4.29) will have to be solved iteratively ($f_z(0)$ is simply a common multiplying factor) for J_{Zig} and ϕ_{ig}, then obtain the group condensed and homogenised diffusion coefficients using the following equations instead of Eqs. (4.14), (4.18) and (4.19).

$$\bar{J}_{ZGK} = -\frac{1}{A_{pcK}} \sum_{i\in K, g\in G} A_i J_{Zig} \tag{4.14a}$$

$$\frac{\partial \bar{\phi}_{GK}}{\partial z} = \frac{1}{A_{pcK}} \sum_{i,g\in G} A_i \phi_{ig} \tag{4.18a}$$

$$D_{GK} = -\frac{\bar{J}_{ZGK}}{\frac{\partial \bar{\phi}_{GK}}{\partial z}} \tag{4.19a}$$

4.4 Finite Lattice - Effect of Leakage

In this section, the method for obtaining the leakage corrected lattice spectrum and flux distribution that goes as input into the calculation of the lattice parameters is described. The flux is written as a product of a slowly varying smooth function and a periodic function of x and y that has the period of the lattice. In this respect it resembles the methods described above. However, the form of the smooth slowly varying function need not be specified. With this, there is no need to solve the transport equation with a complex cross section, and the formulation is in terms of collision probabilities and can therefore be easily implemented in lattice codes. The leakage correction is carried out, with the help of the leakage corrected collision probabilities, during the lattice calculation of the heterogeneous medium i.e. without homogenisation following a lattice calculation. Expressions are derived for axial leakage corrected collision probabilities. These expressions have been coded in the LWR lattice code BOXER3 [7,166] for calculation of the leakage corrected flux distribution, the total leakage and the diffusion coefficients.

4.4.1 Axial leakage corrected collision probabilities

To obtain the leakage corrected collision probabilities, the flux is written as a product of a smooth function $f(z)$ of z and a periodic function $\phi_g(x,y)$ [$S_g(x,y)$ for the source] of x and y. The method adopted is similar to that was used for obtaining the axial diffusion coefficient, described in the previous section. However instead of obtaining the expression of current, expression for flux is obtained.

4.4.1.2 Contribution to Flux from Volume Sources

Consider a lattice which is infinite in the x and y directions but finite with uniform (constant) nuclear properties in the z-direction. The required flux, at a point in the z = 0 plane which is at the origin in the system of coordinates as shown in Fig.4.1, is obtained by multiplying the source density with the volume element, the exponential attenuation factor, and

integrating over all space. The source density is assumed to be factorizable into a function of (x, y) and the energy group and a slowly varying function of z that may be represented by the first few terms of its Taylor expansion.

$$\phi_g(x,y)f(0) = \frac{1}{4\pi}\int_0^{\infty} d\rho \int_0^{2\pi} d\varphi \int_0^{\pi} S_g(x,y)f(z)\, exp\left(-\tau_g/\sin\theta\right)d\theta$$

$$\approx \frac{1}{4\pi}\int_0^{\infty} d\rho \int_0^{2\pi} d\varphi \int_0^{\pi} S_g(x,y)\left\{f(0) + zf_z(0) + \frac{z^2}{2}f_{zz}(0)\right\} exp\left(-\tau_g/\sin\theta\right)d\theta \tag{4.30}$$

$$= \frac{1}{4\pi}\int_0^{\infty} d\rho \int_0^{2\pi} d\varphi \int_0^{\pi} S_g(x,y)\left\{f(0) + \rho\cot\theta f_z(0) + \frac{\rho^2\cot^2\theta}{2}f_{zz}(0)\right\} exp\left(-\tau_g/\sin\theta\right)d\theta$$

Here τ_g is the projection of the optical path length between the area and volume elements in a plane perpendicular to the z axis. The second term gives a vanishing contribution because $\cot\theta$ is anti-symmetric about $\pi/2$ leaving contributions from the first and last terms only. Thus

$$\phi_g(x,y)f(0)$$

$$= \frac{f(0)}{2\pi}\int_0^{\infty} d\rho \int_0^{2\pi} d\varphi\, S_g(x,y)Ki_1(\tau_g) + \frac{f_{zz}(0)}{4\pi}\int_0^{\infty} \rho^2 d\rho \int_0^{2\pi} d\varphi\, S_g(x,y)\left[Ki_{-1}(\tau_g) - Ki_1(\tau_g)\right] \tag{4.31}$$

where the integral over θ has been written in terms of the Bickley functions. Thus, the expression for the flux is made up of two terms. The first is the uncorrected flux for an infinite medium, while the second term gives the correction due to the finiteness of the medium. Assume that it is permissible to write the second derivative as being proportional to the flux itself, i.e. $f_{zz}(0) = -B_z^2 f(0)$. Eq. (4.31) gives the flux at a point due to a source at another point. In the collision probability method, the equations are written in terms of average fluxes and sources in a mesh. The equation for the average flux in the i^{th} mesh is therefore obtained by further integrating over the destination coordinates and dividing out by the area (volume per unit length) of the i^{th} destination mesh.

$$\phi_{i,g} = \frac{1}{2\pi A_i}\left[\int_{A_j} dA \int_0^{\infty} d\rho \int_0^{2\pi} d\varphi\, S_g(x,y) Ki_1(\tau_g) - \frac{B_z^2}{2}\int_{A_j} dA \int_0^{\infty} \rho^2 d\rho \int_0^{2\pi} d\varphi\, S_g(x,y)\left[Ki_{-1}(\tau_g) - Ki_1(\tau_g)\right]\right] \tag{4.32}$$

The integrals represent integrations over the area of cross section of meshes of the lattice cell (fuel assembly in this case) and can be calculated by the same ray tracking technique used for obtaining the collision probabilities. To obtain these integrals similar procedure as used in section 4.2 is used.

With reference to Fig. 4.2, the polar coordinates of the destination point, with the emission point as origin and angle φ relative to the fixed frame are

$$(\rho', \varphi) = (x_2 - x_1, \varphi) \tag{4.33}$$

where, x_2 is the x-coordinate of the destination point in the rotated frame. The φ integration element at the destination point can be written as:

$$\rho'^2 d\varphi = (x_2 - x_1)^2 d\varphi \tag{4.34}$$

The equation for the flux then becomes

$$\Sigma_{gi} A_i \phi_{ig} = \sum_j S_{jg} A_j (K_1 - K_2) \tag{4.35}$$

where,

$$K_1 = \frac{\Sigma_{gi}}{2\pi A_j}\int_0^{2\pi} d\varphi \int dy_1 \int_{a_1}^{b_1} dx_1 \int_{a_2}^{b_2} dx_2 Ki_1\left(\tau_{ijg} + \Sigma_{gi}(b_1 - x_1) + \Sigma_{gj}(x_2 - a_2)\right)$$

$$K_2 = \frac{B_z^2}{2}\frac{\Sigma_{gi}}{2\pi A_j}\int_0^{2\pi} d\varphi \int dy_1 \int_{a_1}^{b_1} dx_1 \int_{a_2}^{b_2} dx_2 (x_2 - x_1)^2 Ki'_{-1}\left(\tau_{ijg} + \Sigma_{gi}(b_1 - x_1) + \Sigma_{gj}(x_2 - a_2)\right)$$

To make the equations resemble the collision probability equations, both sides of the equation is multiplied by $\Sigma_{gi}A_i$ and introduced the factor A_j in the numerators and denominators of the two terms on the right side. With this, both K_1 and K_2 can be interpreted as the collision probability from the region j to the region i. The first is the usual collision probability expression for infinite medium while the second represents the correction due to axial leakage.

4.4.1.3 Final Expressions for Leakage Corrected Collision Probabilities

The same procedure as described in section 4.2 is followed for obtaining the above two integrals. Thus for $i \neq j$,

$$P^{(u)}{}_{jig} = \frac{\Sigma_{gi}}{2\pi A_j}\int_0^{2\pi} d\varphi \int dy_1 \int_0^{p_1} d\xi_1 \int_0^{p_2} d\xi_2 Ki_1(\tau_{ijg} + \Sigma_{gi}\xi_1 + \Sigma_{gj}\xi_2)$$

$$= \frac{1}{2\pi\Sigma_{gj}A_j}\int_0^{2\pi} d\varphi \int dy_1 \left[Ki_3(\tau_{gij}) - Ki_3(\tau_{gij} + \tau_{gi}) - Ki_3(\tau_{gij} + \tau_{gj}) + Ki_3(\tau_{gij} + \tau_{gj} + \tau_{gi})\right] \quad (4.36a)$$

$$P^{(ac)}{}_{jig} = -\frac{B_z^2}{2}\frac{1}{2\pi\Sigma_{gj}A_j}\int_0^{2\pi} d\varphi \int dy_1 L_{ji} \quad (4.36b)$$

$$L_{ji} = \Sigma_{gi}\Sigma_{gj}\int_0^{p_1} d\xi_1 \int_0^{p_2} d\xi_2 \ (p_{12} + \xi_1 + \xi_2)^2 \ \ Ki'_{-1}(\tau_{ijg} + \Sigma_{gi}\xi_1 + \Sigma_{gj}\xi_2)$$

$$= \frac{2}{\Sigma_{gi}\Sigma_{gj}}\left(1 + \frac{\Sigma_{gi}}{\Sigma_{gj}} + \frac{\Sigma_{gj}}{\Sigma_{gi}}\right)\{Ki'_3(\tau_{gij}) - Ki'_3(\tau_{gij} + \tau_{gi}) - Ki'_3(\tau_{gij} + \tau_{gj}) + Ki'_3(\tau_{gij} + \tau_{gj} + \tau_{gi})\} \quad (4.36c)$$

$$+ 2\left(\frac{1}{\Sigma_{gi}} + \frac{1}{\Sigma_{gj}}\right)\{p_{12}\, Ki'_2(\tau_{gij}) - (p_{12} + p_1)\, Ki'_2(\tau_{gij} + \tau_{gi}) - (p_{12} + p_2)Ki'_2(\tau_{gij} + \tau_{gj}) + (p_{12} + p_1 + p_2)Ki'_2(\tau_{gij} + \tau_{gj} + \tau_{gi})\}$$

$$+ \{(p_{12})^2\, Ki'_1(\tau_{gij}) - (p_{12} + p_1)^2\, Ki'_1(\tau_{gij} + \tau_{gi}) - (p_{12} + p_2)^2 Ki'_1(\tau_{gij} + \tau_{gj}) + (p_{12} + p_1 + p_2)^2 Ki'_1(\tau_{gij} + \tau_{gj} + \tau_{gi})\}$$

while for $i = j$,

$$P^{(u)}{}_{iig} = \frac{1}{2\pi\Sigma_{gi}\mathrm{A}_i}\int_0^{2\pi} d\varphi \int dy_1 \left[\tau_{gi} - \left(Ki_3(0) - Ki_3(\tau_{gi})\right)\right] \tag{4.37a}$$

$$P^{(ac)}{}_{iig} = -\frac{{B_z}^2}{4\pi\Sigma_{gi}\mathrm{A}_i}\int dyd\varphi L_{ii} \tag{4.37b}$$

$$L_{ii} = \left[({p_1}^2)Ki'_1(\tau_{gi}) + \frac{2p_1}{\Sigma_i}\left(Ki'_2(0) + 2Ki'_2(\tau_{gi})\right) - \frac{6}{\Sigma_i^2}\left(Ki'_3(0) - Ki'_3(\tau_{gi})\right)\right] \tag{4.37c}$$

The symbols p_1 and p_2 are for the path lengths through the regions *i* and *j* and p_{12} for the path length in between the regions *i* and *j.* The source in the i^{th} mesh can be written in the usual way as follows:

$$S_{ig} = \sum_h \left(\Sigma_{h\to g} + \frac{\chi_g \nu\Sigma_{fh}}{k}\right)\phi_{ih} \tag{4.38}$$

4.5 Results of Calculations using the Proposed Method

To verify the proposed method to obtain the diffusion coefficient as described in the previous sections, a small computer program has been written. The path lengths and other inputs such as mesh division, material distribution and flux, required for this purpose are calculated using the lattice code BOXER3 [7]. For the verification of the method in the case of lattice without any leakage correction to the flux distribution, the program evaluates the integrals in Eq. (4.15) using the integrands given in Eqs. (4.12) and (4.13) and obtain the diffusion coefficients from Eq. (4.19).

To generate the leakage corrected flux distribution, a routine which estimate the integral in Eqs. (4.36b) and (4.37b) was introduced in BOXER3. Diffusion coefficient is obtained from Eq. (4.19) using the computer program mentioned above.

For verifying the proposed methodology, a simple problem of a square pin cell of a typical PWR is considered. The calculations are limited to two energy groups (group 1 is from

10 MeV to 0.625eV and group 2 is energy less than 0.625eV) and isotropic scattering. The infinite medium problem was run using BOXER3 to generate the homogeneous cross sections by the usual flux volume weighting procedure. The diffusion coefficients were obtained by the P1 method and the proposed method [165].

4.5.1 Without Leakage Correction

For the case of an infinite homogeneous medium, the diffusion coefficient by the proposed method reduces to $\frac{1}{3\Sigma_{tr}}$. This result is used to check the correctness and accuracy of the integration algorithm by considering the same lattice cell mentioned above with the same mesh divisions and integration method but having the same material in each of the mesh divisions to simulate an infinite homogeneous region. Table 4.1 show the values of $\frac{1}{3\Sigma_{tr}}$ for the two energy groups and the diffusion coefficient as computed above. The agreement gives the confidence in the numerical computation.

Table 4.1: Diffusion coefficient for an infinite homogeneous medium

Energy group	$D = 1/(3\Sigma_{tr})$	D by Numerical integration using Eqs. (4.12 to 4.19)
1	1.19556	1.19554
2	0.258110	0.258116

The same pin cell with the fuel, clad and water introduced as in the actual pin cell is considered for computing the diffusion coefficient. The pin cell pitch is 1.2 cm and the U^{235} enrichment is 2%. Two cases corresponding to different rod radii are evaluated. In case-1 the fuel pin OD is 0.9 cm with a clad thickness of 0.05 cm. In case-2 the fuel pin OD is 0.75 cm with a clad thickness of 0.025 cm. Table 4.2 shows the comparison of D with $P1$ method $\left(\frac{1}{3\Sigma_{tr}}\right)$ and the proposed method. It is seen that the proposed method gives a slightly different diffusion coefficient (about 0.5% higher) than the P1 results for the fast group but the difference

is nearly 8-10% for the thermal group, which is quite significant. This may be expected as the medium is more heterogeneous in the thermal region and the flux also varies considerably from point to point.

Table 4.2: Comparison of diffusion coefficients by the two methods

Pin cell details	Energy group	D by Proposed method	D by P1 $(1/(3\Sigma_{tr}))$
Fuel OD = 0.8cm Clad OD = 0.9cm Pin cell pitch = 1.2 cm U^{235}enrichment = 2%	1	1.19610	1.19556
	2	0.281014	0.258110
Fuel OD = 0.7cm Clad OD = 0.75cm Pin cell pitch = 1.2 cm U^{235} enrichment = 2%	1	1.21731	1.21684
	2	0.230334	0.214149

The effect of these different diffusion coefficients on the K-effective (K-eff) of a finite sized core is studied. Since the study is for axial diffusion coefficient, the size of the reactor along axial direction is kept finite whereas along X and Y directions it is assumed that the system is infinite (i.e., the problem is that of a homogeneous slab). Since most of the leakage is in the fast group but most of the difference in the diffusion coefficient is in the thermal group (Table 4.2), the difference in the value of K-eff is not expected to be large. The core calculations were performed for core heights (slab thickness) of 50, 75 and 100 cm. These dimensions are chosen because small cores would show greater difference, owing to greater leakage, between the K-effective (K-eff) by the P1 diffusion coefficient and that by the proposed method. For these core heights, the difference in the K-eff by the two methods is expected to be 100 pcm or less. It is thus important that both the Monte Carlo and the diffusion calculations are performed with a high level of precision to distinguish between the performances of the two diffusion coefficients.

The diffusion computations have been obtained by an analytical solution of the two-group diffusion equation with zero incoming current boundary conditions (in the corrected

form $\frac{J}{\phi} = 2.131$). The analytical solution of the two-group diffusion theory equations with zero incoming current boundary conditions for a bare reactor is given in the Appendix -A.

Table 4.3 show a comparison of the K-effective obtained using two group diffusion theory with the same homogenised cross sections but with the two different ways of computing *D*. As for reference, results of Monte Carlo calculation are given in the table. Monte Carlo calculation is for the original heterogeneous lattice cell reflected in the x-y directions but having a finite height and using the same cross section data that was used (as input) in the BOXER3 calculation. The relative error (standard deviation) in the Monte Carlo calculations is about 0.00004. The result in Table 4.3 shows that though the difference in the K-effective by the two methods is not large, the proposed method for obtaining D is better in predicting the K-effective as compared to the standard method.

Table 4.3: Comparison of diffusion theory K-effective

Pin cell details	Core height (cm)	K-effective (deviation with respect to K-effective by Monte Carlo (pcm))		
		Using *D* as $1/3\Sigma_{tr}$ (P1)	Using *D* by Proposed method	Monte Carlo
Fuel OD = 0.8cm Clad OD = 0.9cm Pin cell pitch = 1.2 cm U^{235}enrichment = 2%	50	1.22656 (55)	1.22559 (-24)	1.22589
	75	1.30630 (60)	1.30582 (23)	1.30552
	100	1.33856 (43)	1.33827 (21)	1.33799
Fuel OD = 0.7cm Clad OD = 0.75cm Pin cell pitch = 1.2 cm U^{235} enrichment = 2%	50	1.21354 (41)	1.21269 (-29)	1.21304
	75	1.28391 (56)	1.28349 (23)	1.28319
	100	1.31211 (40)	1.31186 (21)	1.31159

4.5.2 With Leakage Correction

The cases considered and the cross section set used are same as in section 4.5.1. The problem is solved for a given input buckling corresponding to the core size. To check the effect of leakage on the flux distribution, ratio of production to absorption is compared with K-infinity of the lattice. For different core size, K-effective is also computed with BOXER3 (corresponding buckling and leakage corrected collision probability) as well as with Monte Carlo calculations. Monte Carlo calculation is for the original heterogeneous lattice cell reflected in the x-y directions but having a finite height and using the same cross section data that was used as input in the BOXER3 calculation. The results are summarized in Table 4.4.

The good agreement with Monte Carlo values shows that the concept as well as computation of the leakage corrected probabilities are correct. The small disagreement is due to the use of an approximate buckling as input. The actual core flux is not described by a single buckling concept even for a bare reactor. This does not matter as the leakage corrected collision probabilities are used only to calculate the lattice flux distribution and thereby the homogenised cross sections and diffusion coefficients. The core leakage, K-effective and flux distribution are obtained from these cross sections from a few group diffusion calculations.

Table 4.4: Ratio (production by absorption) and K-effective with leakage correction

Pin cell case	Core height (cm)	BOXER3 K-infinity	BOXER3 (production/ absorption)	BOXER3 K-effective (eigenvalue)	K-effective (Monte Carlo)
Case 1	50	1.38541	1.38383	1.22587	1.22589
	75		1.38467	1.30596	1.30552
	100		1.38498	1.33831	1.33799
Case 2	50	1.35278	1.35152	1.21150	1.21304
	75		1.35219	1.28370	1.28319
	100		1.35243	1.31194	1.31159

Comparison of K-effective obtained using two-group diffusion theory with the same homogenised cross sections but with the two different ways of computing D are presented in Table 4.5. The results obtained using diffusion theory parameters generated with and without leakage corrections are also presented. From the table it appears that while the agreement with Monte Carlo improves with the use of leakage corrected cross sections for larger core sizes, it worsens for the smallest size core, ie. 50 cm. This is probably due to transport effects since these are expected to be maximum for the smallest size core. To confirm this, a comparison between diffusion and Monte Carlo results for the above core heights (using the same homogenised cross sections for both) is presented in Table 4.6. It is clear from the table that diffusion value of the K-effective is about 76 pcm lower than transport Monte Carlo value on account of transport theory effects, for the 50 cm core. The difference is almost zero (i.e. of the same order as the Monte Carlo standard error) for the 100 cm core.

Table 4.5: Comparison of diffusion theory K-eff using D with and without leakage correction

Pin cell case	Core height (cm)	K-effective (deviation with respect to K-effective by Monte Carlo (pcm))				
		Diffusion theory parameters without leakage correction		Diffusion theory parameters with leakage correction		Monte Carlo
		$D = 1/(3\Sigma_{tr})$ (P1)	D by proposed method	$D = 1/(3\Sigma_{tr})$ (P1)	D by proposed method	
Case 1	50	1.22656 (55)	1.22559 (-24)	1.22625 (29)	1.22536 (-43)	1.22589
	75	1.30630 (60)	1.30582 (23)	1.30615 (48)	1.30569 (13)	1.30552
	100	1.33856 (43)	1.33827 (21)	1.33847 (36)	1.3382 (16)	1.33799
Case 2	50	1.21354 (41)	1.21269 (-29)	1.21316 (10)	1.21241 (-52)	1.21304
	75	1.28391 (56)	1.28349 (23)	1.28373 (42)	1.28335 (12)	1.28319
	100	1.31211 (40)	1.31186 (21)	1.31201 (32)	1.31177 (14)	1.31159

The somewhat better agreement for the 50 cm core by the P1 method (Table 4.5) can be attributed to cancellation of errors due to homogenisation and transport effects. Once this is taken into account, it is seen that the homogenisation error that is about 100 to 30 pcm using P1 diffusion coefficient and standard infinite lattice homogenisation reduces to about 30 to 10 pcm using the proposed method. This shows that theory developed for the computation of *D* yields better homogenised diffusion theory parameters for large as well as small cores.

Table 4.6: Comparison of diffusion theory and Monte Carlo K-eff for homogeneous cores.

Core height (cm)	$D = \frac{1}{(a_g 3\Sigma_{tr})}$ (B1)	$D = 1/(3\Sigma_{tr})$ (P1 method)	Monte Carlo
50	1.22778 (24)	1.22656 (-76)	1.22749
75	1.30662 (12)	1.30630 (-12)	1.30646
100	1.33868 (14)	1.33856 (5)	1.33849

The B1 method takes better care of the transport effects as may be seen from the results shown in the first column of Table 4.6. In B1 method, for the homogeneous problem one has to divide the diffusion coefficient by the factor $a_g(x)$ [95] given by

$$a_g(x) = \left(\frac{1}{3}x^2 \arctan(x)\right)/(x - \arctan(x))$$

where, $x = \left(\frac{B}{\Sigma_{tg}}\right)^2$. The B1 correction is applied to homogenised diffusion coefficients by both P1 and the proposed method and the results are given in Table 4.7. It is seen that applying B1 correction overcorrects the transport effect as compared to that for the homogeneous case. The use of *D* by the proposed method yield better results for all cases and it improves with leakage correction.

Table 4.7: Comparison of diffusion theory K-effective using B1 corrected *D*

Pin cell case	Core height (cm)	K-effective (deviation with respect to K-effective by Monte Carlo (pcm))				
		Diffusion theory parameters without leakage correction		Diffusion theory parameters with leakage correction		Monte Carlo
		$D = \frac{1}{(a_g 3\Sigma_{tr})}$ (B1)	B1 corrected *D* by proposed method	$D = \frac{1}{(a_g 3\Sigma_{tr})}$ (B1)	B1 corrected *D* by proposed method	
Case 1	50	1.22778 (154)	1.22681 (75)	1.22747 (129)	1.22658 (56)	1.22589
	75	1.30662 (84)	1.30614 (47)	1.30647 (73)	1.30601 (37)	1.30552
	100	1.33868 (52)	1.33839 (30)	1.33859 (45)	1.33832 (25)	1.33799
Case 2	50	1.21464 (132)	1.21379 (62)	1.21427 (101)	1.21352 (40)	1.21304
	75	1.28420 (79)	1.28379 (46)	1.28403 (65)	1.28364 (35)	1.28319
	100	1.31221 (47)	1.31197 (29)	1.31211 (39)	1.31188 (22)	1.31159

4.6 Summary

The method developed for obtaining homogenised diffusion coefficients, for a more accurate treatment of axial diffusion in core calculations, can be introduced in lattice codes based on collision probability / mixed collision probability and interface current methods. The effect of anisotropic scattering in the calculation of the diffusion coefficients can be accounted for, without having anisotropic treatment in the lattice calculations. The effect on spatial and spectral flux distribution due to leakage is taken care in the collision probability estimation normally carried out in CP method. Comparison of core calculations using these homogenised diffusion coefficients with Monte Carlo calculations show that they perform better than the standard method used for this purpose. In the case of small sized core, the transport effects while applying the diffusion theory are prominent. The B1 corrected diffusion coefficient takes

care of the transport effect in the case of homogeneous calculations. The use of B1- corrected diffusion coefficient, which is obtained by the proposed method with leakage correction to the flux distribution, yields better results.

The B1 correction applied here is valid for homogeneous systems (or heterogeneous systems after homogenisation). It may be possible to obtain B1 correction to the diffusion coefficient using the method described in this chapter directly (i.e. without previous homogenization) for heterogeneous systems. It is proposed to attempt such a correction in future.

CHAPTER 5

DEVELOPMENT OF COMPUTER CODE 'FDPEM' BASED ON COMBINATION OF FINITE DIFFERENCE AND POLYNOMIAL EXPANSION METHODS FOR PIN BY PIN CORE CALCULATIONS

5.1 Introduction

The second step in the reactor calculation for obtaining the detailed neutron flux distribution and status of the reactor core is the 3-D core calculation wherein the few group neutron diffusion equation is solved. The homogenized few group cross sections constitute the input to this calculation. These are obtained by a homogenization procedure using the flux distribution generated in the lattice cell calculation as described in chapters 4 and 3 respectively. In case of LWRs, the fuel assembly (which is the main component of the lattice) is complex and can be highly heterogeneous. One fuel assembly (FA) can contain hundreds of fuel pins with different properties, like enrichment, Gd content etc. Normally after two-dimensional lattice cell calculation, flux-volume homogenization of the cross sections is carried out over the entire fuel assembly and these assembly averaged cross sections are used to solve the diffusion equation in the second step (along X and Y directions homogenized FA is considered as one mesh) to obtain the FA averaged power. The nodal method is commonly used for this purpose as it is quite fast. As the safety and operational requirement demands the knowledge of individual pin power, this is inferred from a combination of the results of the lattice and core calculations [104, 167]. Due to the approximations involved in this procedure, there is a need for a method to directly obtain pin by pin power distribution. The flux-volume homogenization over individual pin cells can be easily carried out (at the lattice level) to obtain the few group cross sections of each pin cell for this purpose. However, the pin by pin core level diffusion calculation is computationally expensive owing to the small sized meshes. This

chapter describes the development of a few group diffusion theory code for pin by pin core calculations based on a combination of finite difference and polynomial expansion methods [8] to reduce the computational effort involved in these calculations. The outline of the chapter is as follows: Section 5.2 describes the rationale behind the development of the new method based on combination of finite difference and polynomial expansion method. Theoretical basis of the method is presented in section 5.3. Verification of the code using benchmark problems is described in section 5.4. Summary regarding the code capability and applicability is presented in section 5.5.

5.2 Rationale behind the Development of the Method based on Combination of FD and Polynomial Expansion

Core calculations in light water reactors have been traditionally carried out, for the last several decades, using one of the nodal [132, 168, 169, 170, 171, 172] methods. With a ten-thousand-fold increase in computing power since the seventies and eighties, when these methods appeared, it is to be expected that a more detailed treatment can be carried out now. Core calculations using transport theory without homogenization using the method of characteristics or interface current methods are being attempted [9, 10] to obtain detailed pin by pin power and burnup distributions. Clearly, these will not be possible for routine computing at least as of now and some (improved) variants of methods based on diffusion theory will continue to be in use in the foreseeable future. This chapter discusses the development of a new method to obtain detailed pin by pin power and burnup distributions employing pin cell sized meshes.

In a typical LWR core, abrupt changes of material properties of the medium in directions perpendicular to the fuel rod length (x-y directions) are quite frequent. In fact, each pin could be having a different enrichment, or Gd content. Material properties also change abruptly due to presence of control rods or water gaps. Thus, unless assembly level homogenization has

been carried out at the lattice level, every pin cell could have different properties. Thus, in the x-y directions, the method must be able to explicitly represent this heterogeneity. The finite difference method may be used for this purpose as it is well studied and has been implemented in several diffusion theory codes.

Along the direction parallel to the length of the fuel rods (the z direction) abrupt changes of material properties of the medium (for example near the ends of partially inserted control rods, core reflector interface etc.) are quite infrequent. There are smooth variations of material properties in this direction (due to burnup, Xenon, temperature and void distribution), but these variations are quite slow. This results in a flux variation that is quite smooth along this direction. Thus, it should be possible to represent the core in the z direction by a few divisions that are decided by the locations at which there are abrupt changes in the properties. Within such a division along the z axis, the flux can be represented by expanding in polynomials and the material properties by constant, linear or quadratic polynomials.

Taking into account the nature of variation in material properties as described above, it is felt that a combination of finite difference method in the directions perpendicular to the fuel pins along which the material properties and flux vary rapidly, and a polynomial expansion method along the fuel length may give better results both in terms of computational requirement and accuracy. There have been a number of attempts to use a similar approach (referred to as 'hybrid finite difference and nodal methods') to pin by pin core calculations [173, 148]. The basic difference in these methods and the method described in this chapter is in the treatment of transverse leakage. In the method described in this chapter, transverse leakage is expressed as fourth order function where as it is represented as a quadratic function even though flux is expanded in fourth order in the 'hybrid finite difference and nodal methods' .

Even though the polynomial expansion method in the z direction is also based on the same fourth order polynomial [132] that is used in the nodal method, unlike the nodal methods, there is no need to factorize flux in the three directions. While treating the flux variation along the z direction, it is therefore not necessary to use the quadratic variation of leakage based on the fitting of average fluxes in the current and neighboring meshes. Instead, a fourth order leakage is easily derivable as shown in the section 5.3. This exact treatment of transverse leakage permits the use of long meshes in the z direction thereby partially mitigating the enhanced demands on memory and computing requirements that arise due to the more detailed treatment in the x-y directions. The use of such long meshes poses another problem that needs a solution. With relatively shorter meshes as in finite difference treatment (or somewhat larger sized nodes in the nodal method), a constant cross section and diffusion coefficient can be assumed within a mesh (node) along the axial direction. Instead of constant values within a mesh, the cross sections / diffusion coefficients can be represented using low order polynomials (typically linear or quadratic in the z variable). To keep the discussion simple, constant cross sections is considered. The necessary modification in the method for the case of a linear representation of cross section (along the z direction) is presented in Appendix-B.

5.3 Discretization of the Diffusion Equation by Polynomial Expansion and Finite Difference methods

The problem region (where diffusion equation is to be solved) is divided into cells that are typically about 1 cm (typical pin-cell pitch) in the x-y directions and 20 cm or longer in the z direction. The cells may be of hexagonal, rectangular, or triangular shapes depending upon the basic fuel assembly geometry. For the study presented in this thesis it is assumed that cells are rectangular in shape. Each cell is characterized by the three cell indices ijk and average flux shape function $\Phi_g^{ijk}(z)$ in energy group g that is a function of the z coordinate within the cell but is averaged in the x-y directions over the cell transverse area. The average flux may be

considered to be the cell center-line flux, since center-mesh finite difference method is used to treat the x-y direction. This allows to write down simple finite differenced expressions for the neutron current on any cell (x-y) surface. Quantities that are also averaged over the z coordinate within the cell are denoted by a bar above, for example $\bar{\Phi}_g^{ijk}$ is the volume averaged flux in the cell. The treatment given in this section assumes that the cross sections and diffusion coefficients are constant (i.e. they do not vary with z) within a cell.

5.3.1 Polynomial Expansion Method (PEM) for Longitudinal (Z) Direction

The few group diffusion equation to be solved is

$$\nabla . D_g^{ijk} \nabla \Phi_g^{ijk} - \Sigma_g^{r,ijk} \Phi_g^{ijk} + \frac{\chi_g}{k} \sum_h \nu \Sigma_{fh} \Phi_h^{ijk} + \sum_h \Sigma_{sh \to g} \Phi_h^{ijk} = 0 \tag{5.1}$$

On integrating the diffusion equation over x-y variables for any z, one obtains

$$-\frac{d}{dz} D_g^{ijk} \frac{d}{dz} \Phi_g^{ijk}(z) + \Sigma_g^{r,ijk} \Phi_g^{ijk}(z) = Q_g^{ijk}(z) - \frac{1}{\Delta x}\left[J_{gx+}^{ijk}(z) - J_{gx-}^{ijk}(z)\right] - \frac{1}{\Delta y}\left[J_{gy+}^{ijk}(z) - J_{gy-}^{ijk}(z)\right] \tag{5.2}$$

where

$$\Phi_g^{ijk}(z) = \frac{1}{\Delta x . \Delta y} \int dy \int dx \ \Phi_g^{ijk}(x, y, z)$$

and

$$Q_g^{ijk}(z) = \frac{1}{\Delta x . \Delta y} \int dy \int dx \ Q_g^{ijk}(x, y, z)$$

The transverse leakage represented by the two terms on the right side of Eq. (5.2) are functions of z.

5.3.2 Finite Difference Treatment of Transverse (X-Y) Coupling and Leakage

In the mesh centered form of finite differencing, the mesh average flux is treated as the flux at the center of the mesh and therefore it is possible to write down the following finite difference expression for the current at the right surface of the mesh along x-direction assuming continuity of flux and current at the mesh interface

$$J_{gx+}^{ijk} = c_g^{i,i+1jk}\left(\Phi_{gz}^{ijk} - \Phi_{gz}^{i+1jk}\right) \tag{5.3}$$

where

$$c_g^{i,i+1jk} = \frac{2D_g^{ijk}D_g^{i+1jk}}{\Delta x^{ijk}D_g^{i+1jk} + \Delta x^{i+1jk}D_g^{ijk}} \tag{5.3a}$$

Similar expressions can be written down for currents on the other surfaces of the mesh. The above expression is usually written down for the average flux (treated as the flux at the mesh center) in all directions i.e. including the z direction. However, in the present context of a cell that is long in the z direction and short like the FD mesh in the x-y directions, the expression for current in the x-y directions is also valid for all values of z (with the flux point located at the cell center line parallel to the z-axis). Thus, it can be written down more generally as follows

$$J_{gx+}^{ijk}(z) = c_g^{i,i+1jk}\left(\Phi_g^{ijk}(z) - \Phi_g^{i+1jk}(z)\right) \tag{5.4}$$

This finite difference form of the current is used to write down the net transverse leakage (in x and y directions indicated by the terms on RHS of Eq. (5.2)) as a function of z, as:

$$\begin{aligned}\left(c_g^{i,i+1jk} + c_g^{i,i-1jk} + c_g^{ij,j+1k} + c_g^{ij,j-1k}\right)\Phi_g^{ijk}(z) \\ - \left(c_g^{i,i+1jk}\Phi_g^{i+1jk}(z) + c_g^{i,i-1jk}\Phi_g^{i-1jk}(z) + c_g^{ij,j+1k}\Phi_g^{ij+1k}(z)\right. \\ \left. + c_g^{ij,j-1k}\Phi_g^{ij-1k}(z)\right)\end{aligned} \tag{5.5}$$

The above expression is for normal inner cells. The expressions for the '*c*' coefficients need to be suitably modified for cells at the outer radial (or x-y) boundary that may have some missing neighboring cells.

Once the leakage functions are known, the remaining task is essentially solving the one-dimensional equation for z. The average flux shape function is expanded in polynomials up to the fourth order as follows:

$$\Phi_g^{ijk}(z) = \bar{\Phi}_g^{ijk} f_0(z) + \sum_{n=1}^{N} a_{gn}^{ijk} f_n(z) \tag{5.6}$$

The polynomials (and solution method) used are the same as in the nodal methods based on fourth order polynomials, described in [132], and is given in Eq. (5.7).

$$\begin{aligned} f_0(z) &= 1 \\ f_1(z) &= \frac{z}{\Delta z} = \xi \\ f_2(z) &= 3\xi^2 - \tfrac{1}{4} \\ f_3(z) &= \xi(\xi - \frac{1}{2})(\xi + \frac{1}{2}) \\ f_4(z) &= (\xi^2 - \frac{1}{20})(\xi - \frac{1}{2})(\xi + \frac{1}{2}) \end{aligned} \tag{5.7}$$

$\bar{\Phi}_g^{ijk}$, the volume weighted cell average flux is obtained from the nodal balance equation arrived by integrating eq. (5.1) over the volume and dividing by the cell volume

$$\frac{1}{\Delta z}\left(J_{gz+}^{ijk} - J_{gz-}^{ijk}\right) + \Sigma_{r,g}^{ijk}\bar{\Phi}_g^{ijk} = \bar{\mathrm{Q}}_g^{ijk} - \frac{1}{\Delta x}\left(J_{gx+}^{ijk} - J_{gx-}^{ijk}\right) - \frac{1}{\Delta y}\left(J_{gy+}^{ijk} - J_{gy-}^{ijk}\right) \tag{5.8}$$

where,

$$\bar{\Phi}_g^{ijk} = \frac{1}{\Delta x.\Delta y.\Delta z}\int dz \int dy \int dx\, \Phi_g^{ijk}(x,y,z) = \frac{1}{\Delta z}\int dz\, \Phi_g^{ijk}(z) \tag{5.8a}$$

$$\bar{\mathrm{Q}}_g^{ijk} = \frac{1}{\Delta x.\Delta y.\Delta z}\int dz \int dy \int dx\, \mathrm{Q}_g^{ijk}(x,y,z) = \frac{1}{\Delta z}\int dz\, \mathrm{Q}_g^{ijk}(z) \tag{5.8b}$$

$J_{gx\pm}^{ijk}$ are the x-components of the net current averaged over the x-directed faces of the cell. The face averaged outgoing and incoming currents satisfy the following relationships:

$$\begin{aligned} J_{gz+}^{ijk,out} - J_{gz+}^{ijk,in} &= J_{gz+}^{ijk} \\ J_{gz-}^{ijk,out} - J_{gz-}^{ijk,in} &= -J_{gz-}^{ijk} \\ 2\left[J_{gz\pm}^{ijk,out} + J_{gz\pm}^{ijk,in}\right] &= \phi_{gz\pm}^{ijk} \end{aligned} \tag{5.9}$$

The coefficients a_{g1} and a_{g2} can be related to the upper and lower boundary fluxes ϕ_{gz+}^{ijk} and ϕ_{gz-}^{ijk} and these can be expressed in terms of the partial currents at the boundary (i.e. a_{g1} and a_{g2} are determined by the boundary conditions at the ends of the cell).

$$a_{g1}^{ijk} = \phi_{gz+}^{ijk} - \phi_{gz-}^{ijk} \tag{5.10}$$

$$a_{g2}^{ijk} = \phi_{gz+}^{ijk} + \phi_{gz-}^{ijk} - 2\bar{\Phi}_{g}^{ijk} \tag{5.11}$$

The higher order coefficients a_{g3} and a_{g4} are determined using the weighted residuals equations based on moments weighting scheme (using the functions $f_1(z)$ and $f_2(z)$ as weight functions). The equations for the moments [132] can be obtained by multiplying Eq.(5.2) by the weight functions $f_0(z)$, $f_1(z)$ and $f_2(z)$ and integrating with respect to z over the extent of the cell in the z direction from $z = -\Delta z/2$ to $z = \Delta z/2$ as:

$$\frac{1}{2}\frac{1}{\Delta z}\left[J_{gz+}^{ijk} + J_{gz-}^{ijk}\right] + \frac{1}{\Delta z}\frac{D_g^{ijk}}{\Delta z}a_{g1}^{ijk} + \Sigma_g^{r,ijk}\phi_{g1}^{ijk} = Q_{g1}^{ijk} - \frac{1}{\Delta x}L_{gxz1}^{ijk} - \frac{1}{\Delta \mathrm{y}}L_{gyz1}^{ijk} \tag{5.12}$$

$$\frac{1}{2}\frac{1}{\Delta z}\left[J_{gz+}^{ijk} - J_{gz-}^{ijk}\right] + \frac{3}{\Delta z}\frac{D_g^{ijk}}{\Delta z}a_{g2}^{ijk} + \Sigma_g^{r,ijk}\phi_{g2}^{ijk} = Q_{g2}^{ijk} - \frac{1}{\Delta x}L_{gxz2}^{ijk} - \frac{1}{\Delta \mathrm{y}}L_{gyz2}^{ijk} \tag{5.13}$$

where, the flux moments ϕ_{gn}^{ijk} are given by

$$\phi_{gn}^{ijk} = \frac{1}{\Delta z}\int_{-\Delta z/2}^{+\Delta z/2} dz\, f_n(z)\ \Phi_g^{ijk}(z), \qquad n = 1,2 \tag{5.14}$$

Similar expressions can be written for Q_{gn}^{ijk}, L_{gxn}^{ijk} and L_{gyn}^{ijk} .

Using Eqs. (5.6), (5.7) and (5.14) the following expressions can be obtained for higher order expansion coefficients a_{g3}^{ijk} and a_{g4}^{ijk} in terms of the first and second flux moments:

$$a_{g3}^{ijk} = -120\phi_{g1}^{ijk} + 10a_{g1}^{ijk} \tag{5.15a}$$

$$a_{g4}^{ijk} = -700\phi_{g2}^{ijk} + 35a_{g2}^{ijk} \tag{5.15b}$$

The average z component of the currents on the upper and lower surfaces can be written in terms of the expansion coefficients using the relation $J = -D\frac{d\phi}{dz}$ from the flux expansion Eq. (5.6) as:

$$J_{gz+}^{ijk,out} = -\frac{D_g^{ijk}}{\Delta z}\left[a_{g1}^{ijk} + 3a_{g2}^{ijk} + \frac{1}{2}a_{g3}^{ijk} + \frac{1}{5}a_{g4}^{ijk}\right] + J_{gz+}^{ijk,in} \tag{5.16a}$$

$$J_{gz-}^{ijk,out} = +\frac{D_g^{ijk}}{\Delta z}\left[a_{g1}^{ijk} - 3a_{g2}^{ijk} + \frac{1}{2}a_{g3}^{ijk} - \frac{1}{5}a_{g4}^{ijk}\right] + J_{gz-}^{ijk,in} \tag{5.16b}$$

Eliminating the expansion coefficients from Eq. (5.16) using Eqs. (5.10), (5.11) and (5.15) the following equation for the out-currents in terms of the in-currents, source and leakage moments are obtained

$$\begin{bmatrix} A_{11} & A_{12} \\ A_{21} & A_{22} \end{bmatrix}\begin{bmatrix} J_{gz+}^{ijk,out} \\ J_{gz-}^{ijk,out} \end{bmatrix} = \begin{bmatrix} B_{11} & B_{12} & B_{13} \\ B_{21} & B_{22} & B_{23} \end{bmatrix}\begin{bmatrix} Q_g^{ijk} \\ Q_{g1}^{ijk} - L_{gz1}^{ijk} \\ Q_{g2}^{ijk} - L_{gz2}^{ijk} \end{bmatrix} + \begin{bmatrix} P_{11} & P_{12} \\ P_{21} & P_{22} \end{bmatrix}\begin{bmatrix} J_{gz+}^{ijk,in} \\ J_{gz-}^{ijk,in} \end{bmatrix} - \begin{bmatrix} R_{11} & R_{12} \\ R_{21} & R_{22} \end{bmatrix}\begin{bmatrix} J_{gx+}^{ijk} - J_{gx-}^{ijk} \\ J_{gy+}^{ijk} - J_{gy-}^{ijk} \end{bmatrix} \tag{5.17}$$

$L_{gz}^{ijk} = \frac{1}{\Delta x}L_{gxzn}^{ijk} + \frac{1}{\Delta y}L_{gyzn}^{ijk}$ are the transverse leakage moments. In traditional nodal methods they are approximated by a quadratic polynomial determined by fitting the average leakages in nodes $ijk-1$, ijk and $ijk+1$. In the proposed method, the leakage moments on the right side of Eq. (5.12) and (5.13) as well as the transverse leakage on the right side of Eq. (5.8) can be written using Eq. (5.5). This has the net effect of adding

$$\frac{1}{\Delta x}\left(c_g^{i,i+1jk} + c_g^{i,i-1jk}\right) + \frac{1}{\Delta y}\left(c_g^{ij,j+1k} + c_g^{ij,j-1k}\right) \tag{5.18a}$$

to the removal cross section $\Sigma_g^{r,ijk}$ and adding

$$\frac{1}{\Delta x}\left(c_g^{i,i+1jk}\Phi_{gzn}^{i+1jk} + c_g^{i,i-1jk}\Phi_{gzn}^{i-1jk}\right) + \frac{1}{\Delta y}\left(c_g^{ij,j+1k}\Phi_{gzn}^{ij+1k} + c_g^{ij,j-1k}\Phi_{gzn}^{ij-1k}\right) \tag{5.18b}$$

to the n^{th} order source moments. The n^{th} order flux moments Φ_{gzn}^{ijk} involved in Eq. (5.18b) refer to neighboring cells and hence are deemed to be known. Due to the use of this prescription for the transverse leakage, all transverse leakage moments and transverse leakage currents may be set to zero in Eq. (5.17).

Thus, there is no reason to separately write down and use expressions for the transverse leakage moments (including the zeroth order moment which is the average transverse leakage and appears in the neutron balance equation for the cells) based on the quadratic function obtained by fitting the average leakages of the current and two neighboring cells.

A computer code 'Finite Difference Polynomial Expansion Method' (FDPEM) is developed based on the method described above. The usual inner-outer iteration procedure is adopted for solution of the equations. The inner iteration is for obtaining the leakage and flux corresponding to a fixed fission source, while the outer iteration is for fission source and eigenvalue convergence. The sequence of steps involved in the iteration process are as follows: Starting with guess values of z direction in-currents and average fluxes in each cell, first obtain out-currents using Eq. (5.17). Using these, the average flux and its first and second moments are obtained from Eqs. (5.8), (5.12) and (5.13). The source is then updated for the next group and the calculations are repeated till all cells are covered. Finally go to the next group and repeat the process till all groups are covered. The fission source is estimated along with the eigenvalue and then move to the next outer iteration.

5.4 Verification Studies

To verify the methodology and the code FDPEM, two problems were studied. The first problem involves a pressurised heavy water reactor (PHWR) [174, 175] and the results obtained using FDPEM are compared with those obtained using a standard finite difference (SFD) code. The second is the IAEA 3D PWR benchmark problem [176] and the results

obtained using FDPEM are compared with those described in [176], based on other codes. For the IAEA 3D PWR benchmark problem, comparison of FDPEM results with fine mesh finite difference (SFD) results are also made. Both these problems are solved using the traditional quadratic leakage approximation employed in the nodal method as well as the 4^{th} order polynomial treatment of the transverse leakage moments described in section 5.3.

5.4.1 PHWR Problem

5.4.1.1 Description of the problem and the inputs

The core has 392 fuel channels with each channel containing 12 fuel bundles made up of 37 fuel elements. The lattice pitch and bundle length are 28.6 cm and 49.5 cm respectively. There is a radial heavy water reflector of about 70 cm thick, but axially the reactor is 5.94m long and is bare. No reactivity devices and no variation due to fuel burnup are considered in the simulation for simplicity. The lattice cell containing fuel bundle, D_2O coolant, pressure tube, calandria tube and associated moderator is homogenised and the two energy group cell averaged cross sections used for the study are given in Table 5.1. Fig. 5.1 depicts a radial section (one quarter) of the core indicating the layout of the materials.

Table 5.1: Two group cell averaged cross-section used for PHWR problem

Material	**group**	Σ_a (cm^{-1})	Σ_f (cm^{-1})	$\nu\Sigma_f$ (cm^{-1})	D_g (cm)	Σ_{s1-2} (cm^{-1})
1 (Fuel)	1	1.608E-03	3.144E-04	8.389E-04	1.3718	8.641E-03
	2	3.532E-03	1.735E-03	4.229E-03	0.8947	
2 (Reflector)	1	4.965E-06	0.0	0.0	1.3288	1.140E-02
	2	4.232E-05	0.0	0.0	0.8419	

1	1	1	1	1	1	1	1	1	1	1	2	2	2
1	1	1	1	1	1	1	1	1	1	1	2	2	2
1	1	1	1	1	1	1	1	1	1	1	2	2	
1	1	1	1	1	1	1	1	1	1	1	2	2	
1	1	1	1	1	1	1	1	1	1	2	2	2	
1	1	1	1	1	1	1	1	1	1	2	2		
1	1	1	1	1	1	1	1	1	2	2	2		
1	1	1	1	1	1	1	1	2	2	2			
1	1	1	1	1	1	1	2	2	2	2			
1	1	1	1	1	1	2	2	2	2				
1	1	1	1	2	2	2	2	2					
2	2	2	2	2	2	2							
2	2	2	2	2									
2	2												

Figure 5.1: Core (1/4th) map of PHWR (1: fuel cell, 2: reflector)

The study is carried out with FDPEM employing a combination of the FD method in the X-Y directions with a cell size of 28.6 cm (one pitch) and the fourth order polynomial expansion method in the Z direction. The fourth order polynomial treatment of transverse leakage moments discussed in section 5.3 is used and compared with the quadratic approximation used in nodal methods. The effectiveness of the fourth order polynomial treatment of the transverse leakage moments is studied by varying the cell size along axial direction. The reference results were obtained by the SFD code using a fairly standard mesh employed in PHWR calculations viz., 28.6 cm (one lattice pitch) in the X and Y directions and half a bundle length (24.75 cm) in the Z direction. The K-effective, axial flux distribution and channel powers obtained by the FDPEM code are compared with the reference results obtained using the SFD (24 axial meshes) code. At the outer boundary, a zero incoming current boundary condition is applied. The convergence criteria used for both eigenvalue and flux is 10^{-6}.

5.4.1.2 Results of PHWR Problem Simulation

The relative deviation of the K-effective obtained using the FDPEM code from the reference SFD value is shown in Table 5.2. While both quadratic and fourth order leakage approximations show good agreement with the reference SFD result, the quadratic leakage

approximation gives significant error for long cells (2 or 4 for the entire core length). The reference radial (channel) power distribution (normalised w.r.to the maximum channel power) of a quarter of the core obtained by SFD is shown in Table 5.3.

Table 5.2: Comparison of K-effective by FDPEM and SFD for PHWR

No. of axial cells	$(K_{SFD} - K_{FDPEM}) / K_{SFD}$ (pcm)	
	FDPEM-2nd order leakage	FDPEM-4th order leakage
24	1.5	1.5
12	1.4	1.5
6	3.8	1.5
4	19	1.5
2	179	1.4

Table 5.3: Radial (channel) power distribution of PHWR using SFD with 24 axial meshes

1.000	0.984	0.953	0.907	0.848	0.776	0.694	0.603	0.506	0.406	0.310
0.984	0.969	0.938	0.892	0.833	0.762	0.681	0.591	0.494	0.394	0.298
0.953	0.938	0.907	0.863	0.805	0.735	0.654	0.566	0.471	0.372	0.276
0.907	0.892	0.863	0.819	0.762	0.694	0.616	0.529	0.437	0.341	0.251
0.848	0.833	0.805	0.762	0.707	0.641	0.566	0.482	0.393	0.305	
0.776	0.762	0.735	0.694	0.641	0.578	0.506	0.426	0.342	0.261	
0.694	0.681	0.654	0.616	0.566	0.506	0.438	0.364	0.293		
0.603	0.591	0.566	0.529	0.482	0.426	0.364	0.304			
0.506	0.494	0.471	0.437	0.393	0.342	0.293				
0.406	0.394	0.372	0.341	0.305	0.261					
0.310	0.298	0.276	0.251							

The radial (channel) powers (of quarter core) obtained by FDPEM employing 24 and 2 axial cells are compared with reference channel powers and the % deviations ($\%\ \text{deviation} = \frac{Chann\quad power\ by\ SFD - Channe\quad power\ by\ FDPEM}{Channel\ Power\ by\ SFD} * 100$) are given in Tables 5.4 and 5.5 respectively. Even with two axial cells the % deviation in channel powers, with fourth order representation of the leakage, is less than 0.5%. As can be seen from Fig.5.2, the axial neutron flux distribution obtained by FDPEM employing 2 axial cells is in good agreement with that obtained by SFD code.

Table 5.4: % deviation in channel (radial) power obtained by FDPEM (fourth order leakage and 24 axial cells) from reference results (SFD-24 axial meshes) for PHWR

0.005	0.005	0.004	0.003	0.003	0.002	-0.002	-0.002	-0.003	-0.007	-0.013
0.005	0.004	0.004	0.004	0.002	0.000	0.000	0.000	-0.003	-0.007	-0.009
0.004	0.004	0.003	0.002	0.002	0.002	0.000	0.000	-0.003	-0.004	-0.010
0.003	0.004	0.002	0.002	0.000	0.000	-0.002	-0.003	-0.003	-0.004	-0.005
0.003	0.002	0.002	0.000	0.000	0.000	0.000	-0.003	-0.003	-0.004	
0.002	0.000	0.002	0.000	0.000	0.000	-0.003	-0.003	-0.004	0.000	
-0.002	0.000	0.000	-0.002	0.000	-0.003	-0.003	0.000	-0.005		
-0.002	0.000	0.000	-0.003	-0.003	-0.003	0.000	0.000			
-0.003	-0.003	-0.003	-0.003	-0.003	-0.004	-0.005				
-0.007	-0.007	-0.004	-0.004	-0.004	0.000					
-0.013	-0.009	-0.010	-0.005							

Table 5.5: % deviation in channel (radial) power obtained by FDPEM (fourth order leakage and 2 axial cells) from reference results (SFD-24 axial meshes) for PHWR

0.004	0.004	0.008	0.013	0.016	0.017	0.011	-0.009	-0.055	-0.147	-0.308
0.004	0.007	0.010	0.013	0.018	0.019	0.014	-0.002	-0.043	-0.124	-0.262
0.008	0.010	0.013	0.018	0.021	0.023	0.020	0.007	-0.023	-0.086	-0.187
0.013	0.013	0.018	0.021	0.028	0.029	0.030	0.020	0.000	-0.039	-0.111
0.016	0.018	0.021	0.028	0.032	0.035	0.035	0.033	0.020	-0.004	
0.017	0.019	0.023	0.029	0.035	0.041	0.045	0.040	0.039	0.020	
0.011	0.014	0.020	0.030	0.035	0.045	0.048	0.047	0.045		
-0.009	-0.002	0.007	0.023	0.033	0.040	0.047	0.052			
-0.055	-0.043	-0.023	0.000	0.020	0.039	0.045				
-0.147	-0.121	-0.082	-0.039	-0.004	0.020					
-0.308	-0.262	-0.187	-0.111							

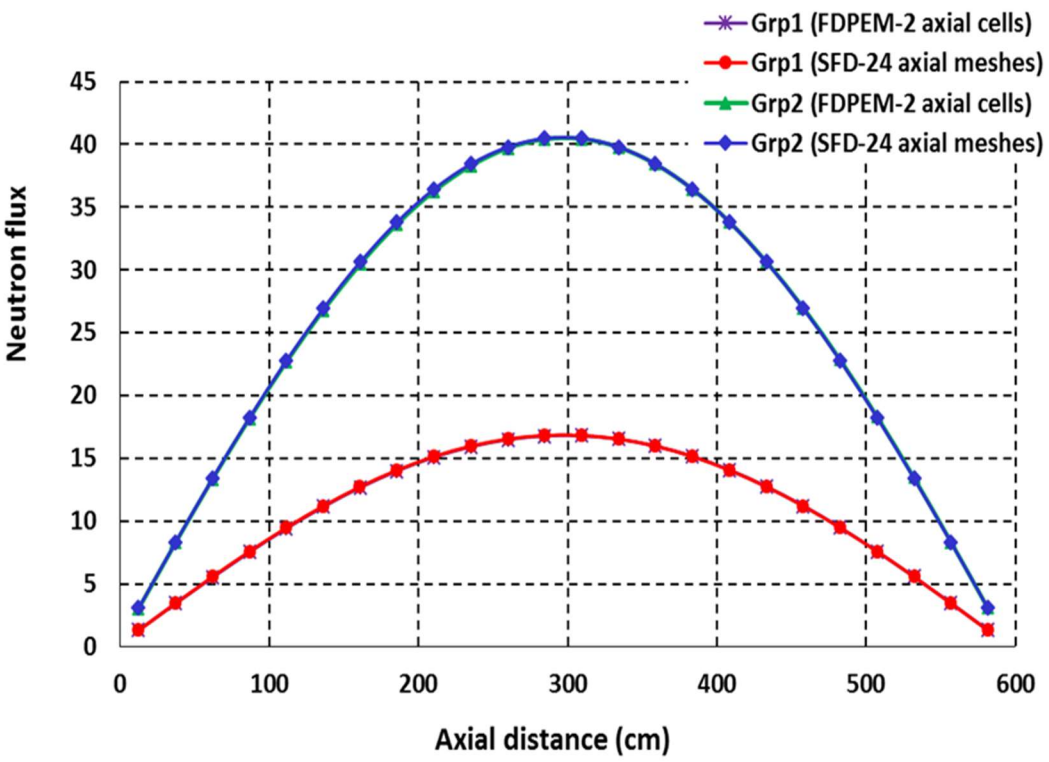

Figure 5.2: Comparison of axial neutron flux distribution at the radial center for PHWR core by FDPEM (2 axial cells) and SFD (24 axial meshes)

5.4.2 IAEA PWR Benchmark Problem

5.4.2.1 Description of the Problem and the Inputs

The core contains 177 fuel assemblies (FAs) and 64 reflector assemblies (RAs) as shown in Fig. 5.3. The FAs and RAs have the same pitch viz., 20 cm. There are 9 fully rodded FAs and 4 partially rodded FAs. The rods are inserted in the upper 80 cm of the active core height in the partially rodded FAs. The active height of the fuel assemblies is 340 cm and there is a 20 cm axial reflector region at the bottom and top of the core as shown in Fig. 5.3. Thus, there is some variation in the material properties along the direction of the Z axis, and the effect of varying the cell size along the Z direction on the eigenvalue and the power distribution is studied.

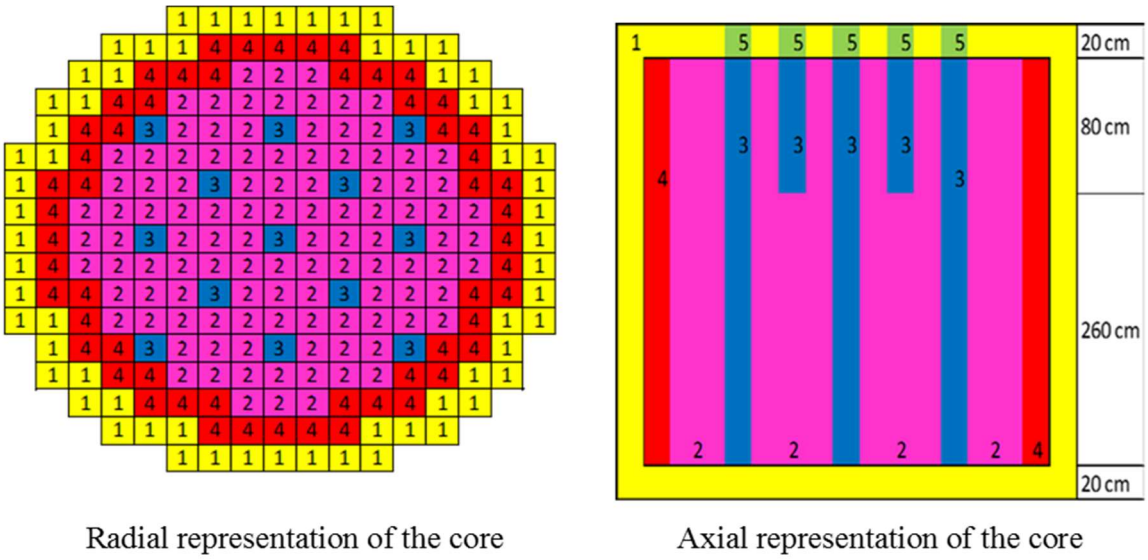

Radial representation of the core Axial representation of the core

Figure 5.3: Core Map of IAEA PWR Benchmark

In order to have fine cell F-D method along X and Y directions, each fuel assembly is divided into 12x12. The material cross sections used in the study are given in Table 5.6. At the outer boundary, a zero incoming current boundary condition is applied. The convergence criteria used for both eigenvalue and flux is 10^{-6}.

Table 5.6: Cross sections used in the IAEA PWR benchmark

Material		Group G	Σ_{ag} (cm^{-1})	$\nu\Sigma_{fg}$ (cm^{-1})	Σ_s1-G (cm^{-1})	D_g (cm)
1	Reflector	1	0.0	0.0	0.0	2.0
		2	0.01	0.0	0.04	0.3
2	Fuel 1	1	0.01	0.0	0.0	1.5
		2	0.085	0.135	0.02	0.4
3	Fuel1 + CR	1	0.01	0.0	0.0	1.5
		2	0.13	0.135	0.02	0.4
4	Fuel 2	1	0.01	0.0	0.0	1.5
		2	0.08	0.135	0.02	0.4
5	Reflector + CR	1	0.0	0.0	0.0	2.0
		2	0.055	0.0	0.04	0.3

The IAEA 3D benchmark problem is solved using both quadratic and 4^{th} order polynomial approximation of the transverse leakage moments. To check the effectiveness of the new method, the benchmark is analysed with various cell sizes along the Z-axis.

The reference solution [176] is the one obtained using the PARCS code that solves the 2-group neutron diffusion equation by ANM. In the PARCS code, the core is divided radially into 2x2 nodes per assembly, with the size of each node being 10 cm. Axially, the active core height (340 cm) is divided into 17 uniform axial nodes and one axial node each for the bottom and top reflector regions. Thus, each of the nodes is 20 cm long.

5.4.2.2 Results of IAEA PWR Benchmark Simulation

The K-effective obtained by the two methods for treating the transverse leakage moments are compared with the PARCS reference results in Table 5.7. The benchmark is analysed by full FD using SFD with 190 axial meshes, each axial mesh size is 2 cm. All the results agree within 10-20 pcm. The fourth order treatment of leakage moments gives good results even with 6 cells whereas the quadratic leakage model fails to give any meaningful result for this case.

Table 5.7: K-effective by FDPEM, SFD and PARCS codes for the IAEA PWR benchmark

No. of cells along Z	Cell size (cm)	$(K_{PARCS} - K_{eff}) / K_{PARCS}$ (pcm)		
		K_{eff} by FDPEM (quadratic leakage)	K_{eff} by FDPEM (4^{th} order leakage)	K_{eff} by SFD
19	20 (uniform)	14	14	
8	20, 4*65, 2*40, 20	30	20	
6	20, 20,110,130, 80, 20	-	21	
190	2 (uniform)			11

Table 5.8 gives a comparison of the FA powers obtained by FDPEM, using second order transverse leakage moments and 19 axial cells each of 20 cm length, with the reference FA power obtained by the PARCS. The maximum deviation in FA power is 2.76% and RMS is 1.212. The same comparison is shown in Table 5.9 but with fourth order representation for transverse leakage moments. In this case, the maximum deviation is 2.76% and RMS is 1.214. The FA powers are in good agreement with both the leakage approximations as the number of axial cells employed is adequate for both cases.

Table 5.8: Comparison of FA powers by PARCS and FDPEM-with quadratic leakage

0.7264	1.2742	1.4156	1.1884	0.6097	0.9524	0.9607	0.7798	PARCS
0.7305	1.2923	1.4314	1.2024	0.6096	0.9557	0.9567	0.7672	FDPEM
-0.57	-1.42	-1.11	-1.17	0.02	-0.35	0.41	1.61	(PARCS-FDPEM)*100/PARCS
1.2742	1.3899	1.4248	1.2856	1.0685	1.0543	0.9768	0.7600	
1.2923	1.4066	1.4399	1.2976	1.0771	1.0558	0.9719	0.7470	
-1.42	-1.20	-1.06	-0.93	-0.80	-0.14	0.50	1.71	
1.4156	1.4248	1.3627	1.3065	1.1785	1.0888	1.0016	0.7152	
1.4314	1.4399	1.3737	1.3166	1.1841	1.0883	0.9948	0.6961	
-1.11	-1.06	-0.81	-0.77	-0.47	0.05	0.68	2.67	
1.1884	1.2856	1.3065	1.1751	0.9702	0.9238	0.8698		
1.2024	1.2976	1.3166	1.1826	0.9750	0.9209	0.8551		
-1.17	-0.93	-0.77	-0.64	-0.49	0.31	1.70		
0.6097	1.0685	1.1785	0.9702	0.4766	0.7015	0.6150		
0.6096	1.0771	1.1841	0.9750	0.4727	0.6974	0.5980		
0.02	-0.80	-0.47	-0.49	0.81	0.58	2.76		
0.9524	1.0543	1.0888	0.9238	0.7015	0.6017			
0.9557	1.0558	1.0883	0.9209	0.6974	0.5857			
-0.35	-0.14	0.05	0.31	0.58	2.67			
0.9607	0.9768	1.0016	0.8698	0.6150				
0.9567	0.9719	0.9948	0.8551	0.5980				
0.41	0.50	0.68	1.70	2.76				
0.7798	0.7600	0.7152						
0.7672	0.7470	0.6961						
1.61	1.71	2.67						

Table 5.9: Comparison of FA powers by PARCS and FDPEM-with fourth order leakage

0.7264	1.2742	1.4156	1.1884	0.6097	0.9524	0.9607	0.7798	PARCS
0.7306	1.2923	1.4314	1.2024	0.6096	0.9557	0.9567	0.7672	FDPEM
-0.57	-1.42	-1.12	-1.18	0.02	-0.35	0.41	1.61	(PARCS- FDPEM)*100/PARCS
1.2742	1.3899	1.4248	1.2856	1.0685	1.0543	0.9768	0.7600	
1.2923	1.4067	1.4399	1.2976	1.0771	1.0558	0.9719	0.7470	
-1.42	-1.21	-1.06	-0.94	-0.80	-0.14	0.51	1.71	
1.4156	1.4248	1.3627	1.3065	1.1785	1.0888	1.0016	0.7152	
1.4314	1.4399	1.3737	1.3166	1.1841	1.0883	0.9947	0.6961	
-1.12	-1.06	-0.81	-0.77	-0.47	0.05	0.68	2.68	
1.1884	1.2856	1.3065	1.1751	0.9702	0.9238	0.8698		
1.2024	1.2976	1.3166	1.1826	0.9750	0.9209	0.8550		
-1.18	-0.94	-0.77	-0.64	-0.49	0.31	1.70		
0.6097	1.0685	1.1785	0.9702	0.4766	0.7015	0.6150		
0.6096	1.0771	1.1841	0.9750	0.4728	0.6974	0.5980		
0.02	-0.80	-0.47	-0.49	0.80	0.58	2.76		
0.9524	1.0543	1.0888	0.9238	0.7015	0.6017			
0.9557	1.0558	1.0883	0.9209	0.6974	0.5857			
-0.35	-0.14	0.05	0.31	0.58	2.67			
0.9607	0.9768	1.0016	0.8698	0.6150				
0.9567	0.9719	0.9947	0.8550	0.5980				
0.41	0.51	0.68	1.70	2.76				
0.7798	0.7600	0.7152						
0.7672	0.7470	0.6961						
1.61	1.71	2.68						

Table 5.10 shows comparison of FA powers obtained by FDPEM using fourth order representation of the transverse leakage and 19 cells along the Z-axis, with the same code and leakage representation but only 6 cells along the Z axis. The table also shows comparison of the FA powers obtained by FDPEM (4^{th} order leakage and 6 axial cells) and SFD (190 axial meshes). The maximum difference in FA power is 0.06%. This is an interesting result as it shows that for the relatively more complex problem of the PWR, even with a very coarse division into cells along Z-axis, the 4^{th} order transverse leakage moments give accurate estimates of the K-effective and the assembly power distribution.

Table 5.10: % Deviation of FA powers obtained by FDPEM with fourth order leakage (Case a: 19 axial cells, Case b: 6 axial cells) and SFD (Case c: 190 axial meshes) for IAEA PWR benchmark

-0.056 -0.058	-0.050 -0.051	-0.046 -0.048	-0.032 -0.033	-0.012 -0.012	0.038 0.035	0.057 0.055	0.060 0.059	(Case a-Case b)*100/Case a (Case c-Case b)*100/Case c
-0.050 -0.051	-0.057 -0.058	-0.068 -0.068	-0.039 -0.040	0.002 0.000	0.037 0.034	0.056 0.053	0.060 0.058	
-0.046 -0.048	-0.068 -0.068	-0.139 -0.138	-0.050 -0.052	0.004 0.001	0.036 0.033	0.052 0.050	0.054 0.053	
-0.032 -0.033	-0.039 -0.040	-0.050 -0.052	-0.024 -0.026	0.009 0.007	0.038 0.036	0.047 0.046		
-0.012 -0.012	0.002 0.000	0.004 0.001	0.009 0.007	0.009 0.010	0.040 0.038	0.044 0.044		
0.038 0.035	0.037 0.034	0.036 0.033	0.038 0.036	0.040 0.038	0.039 0.040			
0.057 0.055	0.056 0.053	0.052 0.050	0.047 0.046	0.044 0.044				
0.060 0.059	0.060 0.058	0.054 0.053						

The axial neutron flux distributions in three selected FAs obtained by FDPEM (using fourth order treatment of the transverse leakage) and SFD are shown in Figures 5.4, 5.5 and 5.6. The figures show that even with very few axial cells, the method correctly reproduces the details of the axial flux distortions due to the reflector and control rods.

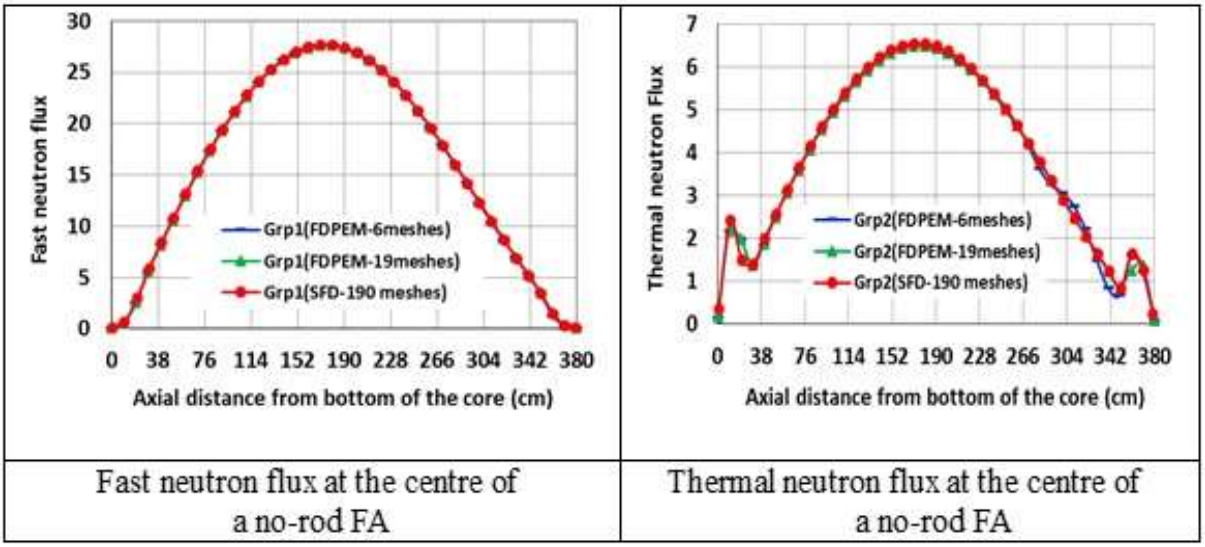

Fast neutron flux at the centre of a no-rod FA | Thermal neutron flux at the centre of a no-rod FA

Figure 5.4: Axial flux distribution at the center of a no-rod FA of IAEA PWR benchmark by FDPEM (6 and 19 axial cells) and SFD (190 axial meshes)

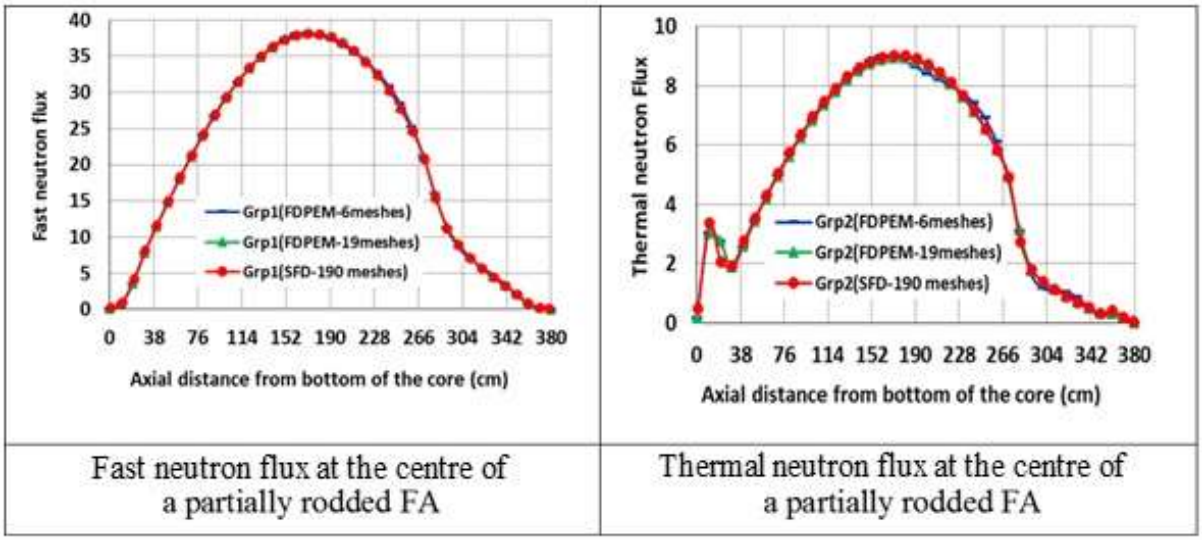

Fast neutron flux at the centre of a partially rodded FA | Thermal neutron flux at the centre of a partially rodded FA

Figure 5.5: Axial flux distribution at center of a partially rodded FA of IAEA PWR benchmark by FDPEM (6 and 19 axial cells) and SFD (190 axial meshes)

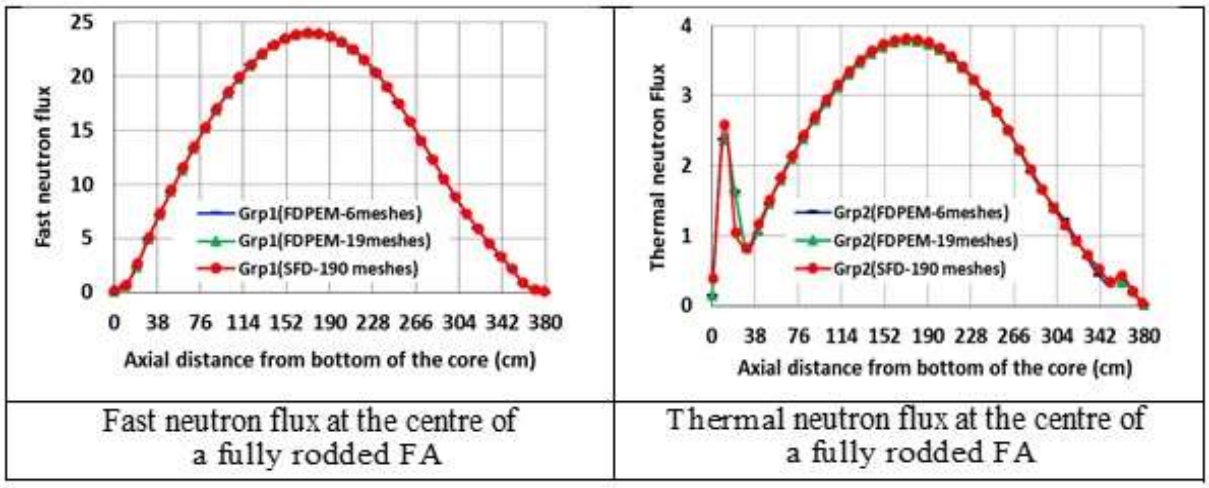

Figure 5.6: Axial flux distribution at the center of a fully rodded FA of IAEA PWR benchmark by FDPEM (6 and 19 axial cells) and SFD (190 axial meshes)

Comparison of the time taken for the solution by full FD (SFD) and FDPEM codes was made. In the case of full FD, 190 axial meshes (of size 2 cm) is required to obtain the correct result. For the convergence criteria of 10^{-6} for both flux and K-effective, the time taken by FDPEM employing 6 axial cells is $¼^{th}$ of that by SFD with 190 meshes. With increasing number of axial cells, the time taken by FDPEM increases and with 19 axial cells it is about same as that by SFD code (with 190 meshes). As seen above, 6 axial divisions are adequate to represent the problem and hence there is substantial savings in computing time.

5.5 Summary

A method for performing pin by pin few group diffusion theory calculations at the core level for light water reactors is developed. It is a hybrid of the finite difference method (in radial i.e. x-y directions) and a fourth order polynomial expansion method (in the axial i.e. z direction along the fuel length) with a more accurate (fourth order) treatment of the transverse leakage. This treatment permits the use of long cells in the z direction, and thereby mitigates the extra computational burden associated with the small sized transverse meshes used in pin

by pin level core calculations. For very long cells, it may not be possible to assume constancy of cross sections within a cell. The theoretical treatment is therefore generalised to permit a linear (axial) variation of cross sections and diffusion coefficients within a cell. With this additional feature, the method permits the use of very few axial divisions and is expected to be useful in pin by pin core calculations. The computer code FDPEM developed based on the method is verified using two benchmark problems. The principal quantities of interest, like K-effective, axial and radial power distributions, obtained by FDPEM even with very few axial cells show good agreement with the reference results. The code FDPEM can be used to obtain the pin power distribution of advanced LWRs like EPR. The method can be extended to treat the hexagonal meshes as in VVER type reactors.

CHAPTER 6

CONCLUSION AND SCOPE OF FUTURE WORK

In the research work presented in the thesis, the development of new methods for the reactor physics analysis of LWRs is described. To obtain the detailed flux distribution and K-effective of the reactor, the best way is by performing full core calculations in fine energy groups using transport theory or by continuous energy Monte Carlo method. These methods are already being attempted and successfully implemented. However, even with the present computational capability, considering the complexity and heterogeneity of advanced reactor systems, these methods appear to be impractical for routine reactor analysis. This necessitates applying some approximations and simplifying assumptions for obtaining the required solution.

In the traditional approach, the reactor physics analysis is normally carried out in a two-step process. The first step is the lattice calculations wherein the two-dimensional neutron transport equation is solved for obtaining the detailed spectrum and spatial flux distribution within a representative region called the lattice cell. This is followed by lattice homogenization that provides the few group homogenized cross sections and diffusion coefficients which forms the input for the second step of the calculation. It is important that the few group diffusion theory parameters are carefully generated so that reaction rates and leakage rates in the lattice cell volume are preserved. While the homogenized cross sections may be generated by flux-volume weighted homogenization of the individual material cross sections, a special treatment is required for the generation of the diffusion coefficient. In the second step, the few group neutron diffusion equation is solved to obtain the three-dimensional flux/power distribution for the reactor core. For the reason mentioned in the first paragraph, it is worth examining the possibilities of developing improved computational methods for both these steps. The aim of the work described in this thesis has been to develop methods / codes for each of the steps of

the computation, so that detailed pin wise power distribution and the status of the reactor core can be estimated accurately.

Towards this aim (as regards the first step in the two-step process), the BOXER3 code was developed as a multi-group transport theory based lattice and burnup code for simulating the fuel assemblies of LWRs. The code has the capability to solve the neutron transport equation with three methods viz: Collision Probability (CP) method, combination of CP and interface current method and the MOC. The solution by MOC enables the treatment of anisotropic scattering. The availability of three options for obtaining the transport solution combined with other features like a new method for normalizing the collision probabilities, solution of burnup equations with the predictor- corrector method, calculation of pin-dependent Dancoff factors, inclusion of leakage corrected collision probabilities to obtain the leakage corrected fine-group flux distribution and a new formula for obtaining the axial diffusion coefficient, makes the code an advanced tool for lattice calculations of LWRs.

The code and the method have been verified extensively. Verification of the code through analyses of benchmarks is also discussed in the thesis. The agreement of the results with that of other codes are fairly good for the lattice without any Gd pins. It is observed that burnup simulation with pins containing Gd burnable absorber poses special difficulties. Even with the predictor-corrector method employing fairly short burnup steps of 1.0 GWd/Te and using different burnup zones to represent each of the annular divisions of a Gd-containing fuel pin, the K- infinity showed deviations of about 700 to 800 pcm for the FA lattice with Gd bearing pins. To overcome this problem, an improved method for burnup solutions such as the projected predictor-corrector method is proposed to be implemented in the code in future.

A new method for obtaining the leakage corrected flux distribution in the lattice calculations that may be used in the homogenization procedure, has been developed and is described in the thesis. The homogenized cross sections are traditionally obtained by a flux

volume weighting procedure. This is followed by a P1 / B1 calculation for obtaining the leakage corrected spectrum and the few group reaction cross sections and diffusion coefficients. The procedure accounts (at least approximately) for the change in cell spectrum, but not for the altered spatial distribution of the flux. To account for both these effects, the leakage correction is carried out, with the help of the leakage corrected collision probabilities, during the lattice calculation of the heterogeneous medium. The flux distribution thus obtained is then used to generate the few group cross sections and the homogenised diffusion coefficients.

The development of a method for obtaining the axial diffusion coefficient also forms a part of the thesis. As stated above, the traditional method involves flux volume weighted homogenization of the cross sections followed by solution of the P1 or B1 equations which yields the diffusion coefficient. The method described in the thesis on the other hand prescribes a new method for obtaining the homogenized diffusion coefficient that is theoretically more satisfactory and also gives improved numerical results. It is based on a derivation of Fick's law (that is the net current is proportional to the flux gradient in the axial direction with diffusion coefficient being the proportionality constant) in the heterogeneous medium of the lattice. The formalism developed in the present work is particularly suitable for implementation in lattice codes employing CP method for its solution. The method is incorporated in the lattice code BOXER3. Comparisons of core calculations using the homogenised diffusion coefficients obtained by the method proposed in the thesis, with Monte Carlo calculations show that they perform better than the standard methods used for this purpose.

The research has also focused on new approaches for core simulations. In the second step (3-D core calculations for the solution of diffusion equation in few energy groups), a new method that uses a combination of the finite difference (FD) along the X and Y directions and the polynomial expansion method along Z-direction is developed. Though there have been a few studies on the use of combined FD and polynomial expansion method for core calculations,

the treatment of transverse leakage by a fourth order polynomial instead of the usual quadratic expansion represents an improvement. Another new feature is the relaxation of the assumption of uniform material properties in a mesh. As the irradiation proceeds, the cross sections and diffusion coefficient varies along the length of the fuel because of the axial flux shape. Other factors that cause the non-uniformity along the axial direction are the temperature and density variations of the coolant. The treatment of the effect of this non-uniformity on cross sections and diffusion coefficient within a mesh, together with the use of a fourth order polynomial expansion for flux (in the axial i.e. z direction along the fuel length) and the transverse leakage in the diffusion theory code, permits the use of very few axial divisions and is therefore economical in detailed pin by pin core calculations. A code called FDPEM based on the new method has been developed. The benchmark studies on LWR core calculations carried out using the code FDPEM show good agreement in the principal quantities of interest, (viz., the K- effective and the axial and radial power distributions) between results obtained by FDPEM and reference results and substantial savings in computer time over the more elaborate finite difference method. The code can therefore be used to obtain the detailed (pin wise) flux/power distribution of the LWR core efficiently without compromising on the accuracy.

The developments discussed in the thesis have been directly applied to square pitch heterogeneous LWR lattices and cores. They represent an important advancement in the methods for lattice and core calculations of such reactors. A similar development is proposed to be carried out for the case of hexagonal geometry that appears in VVER type of reactors in future. Other developments proposed to be carried out in future are as follows:

It is proposed to implement the improvement in the treatment of burnup involving Gd bearing pins mentioned above. Another proposed development is to obtain a B1 corrected diffusion coefficient of heterogeneous lattices. It is also proposed to extend the numerical studies on obtaining homogenized diffusion coefficient by the proposed method to the more

complex lattice calculations of LWRs as the studies described in the thesis were limited to simple pin cells in two groups. Finally, it is proposed to study the application of acceleration techniques for speeding up the convergence of the iteration process in the solution of the transport / diffusion equation.

APPENDIX – A

Analytical solution of the two-group diffusion theory equations with zero incoming current boundary conditions

Two group equations for a bare slab reactor

Consider a bare homogeneous slab reactor between $z = -H/2$ and $z = +H/2$. The two group equations for a slab that is finite in the z direction may be written in standard notation (with k written for the k_{eff}) in the form

$$D_1 \frac{d^2\phi_1}{dz^2} - \Sigma_{r1}\phi_1 + \Sigma_{21}\phi_2 + \frac{\nu\Sigma_{f1}\phi_1}{k} + \frac{\nu\Sigma_{f2}\phi_2}{k} = 0 \tag{A1}$$

$$D_2 \frac{d^2\phi_2}{dz^2} - \Sigma_{r2}\phi_2 + \Sigma_{12}\phi_1 = 0 \tag{A2}$$

where,

$$\Sigma_{r1} = \Sigma_{a1} + \Sigma_{12} \tag{A1a}$$

$$\Sigma_{r2} = \Sigma_{a2} + \Sigma_{21} \tag{A2a}$$

Solution of the equations

Let us write the solution in the form

$$\phi = \cos Bz \tag{A3}$$

so that

$$\frac{d^2\phi}{dz^2} = -B^2\phi \tag{A4}$$

With this substitution, Eqs. (A1) and (A2) above can be re-written in the form

$$-D_1B^2\phi_1 - \Sigma_{r1}\phi_1 + \Sigma_{21}\phi_2 + \frac{\nu\Sigma_{f1}\phi_1}{k} + \frac{\nu\Sigma_{f2}\phi_2}{k} = 0 \tag{A5}$$

$$-D_2B^2\phi_2 - \Sigma_{r2}\phi_2 + \Sigma_{12}\phi_1 = 0 \tag{A6}$$

The second of the above equations yields,

$$\phi_2 = \frac{\Sigma_{12}\phi_1}{D_2 B^2 + \Sigma_{r2}} \tag{A7}$$

On substituting Eq. (A7) in Eq. (A5) the result is

$$D_1 D_2 B^4 + \left(D_1\Sigma_{r2} + D_2\Sigma_{r1} - \frac{D_2\nu\Sigma_{f1}}{k}\right)B^2 + \left[\Sigma_{r1}\Sigma_{r2} - \frac{\Sigma_{r2}\nu\Sigma_{f1}}{k} - \Sigma_{12}\left(\Sigma_{21} + \frac{\nu\Sigma_{f2}}{k}\right)\right] \tag{A8}$$

Eq. (A8) is a quadratic in B^2 and has one positive root, which is refer to as B_1^2, and corresponds to the material buckling, while the other root, $-B_2^2$, (where B_2^2 is positive) is negative. Due to symmetry of the flux about the origin, it is clear that the flux would involve only the symmetric functions (viz. cosine and hyperbolic cosine) and hence the general solution for the first group may be written as follows

$$\phi_1 = A\cos B_1 z + C\cosh B_2 z \tag{A9}$$

Due to the relation (A7) between the fast and thermal solutions, the general solution for the second group flux is easily seen to be

$$\phi_2 = \Sigma_{12}\left(\frac{A}{D_2 B_1^2 + \Sigma_{r2}}\cos B_1 z + \frac{C}{-D_2 B_2^2 + \Sigma_{r2}}\cosh B_2 z\right) \tag{A10}$$

Boundary conditions

It is possible to write down the following relation starting from the zero incoming current boundary condition

$$\phi + \delta\frac{d\phi}{dz} = 0 \tag{A11}$$

where $\delta = 2D$. Based on the asymptotic solution of the Milne problem in transport theory [4], the above expression for δ can be corrected to $\delta = 2.131D$. This boundary condition is employed. Due to the symmetry of the problem, it is enough to apply the boundary condition at the right boundary. Applying this boundary condition, to the solutions given by Eqs. (A9) and (A10), obtain

$$\left(\cos\frac{B_1H}{2} - B_1\delta_1\sin\frac{B_1H}{2}\right)A + \left(\cosh\frac{B_2H}{2} + B_2\delta_1\sinh\frac{B_2H}{2}\right)C = 0 \tag{A12}$$

$$\frac{\cos\frac{B_1H}{2} - B_1\delta_2\sin\frac{B_1H}{2}}{D_2B_1^2 + \Sigma_{r2}}A + \frac{\cosh\frac{B_2H}{2} + B_2\delta_2\sinh\frac{B_2H}{2}}{-D_2B_2^2 + \Sigma_{r2}}C = 0 \tag{A13}$$

The system of equations (A12) and (A13) has a non-trivial solution if the determinant of the coefficient matrix is zero. This is the criticality condition. In all practical situations the argument (B_2H) of the hyperbolic function is so large that we may replace, without any perceptible error, both the hyperbolic sine and cosine functions by the exponential function. This enables us to write down a simple formula for the critical height.

$$\frac{\cos\frac{B_1H}{2} - B_1\delta_1\sin\frac{B_1H}{2}}{\cos\frac{B_1H}{2} - B_1\delta_2\sin\frac{B_1H}{2}} = \beta \tag{A14}$$

where,

$$\beta = \left(\frac{-D_2B_2^2 + \Sigma_{r2}}{D_2B_1^2 + \Sigma_{r2}}\right)\left(\frac{1 + B_2\delta_1}{1 + B_2\delta_2}\right) \tag{A14a}$$

Eq. (A14) is easily solved for H and get

$$H = \frac{\pi}{B_1} + 2\varphi_2 \tag{A15}$$

where,

$$\varphi_2 = \tan^{-1}\frac{B_1(\delta_1 - \delta_2\beta)}{(1 - \beta)} \tag{A15a}$$

Eq. (A15) allows us to obtain the height for a given K-eff. Often one is interested in the k_{eff} as a function of height. For this, one assumes a guess value of the k_{eff}, and uses it to obtain B_1 and B_2 by solving Eq. (A8). These are used to obtain the critical height using Eq. (A15). If the height is different from the height of the slab, one has to adjust k_{eff} and obtain the critical height again.

APPENDIX – B

Combined polynomial expansion and finite difference method with linearly varying cross sections within a cell

Since the proposed method permits the use of very long meshes, the assumption that cross sections and diffusion coefficients are constant within a cell may not be correct owing to burnup, temperature and moderator density variation along the z direction within a cell. A linear representation of the cross sections and diffusion coefficients might be adequate as these variations are slow. In this appendix, the modification required in the formulation for linear variation is given. Extension to a quadratic variation is also fairly straightforward.

The main difference from the case of constant cross sections is that the equations for the average flux and first moment involve higher moments and the equation for the second moment involves the third moment which is not calculated. Hence instead of using the average flux and its moments as unknowns, the average flux and expansion coefficients are unknowns and write the conservation equation and the two weighted residuals equations in terms of the expansion coefficients and the average flux. The remaining two equations are written down for the incoming currents that are assumed to be known quantities (from boundary conditions or previous iterations). Assume the following linear variation of removal and other cross sections, and the diffusion coefficient,

$$\Sigma_g^r(z) = \Sigma_g^{r0} + \Sigma_g^{r1}.z,$$

$$\Sigma_g^x(z) = \Sigma_g^{x0} + \Sigma_g^{x1}.z$$

$$D_g(z) = \mathrm{D}_g^0 + \mathrm{D}_g^1.z$$

And the one-dimensional transverse integrated equation becomes

$$-\left(D_g^0 + \mathrm{D}_g^1 z\right)\frac{d^2\bar{\phi}_{zg}^{ijk}}{dz^2} + \left(\Sigma_g^{r0} + \Sigma_g^{r1}.z\right)\bar{\phi}_{zg}^{ijk} = \bar{Q}_{gz}^{ijk} - \frac{1}{\Delta x}L_{gx}^{ijk} - \frac{1}{\Delta y}L_{gy}^{ijk} \qquad \text{(B1)}$$

or,

$$-\left(D_g^0 + \mathrm{D}_g^1 z\right)\frac{d^2\bar{\phi}_{zg}^{ijk}}{dz^2} + \left(\Sigma'^{r0}_g + \Sigma'^{r1}_g . z\right)\bar{\phi}_{zg}^{ijk} = \bar{Q}'^{ijk}_{gz} \tag{B2}$$

where transverse leakage terms are clubbed the with the removal and source terms as discussed in chapter5 of the thesis.

$$\Sigma'^{r}_g = \Sigma^r_g + \left(c_g^{i,i+1jk} + c_g^{i,i-1jk} + c_g^{ij,j+1k} + c_g^{ij,j-1k}\right) \tag{B3}$$

$$\bar{Q}'^{ijk}_g = \bar{Q}^{ijk}_g + \left(c_g^{i,i+1jk}\bar{\Phi}_g^{i+1jk} + c_g^{i,i-1jk}\bar{\Phi}_g^{i-1jk} + c_g^{ij,j+1k}\bar{\Phi}_g^{ij+1k} + c_g^{ij,j-1k}\bar{\Phi}_g^{ij-1k}\right) \tag{B4}$$

As before, the solution of the problem consists of finding the five unknown expansion coefficients $\bar{\Phi}_g^{ijk}$, a_1, a_2, a_3 and a_4. As there are five unknowns, total of five equations are needed. The first two are obtained from the equations for the incoming currents $J_{gz+}^{ijk,in}$ and $J_{gz-}^{ijk,in}$ viz.,

$$J_{gz+}^{ijk,in} = \frac{\bar{\Phi}_g^{ijk}}{4} + a_1\left(\frac{\mathrm{D}_g^0}{2.\Delta z} + \frac{\mathrm{D}_g^1}{4} + \frac{1}{8}\right) + a_2\left(\frac{3\mathrm{D}_g^0}{2.\Delta z} + \frac{3\mathrm{D}_g^1}{4} + \frac{1}{8}\right) + a_3\left(\frac{\mathrm{D}_g^0}{4.\Delta z} + \frac{\mathrm{D}_g^1}{8}\right) + a_4\left(\frac{\mathrm{D}_g^0}{10.\Delta z} + \frac{\mathrm{D}_g^1}{20}\right) \tag{B5}$$

$$J_{gz-}^{ijk,in} = \frac{\bar{\Phi}_g^{ijk}}{4} - a_1\left(\frac{D_g^0}{2.\Delta z} + \frac{D_g^1}{4} + \frac{1}{8}\right) + a_2\left(\frac{3D_g^0}{2.\Delta z} + \frac{3D_g^1}{4} + \frac{1}{8}\right) - a_3\left(\frac{D_g^0}{4.\Delta z} + \frac{D_g^1}{8}\right) + a_4\left(\frac{D_g^0}{10.\Delta z} + \frac{D_g^1}{20}\right) \tag{B6}$$

Multiplication of Eq.B2 with the weight functions

$$w_0(z) = 1, \quad w_1(z) = \frac{z}{\Delta z}, \quad w_2(z) = \frac{3z^2}{\Delta z^2} - \frac{1}{4}$$

and integrating over z yields the remaining three equations for finding the unknowns $\bar{\Phi}_g^{ijk}$, a_1, a_2, a_3 and a_4. Multiplying Eq.B2 with $w_0(z)$ and integrating over z gives

$$\Sigma'^{r0}_g\bar{\Phi}_g^{ijk} + \left(\frac{\Sigma'^{r1}_g\Delta z}{12} - \frac{\mathrm{D}_g^1}{\Delta z}\right)a_1 - \frac{6D_g^0}{\Delta z^2}a_2 - \left(\frac{\Sigma'^{r1}_g\Delta z}{120} + \frac{\mathrm{D}_g^1}{2.\Delta z}\right)a_3 - \frac{2D_g^0}{5\Delta z^2}a_4 = \bar{Q}'^{ijk}_0 \tag{B7}$$

Multiplying Eq.B1 with $w_1(z)$ and integrating over z gives

$$\frac{\Sigma'^{r1}_g \Delta z}{12}\bar{\Phi}^{ijk}_g + \frac{\Sigma'^{r1}_g}{12}a_1 + \left(\frac{\Sigma'^{r1}_g \Delta z}{60} - \frac{D^1_g}{\Delta z}\right)a_2 - \left(\frac{D^0_g}{2\Delta z^2} + \frac{\Sigma'^{r1}_g}{120}\right)a_3 - \left(\frac{\Sigma'^{r1}_g \Delta z}{2100} + \frac{D^1_g}{10.\Delta z}\right)a_4 = \bar{Q}'^{ijk}_1 \quad \text{(B8)}$$

Multiplying Eq.B1 with $w_2(z)$ and integrating over z gives

$$\left(\frac{\Sigma^{r1}_g \Delta z}{60} + \frac{\mathrm{D}^1_g}{\Delta z} - \frac{\mathrm{D}^1_g}{\Delta z^2}\right)a_1 + \frac{\Sigma'^{r}_g}{20}a_2 - \left(\frac{\Sigma^{r1}_g \Delta z}{1680} + \frac{\mathrm{D}^1_g}{4\Delta z} - \frac{\mathrm{D}^1_g}{10.\Delta z^2}\right)a_3 - \left(\frac{D^0_g}{5\Delta z^2} + \frac{\Sigma^{r1}_g}{700}\right)a_4 = \bar{Q}'^{ijk}_2 \quad \text{(B9)}$$

The set of equations [Eqs. (B5) to (B9)] are linear in the expansion coefficients and are solved simultaneously to yield the flux distribution in a node for a given source and in currents. Definition of c_g is as per the definition given in equation (5.3a). It is assumed that the quantities c_g that depend upon the diffusion coefficients in the given node and the neighbouring node also vary linearly with z. Calculation of the moments of the terms pertaining to the source and removal (together with the contributions coming from the transverse leakage terms), requires calculation of integrals of the product of the flux and a linear function and the weight function. This is done as follows:

For any linear function,

$$X(z) = X^0 + X^1.z \quad \text{(B10)}$$

the 0th order moment of $X(z)\bar{\phi}^{ijk}_{zg}$ is

$$\int w_0(z)\, X(z)\, \bar{\phi}^{ijk}_{zg}\, dz = X^0\bar{\Phi}^{ijk}_g + \frac{X^1\Delta z}{12}a_1 - \frac{X^1\Delta z}{120}a_3 \quad \text{(B11)}$$

Likewise, the 1st and 2nd order moments of $X(z)\bar{\phi}^{ijk}_{zg}$ are

$$\int w_1(z)\, X(z)\, \bar{\phi}^{ijk}_{zg}\, dz = \frac{X^1\Delta z}{12}\bar{\Phi}^{ijk}_g + \frac{X^0}{12}a_1 + \frac{X^1\Delta z}{60}a2 - \frac{X^0}{120}a_3 - \frac{X^1\Delta z}{2100}a4 \quad \text{(B12)}$$

$$\int w_2(z)\, X(z)\, \bar{\phi}^{ijk}_{zg}\, dz = \frac{X^1\Delta z}{60}a_1 + \frac{X^0}{20}a2 - \frac{X^1\Delta z}{1680}a_3 - \frac{X^0}{700}a4 \quad \text{(B13)}$$

REFERENCES

1. Samuel Glasstone and Alexander Sesonske, 'Nuclear Reactor Engineering', CBS publishers & distributors, 1998.

2. S. A. Bhardwaj, 'Indian Nuclear Power Programme - Past, Present and Future', Sadhana **38**, Part 5, pp. 775–794, Indian Academy of Sciences, October 2013.

3. Annual report of NPCIL for 2016-17 and 2017-18, available on-line.

4. G.I. Bell, S. Glasstone. 'Nuclear reactor theory', Van Nostrand Reinhold Company, New York, 1970.

5. E. E. Lewis, W. F. Miller, 'Computational methods of neutron transport'. American Nuclear Society, Lagrange Park. Originally published by Wiley- Inter science, 1984.

6. F. Leszczynski, D. López Aldama, and A. Trkov, 'WIMS-D Library Update', STI/PUB/1264, International Atomic Energy Agency, 2007.

7. Sherly Ray, S. B. Degweker, Rashmi Rai, and K. P. Singh, 'A Collision Probability and MOC-Based Lattice and Burnup Code for Analysis of LWR Fuel Assemblies'. Nuclear Science and Engineering, volume 184 (473–494), December 2016. http://dx.doi.org/10.13182/NSE15-127.

8. Sherly Ray, S.B. Degweker, Umasankari Kannan, 'A hybrid method for reactor core simulations employing finite difference and polynomial expansion with improved treatment of transverse leakage'. Annals of Nuclear Energy 131 (2019) 102–111. https://doi.org/10.1016/j.anucene.2019.03.028

9. Joo Han Gyu., Cho Jin Young., Kim Kang Seog., Lee Chung Chan., Zee Sung Quun, 'Methods and Performance of a Three-Dimensional Whole-Core Transport Code DeCART', PHYSOR 2004-The Physics of Fuel Cycles and Advanced Nuclear Systems:

Global Developments Chicago, Illinois, April 25-29, on CD-ROM, American Nuclear Society, Lagrange Park, IL, 2004.

10. Richard Sanchez, ‘Prospects in deterministic three-dimensional whole-core transport calculations’, 2012, http://dx.doi.org/10.5516/NET.01.2012.501.
11. Sho Takano, Akiyuki Tsuchiya, Akiko Toishigawa, Shingo FUJIMAKI and Tadashi IKEHARA, ‘Commercial BWR Whole Core Calculations with MCNP5’, Progress in Nuclear Science and Technology, Vol. 2, pp.267-273, 2011.
12. R. E. MacFarlane, D. W. Muir, R. M Boicourt, A. C. Kahler, ‘The NJOY Nuclear Data Processing System, Version 2012’, LA-UR-12-27079, 2012.
13. D.E. Cullen, ‘PREPRO 2017: 2012 ENDF/B Pre-processing Codes’, IAEA-NDS-39, Rev. 17 (May 4, 2017).
14. J. R. Askew, F.J. Fayers, and P. B. Kemshell, ‘A General Description of the Lattice Cell Code WIMS’, Journal of the British Nuclear Energy Society, 1966.
15. Y. Ishiguro, ‘PEACO-II: a code for calculation of effective cross sections in heterogeneous systems’, JAERI-M 5527, 1974.
16. Naoki Sugimura and Akio Yamamoto, ‘Resonance Treatment Based on Ultra-fine-group Spectrum Calculation in the AEGIS Code’, Journal of Nuclear Science and Technology, Vol. 44, No. 7, p. 958–966 (2007).
17. Zhang, Q., Wu, H., Cao, L., and Zheng, Y., ‘An improved resonance self-shielding calculation method based on equivalence theory’. Nuclear Sci. Eng. 179, 233–252. doi: 10.13182/NSE13-108, 2015.
18. Rudi. J. J. Stammler and Maximo. J. Abbate, ‘Methods of Steady-state Reactor Physics in Nuclear Design’, London: Academic Press Inc, 1983.

19. Dermott E. Cullen, 'Nuclear cross section preparation'- In CRC handbook of nuclear reactor calculations, Volume I, CRC Press, Boca Raton, Florida, 1986.

20. Wolfgang Rothenstein and M. Segev, 'Unit cell calculations'- In CRC handbook of nuclear reactor calculations, Volume I, CRC Press, Boca Raton, Florida, 1986.

21. R. Goldstein and E. R. Cohen, 'Theory of resonance absorption of neutrons', Nuclear Sci. Eng. 13(1962)132-140, 1962.

22. Wolfgang Rothenstein, 'Collision Probabilities and Resonance Integrals for Lattice's, Nuclear Science and Engineering: 7, 162-171 (1960).

23. A.M. Weinberg, E. P. Wigner, 'The physical theory of neutron chain reactors'. University of Chicago Press, Chicago, 1958.

24. Carlvik, 'Dancoff Correction in Square and Hexagonal Lattices', AE-257, Aktiebolaget Atomenergi, Stockholm, Sweden, 1967.

25. Naoki Sugimura, Akio Yamamoto, 'Evaluation of Dancoff factors in complicated geometry using the method of characteristics'. Journal of Nuclear Science Technology, 43:1182, 2006.

26. G. I. Bell, 'A Simple Treatment for Effective Resonance Integrals in Dense Lattices', Nuclear Science and engineering, 5, 138 (1959).

27. Dan Gabriel Cacuci, 'Handbook of Nuclear Engineering', 2010.

28. R. Sanchez and N. J. McCormick, 'A Review of Neutron Transport Approximations, Nuclear Science and Engineering: 80, 481-535 (1982).

29. J.R. Askew, 'A characteristics formulation of the neutron transport equation in complicated geometries', Report AEEW-M 1108, United Kingdom atomic energy establishment, Winfrith, 1972.

30. H. Honek, ‘THERMOS, a Thermalization transport theory code for reactor lattice calculations’, Brookhaven National Laboratory report, 1961.

31. H. C. Huria, ‘MURLI - A Multi-group Integral Transport Code for Thermal Reactor Investigations’, Atomkernenergie, 31(1978) 77 (Also IAEA - TECDOC - 314(1984)).

32. K. Tsuchihashi, ‘CLUP-77: A Fortran Program of Collision Probabilities for Square Clustered Assembly’, JAERI 1196, Japan Atomic Energy Research Institute, 1970 (Jan. 1971).

33. A. J. Janssen, C. M. Caspers, ‘THERMOGENE, an integral transport program for arbitrary X–Y geometry systems. Part 1. Basic theory of program and calculated results’. Atomkernenergie 21 (l), 27–35 (1973).

34. A. J. Janssen, P. Brand, L. M. Caspers, ‘THERMOGENE, an integral transport program for arbitrary x–y geometry systems. III. Calculation of actual light water reactor lattices’. Atomkernenergie 22 (1), 14–23 (1974).

35. S. Chandrasekhar, Radiative Transfer, Dover, New York, 1960.

36. B. Carlson, and G. Bell, ‘Solution of the Transport Equation by the S_N method’, Proc. U.N. Intl. Conf. Peaceful Uses of Atomic Energy, 1958.

37. K. D. Lathrop, React. Technol., 15,107 (1972).

38. B. G. Carlson, Nuclear Science and Engineering, 61,408 (1976).

39. K. D. Lathrop, Nuclear Science and Engineering, 32, 357 (1968).

40. B. G. Carlson and K. D. Lathrop, ‘Discrete Ordinates Angular Quadrature of the Neutron Transport Equation’, Los Alamos Scientific Laboratory Report, LA-3186, 1965.

41. K. D. Lathrop, ‘Remedies for Ray Effects’, Nuclear Science and Engineering, Vol. 45, pp. 255-268, 1971.

42. E. E. Lewis and Miller W.F. Jr., Neutron Transport, American Nuclear Society, LaGrange Park, IL, 1993.
43. J. K. Fletcher, 'The Solution of the Multigroup Neutron Transport Equation Using Spherical Harmonics', Nuclear Science and Engineering, Vol. 84, pp. 33-46, 1983.
44. B.G. Carlson, 'Tables of Equal Weight Quadrature EQN Over the Unit Sphere', Los Alamos Scientific Laboratory Report, LA-4734, 1971.
45. J.F. Carew and G. Zamonsky, 'Uniform Positive-Weight Quadratures for Discrete Ordinate Transport Calculations', Nuclear Science and Engineering, Vol. 131, pp. 199-207, 1999.
46. G. Longoni et al., 'Investigation of New Quadrature Sets for Discrete Ordinates Method with Application to Non-conventional Problems', Trans. Am. Nucl. Soc., Vol. 84, pp. 224-226, 2001.
47. K. Lathrop, 'Spatial Differencing of the Transport Equation: Positivity vs. Accuracy', 1969, https://doi.org/10.1016/0021-9991(69)90015-1.
48. W. Reed, and T. R. Hill, 'Triangular Mesh Methods for the Neutron Transport Equation' (LA-UR-73-479), Los Alamos Scientist Laboratory Report, 1973.
49. V. Kumar and S. V. G. Menon, 'Discrete Ordinates Scheme for Quadrilateral Meshes', Annals of Nuclear Energy, Vol. 15, No. 6, pp. 317-322, 1988.
50. K. D. Lathrop, 'A FORTRAN-IV program for solving multi-group transport equation with anisotropic scattering', LA-3373, 1965.
51. W. W. Engle Jr., 'A users' manual for ANISN: A one Dimensional Discrete Ordinates Transport Code with Anisotropic Scattering' K-1693, 1967.
52. F. R. Mynatt, W. A. Rhoades, 'DOT III: Two-Dimensional Discrete Ordinates Transport Code', ORNL-TM-4280, 1973.

53. K. D. Lathrop, F. W. Brinkley, ‘Theory and Use of the General-Geometry TWOTRAN Program’, LA-4432, 1970.

54. K. D. Lathrop, ‘THREETRAN — A Program to Solve the Multi-group Discrete Ordinates Transport Equation in (x, y, z) Geometry’, LA-6333-MS, Los Alamos Scientific Laboratory (1976).

55. T. Seed and W. Miller Jr., ‘TRIDENT: a new triangular mesh discrete ordinates code’ (LA-UR-77-2511), Los Alamos National Laboratory, 1978.

56. M. DeHart, (2003), ‘NEWT: A New Transport Algorithm for Two-Dimensional Discrete Ordinate Analysis in Non-Orthogonal Geometry’, Oak Ridge National Laboratory, 2003.

57. J. Morel and E. Larsen, ‘A Multiple Balance Approach for Differencing the SN Equations’, Nuclear Science and Engineering, 105, 1–15, 1990.

58. Changyuan Liu, ‘Discrete Ordinates Methods for Transport Problems with Curved Spatial Grids’, A dissertation submitted in partial fulfilment of the requirements for the degree of Doctor of Philosophy (Nuclear Engineering and Radiological Sciences) in The University of Michigan, 2015.

59. W. B. Bickley and J. Naylor, ‘A Short Table of the Functions Ki„(x) from n = 1 to 16’, Phil. Mag. 20, 343 (1935).

60. A. Ahlin, ‘Instructions for the Use of the CLUCOP Programme’, RFN-202, ENEA computer Programme Library (Nov. 1965).

61. C. Daolio, ‘PROCOPE -A Code to Evaluate Collision Probabilities in Pin Clusters and Infinite Rod Lattices’, EUR 3296.e, European Atomic Energy Community – EURATOM, 1967.

62. L. Amyot and P. Benoist, ‘First Flight Collision Probabilities in Pin Clusters and Rod Lattices’, Nuclear Science and Engineering, 28, 215-225, 1967.

63. D. W. Anderson, ‘The WIMS'E' Module W-PIJ -A Two-Dimensional Collision Probability Code with General Boundary Conditions’, AEEW-R 862, U.K. Atomic Energy Authority, Winfrith (1973).

64. Richard Sanchez, ‘Approximate Solutions of the Two-Dimensional Integral Transport Equation by Collision Probability Methods’, Nuclear Science and Engineering: 64, 384-404 (1977).

65. H. C. Huria, ‘Manager's Manual for the Code MURLI-CLUSTER (CLIMAX)’, Bhabha Atomic Research Centre (1984).

66. F. J. Fayers, W. Davison, C. H. George and M. J. Halsall, ‘LWRWIMS- a modular computer code for the evaluation of light water reactor lattices, Part 1, description of methods’. AEEW-R 785, Winfrith, 1972.

67. S. B. Degweker, ‘BOXER3: a three dimensional integral transport code for PHWR supercell’. Report No. BARC-1295 Bhabha Atomic Research Centre, India, 1985.

68. H.C. Chow and M.H.M. Roshd, ‘SHETAN - a three-dimensional integral transport code for reactor analysis’, AECL-6878, 1980.

69. P. D. Krishnani and K. R. Srinivasan, ‘A Method for Solving Integral Transport Equation for Pressurized Heavy Water Reactor Cluster Geometry’, Nuclear Science and Engineering, 78, 97-103, 1981.

70. P. D. Krishnani, ‘CLUB- A Multigroup Integral Transport Theory Code for Analysis of Cluster Lattices’, Annals of Nuclear Energy, 9, 255-260, 1982.

71. P. D. Krishnani, ‘Interface Current Method for PHWR Cluster Geometry with Anisotropy in the Angular Flux at Interfaces’, Annals of Nuclear Energy, 9, 287-296, 1982.

72. P. D. Krishnani, ‘CLUB- A Multi-group Integral Transport Code for Lattice Calculations of PHWR cells’. Report BARC/1992/E/017, 1992.

73. A. Kavenoky and R. Sanchez, ‘The APOLLO assembly spectrum code’, In Int. Topl. Mtg. Advances in Reactor Physics, Mathematics and Computation, Paris, France, 1461 (1987).

74. G. Marleau, Hérbert A., Roy R., ‘A User Guide for DRAGON Version 4’, Institut de genie nucléaire, Département de génie mécanique, École Polytechnique de Montréal (2011).

75. Suhail Ahmad Khan, Arvind Mathur, V. Jagannathan ‘Development of Interface Current Method Based on 2D Collision Probability for 2D Hexagonal geometry’, BARC/2015/E/012, 2015.

76. M. Halsall, ‘CACTUS, a characteristics solution to the neutron transport equations in complicated geometries’, Report AEEW-R 1291, UKAEA Atomic Energy Establishment, Winfrith (United Kingdom), 1980.

77. K. Takeuchi, ‘Numerical Solution to Space-Angle Energy-Dependent Neutron Integral Transport Equation’, Journal of Nuclear Science and Technology, 8,141 (1971).

78. N. Sasamoto and K. Takeuchi, ‘An Improvement of the PALLAS, Discrete-Ordinates Transport Code’ Nuclear Science and Engineering 71,330 (1979).

79. Edward. W. Larsen and Raymond. E. Alcouffe, ‘Linear characteristic method for spatially discretizing the discrete ordinates equations in (X,Y)-geometry’, presented in ANS/ENS Joint Topical Meeting, Mathematical Methods in Nuclear Engineering, Munich, 1981.

80. M. J. Halsall: ‘Neutron Transport in WIMS by the Characteristics Method’, Proc. ANS Topi Mtg on National Criticality Technologies, San Diego, California, 53 (1993).

81. J. L. Hutton, J. Phenix, A. F. Course, ‘Advanced Modelling Methods in WIMSE’, Proc. PHYSOR 90, Marseille, France, Vol. 2, IX-14, (1990)

82. I. R. Suslov, ‘Solution of Transport Equation in 2- and 3-Dimensional Irregular Geometry by the Method of Characteristics’, Proceedings of International Conference on Mathematical Methods and Supercomputing in Nuclear Applications, p. 752, Karlsruhe, Germany, April 19-23, 1993.
83. D. Knott, M. Edenius, ‘Validation of the CASMO-4 Transport Solution’, Proc. Mathematical Methods and Supercomputing in Nuclear Applications, Karlsruhe, Vol.2, 547 (1993).
84. K. Smith, J. Rhodes, ‘CASMO-4 characteristics methods for two-dimensional PWR and BWR core calculations’, ANS/ENS International Winter Meeting and Embedded Topical Meetings, Washington, D.C (2000).
85. N. Z. Cho, S. G. Hong: ‘CRX: A Transport Theory Code for Cell and Assembly Calculations Based on Characteristic Method’, PHYSOR 96, Vol. 1, A-250 (1996).
86. G. Marleau, A. Hébert, R. Roy, ‘A User Guide for DRAGON 3.06’, Report IGE-174 Rev. 7, Institut de génienucléaire, ÉcolePolytechnique de Montréal, Montréal, Québec (2008).
87. Rhodes, K. Smith, D. Lee, ‘CASMO-5 development and applications. Advances in nuclear analysis and simulation (PHYSOR 2006)’, ANS Topical Meeting on Reactor Physics, Vancouver, BC, Canada. 2006 September 10–14 (2006).
88. T. Mazumdar, S. B. Degweker, ‘Solution of Neutron Transport Equation by Method of Characteristics’, Annals of Nuclear Energy, 77, 522 (2015).
89. T. Mazumdar, S. B. Degweker, ‘Solution of the neutron transport equation by the Method of Characteristics using a linear representation of the source within a mesh’, Annals of Nuclear Energy, 108:132-150, 2017.
90. H. Bateman, ‘The solution of a system of differential equations occurring in the theory of radio-active transformations’, Proc. Cambridge Phil. Soc., 15, p. 423 (1910).

91. D. Knott and A. Yamamoto, ‘Lattice Physics Computations’, Handbook of Nuclear Engineering, Springer, 2010.

92. A. Yamamoto, M. Tatsumi, N. Sugimura, ‘Projected Predictor-Corrector Method for Lattice Physics Burnup Calculations’, Nuclear Science and Engineering, 163, 144 (2009).

93. Akio Yamamoto, Tomohiro Endo1, Masato Tabuchi, Naoki Sugimura, Tadashi Ushio, Masaaki Mori, Masahiro Tatsumi and Yasunori Ohoka, ‘AEGIS: An Advanced Lattice Physics Code for Light Water Reactor Analyses’, Nuclear Engineering and Technology, Vol.42, No.5, October 2010.

94. Munenari Yamamoto, ‘Coarse Time-Step Integration Method for Burnup Calculation of LWR Lattice Containing Gadolinium-Poisoned Rods’, Journal of Nuclear Science and Technology, 22[1], Pp. 1~15 (January 1985).

95. S. Choi, K. S. Smith, H. Kim, T. Tak, D. Lee, ‘On the diffusion coefficient calculation in two-step light water reactor core analysis’, Journal of Nuclear Science and Technology, 54(6) 705-715, 2017.

96. P. Benoist, ‘Theory of the Diffusion Coefficient of Neutronics in a Lattice Containing Cavities’, Report No. CEA-R-2278, January 21, 1964.

97. P. Benoist, ‘Streaming Effects and Collision Probabilities in Lattices’, Nuclear Science and Engineering, 34, 285-307, 1968.

98. V. Deniz, ‘Study of the Kinetics of Thermalized neutron populations in multiplying or non-multiplying Heterogeneous media’, Nuclear Science and Engineering. 28, 397, 1967.

99. V. Deniz, ‘A new consistent definition of the homogenized diffusion coefficient of a lattice, limitations of the homogenization concept, and discussion of previously defined coefficients’, Report BARC -989, 1978.

100. E. M. Gelbard, ‘Streaming in Lattices’, Advances in Nuclear Science and Technology (Eds. Lewins J., Becker M.) Vol. 15, Springer, Boston, MA, 1983.

101. P. Kohler, ‘A New Definition of the Cell Diffusion Coefficient’, Nuclear Science and Engineering, 57, 333-344, 1975.

102. Edward. W. Larsen, ‘Neutron transport and diffusion in inhomogeneous media-II’, Nuclear Science and Engineering, 60, 357-368, 1976.

103. K. Koebke, ‘A new approach to homogenisation and group condensation’, Proc. Specialists Meeting on Homogenisation Methods in Reactor Physics, Lugano, 13-15 Nov. 1978, IAEA-TECDOC-231, 1978.

104. K. S. Smith, ‘Assembly Homogenisation Techniques for Light Water Reactor Analysis’. Progress in Nuclear Energy, 17(3), 303-335, 1986.

105. R. Sanchez, ‘Assembly homogenization techniques for core calculations’, Progress in Nuclear Energy 51 (1), 14-31, 2009.

106. S. V. G. Menon, D. C. Sahni, ‘Relation between Koebke’s equivalence theory and Benoist’s cell homogenisation procedure’, Nuclear Science and Engineering, 84, 380-383, 1983.

107. A. Kavenoky, ‘The SPH Homogenization Method’, Proc. Specialists Meeting. Homogenization Methods in Reactor Physics, Lugano, Switzerland, November 13-15, 1978, IAEA-TECDOC-231, p. 181. 1978.

108. A. Hébert, ‘A consistent technique for the pin-by-pin homogenization of a pressurized water reactor assembly’, Nuclear Science and Engineering, 113, 227-238, 1993.

109. R. Sanchez, Zmijarevic I., ‘Diffusion piecewise homogenization via flux discontinuity factors’, International Conference on Mathematics and Computational Methods Applied to Nuclear Science and Engineering (M&C 2011,) Rio de Janeiro, RJ, Brazil, May 8-12, 2011.

110. T.S. Poveshchenko, N. I Laletin, ‘About calculation of axial diffusion coefficient in nuclear reactor cell’, Proc. Int. Conf. PHYSOR-2004, CD 700310, 2004.

111. T. S. Poveshchenko, N. I. Laletin, ‘Method for Calculating the Neutron Diffusion Coefficient in a Nuclear Reactor Cell. Atomic Energy’, 120(3), July, 2016, (Russian Original Vol. 120, No. 3, March, 2016), DOI 10.1007/s10512-016-0112-0), 2016.

112. J. R. Lamarsh, ‘Introduction to Nuclear Engineering’, Addison-Wesley Publishing Company, 1965.

113. S. V. G. Menon, D. C. Khandekar, and M. S. Trasi, ‘Iterative solutions of finite difference diffusion equations’, Tech. Rep. BARC- 1129, 1981.

114. James J. Duderstadt, Louis J. Hamilton, ‘Nuclear Reactor Analysis’, Wiley, New York, 1976.

115. W. R. Cadwell, ‘PDQ-7 Reference Manual’, WAPD-TM-678, Bettis Atomic Power Laboratory, 1967.

116. K. D. Lathrop, ‘Computational procedure for multi-dimensional core analysis’, LA- UR-78-888, 1978.

117. D. R. Vondy, T. B. Fowler and C. U. Cunningham, ‘VENTURE: A Code Block for Solving Multi-group Neutronics Problems Applying the Finite-Difference Diffusion-Theory Approximation to Neutron Transport’, ORNL-5062, 1975.

118. K. L. Derstlne, ‘DIF3D: A code to Solve One-, Two-, and Three-Dimensional Finite Difference Diffusion Theory Problems’, ANL-82-64, Argonne National Laboratory, 1984.

119. K, Balakrishnan and K.R. Srinivasan, ‘A Two Group Three Dimensional Diffusion Theory Programme’, RED/TPS/136 (1966). (Also, IAEA - TECDOC - 314 (1984)).

120. V. Jagannathan, A. K. Kulkarni and R. P. Jain, ‘COMESH - A Corner Mesh Finite Difference Code to Solve multi-group Diffusion Equations In Multi-dimensions’, BARC-1367,1987.

121. K.R. Srinivasan, ‘TAQUIL and TRIVENI-Computer Codes for fuel Management of PHWRs,' PHWR 500/PHY/18, 1986) (Also IAEA - TECDOC - 314 (1984)), 1986.

122. L.A. Semenza, E.E. LEWIS, and E.C. ROSSOW, ‘The Application of the Finite Element Method to the Multi-group Neutron Diffusion Equation’, Nuclear Science and Engineering, 47, 302 (1972).

123. C. M. Kang and K. F. Hansen, ‘Finite Element Methods for Reactor Analysis’, Nuclear Science and Engineering: 51, 4 5 6 - 4 9 5 (1973).

124. A. Kavenoky and J. J. Lautard, Nuclear Science and Engineering, 64, 563, 1977.

125. H. P. Franke, Atomkernenergie 30, 88, 1977.

126. S. A. Hosseini, N. Vosoughi, ‘Development of two-dimensional, multi-group neutron diffusion computer code based on GFEM with unstructured triangle elements’, Annals of Nuclear Energy, 51, 213-226, 2013.

127. Takeharu ISE, Toshio Yamazaki and Yasuaki Nakahara, ‘FEM-BABEL: A Computer Program for Solving Three-Dimensional Neutron Diffusion Equation by the Finite Element Method’. JAERI 1256, 1978.

128. V. Jagannathan, ‘Evaluation of the finite-element-synthesis model using the 3-D finite-element technique’, Annals of Nuclear Energy, vol. 10, no. 11, pp. 569–578, 1983.

129. K. S. Smith, ‘An analytic nodal method for solving the two-group, multidimensional, static and transient neutron diffusion equations’, Nuc. Engr. Thesis, Department of Nuclear Engineering, Mass. Inst. of Technology, Cambridge, MA, 1979.

130. S. Langenbuch, W. Maurer, and W. Werner, ‘Coarse-Mesh Flux Expansion Method for the Analysis of Space-Time Effects in Large Light Water Reactor Cores’, Nuclear Science and Engineering 63,437 (1977).

131. K.S. Smith, D.M Ver Planck, and M. Edenius, ‘An Advanced Nodal Method for LWR Analyses’, Trans. Am. Nucl. Soc., 50,532 (1985).

132. R. D. Lawrence, ‘Progress in Nodal Methods for the Solution of the Neutron Diffusion and Transport Equations’, Progress in Nuclear Energy, Vol. 17, No. 3, pp. 271-301, 1986.

133. M. R. Wagner, ‘Nodal synthesis method and imbedded flux calculations’, Trans. Am. Nucl. Soc. 18, 152, 1974.

134. P. T. Antonopoulous, ‘Large mesh model development study’, Thesis, Department of Nuclear Engineering, Mass. Inst. Tech., Cambridge, MA, 1972.

135. R. A. Shober, R. N. Sims and A. F. Henry, ‘Two Nodal Methods for Solving Time-Dependent Group Diffusion Equations’, Nuclear Science and Engineering, 64:2, 582-592, 1977. DOI: 10.13182/NSE77-A27392.

136. F. Bennewitz, H. Finnemann and M. R.Wagner, ‘Higher-order corrections in nodal reactor calculations’, Trans. Am. Nucl. Soc. 22, 250, 1975.

137. M. Makai and J. Arkuszewski, ‘A hexagonal coarse-mesh program based on symmetry considerations’, Trans. Am. Nucl. Soc. 38, 347, 1981.

138. D. L. Delp, D. L. Fischer, J. M. Harriman and M. J. Stedwell, ‘FLARE, A three-dimensional boiling water reactor simulator’, GEAP-4598, General Electric Company, 1964.

139. H. Finnemann, ‘A consistent Nodal Method for the Analysis of Space-Time Effects in large LWR's’, In: Proceedings of the Joint NEACRP/CSNI Specialists' Meeting on New

Developments in Three-Dimensional Neutron Kinetics and Review of Kinetics Benchmark Calculations, Garching (Munich) January 22-24, 133-170, 1975.

140. D. M. Ver Planck, ‘A Nodal Code Analysis Program for Light Water Reactors’, EPRI-NP 2792 CCM, 1983.

141. R. D. Lawrence, ‘DIF3D Nodal Neutronics Option for Two-and Three-Dimensional Diffusion-Theory Calculations in Hexagonal Geometry’, ANL-83-1, Argonne National Laboratory, USA, 1983.

142. Arvind Kumar, R. Srivenkatesan, ‘Nodal Expansion Method for Reactor Core Calculations’, B.A.R.C.-1249, 1984.

143. B. Mahalakshmi, P. Mohanakrishnan, ‘NODHEX: A 2-D diffusion code based on the nodal expansion method in hexagonal geometry and its validation’, https://doi.org/10.1016/0306-4549(93)90073-X, Annals of Nuclear Energy, Volume 20, Issue 12, Pages 799-808, December 1993.

144. P. J. Turinsky, R. M. K. Al-Chalabi, P. Engrand, H. N. Sarsour, F. X. Faure, and W. Guo, ‘NESTLE: A Few-Group Neutron Diffusion Equation Solver Utilizing the Nodal Expansion Method for Eigenvalue, Adjoint, Fixed Source Steady-State and Transient Problems’, EGG-NRE-11406, EG&G Idaho, (June 1994).

145. U. Grundmann, U. Rohde, ‘DYN3D - A 3-dimensional Core Model for Steady State and Transient Analysis in Thermal Reactors’, Proceedings of the International Conference on the Physics of Reactors "PHYSOR 96", Mito (Japan), 16-20 Sept. 1996.

146. U. Grundmann, ‘HEXNEM – A Nodal Method for the Solution of the Neutron Diffusion Equation in Hexagonal Geometry’, Proceedings of the M&C’99 - Conference on

Mathematics and Computations in Nuclear Applications, pp. 1086-1095, Madrid, September, 27 – 30, 1999.

147. Tej Singh and Tanay Mazumdar, 'Development of a Nodal Expansion Method based space-time kinetics code for hexagonal geometry', 2017. http://dx.doi.org/10.1016/j.anucene.2017.07.012.

148. Deokjung Lee, Thomas J. Downar, 'A Nodal and Finite Difference Hybrid Method for Pin-by-Pin Heterogeneous Three-Dimensional Light Water Reactor Diffusion Calculations', Nuclear Science and Engineering, 146, 319–339, 2004.

149. P. D. Krishnani, 'Analysis of 2-D LWR benchmarks with an interface current method for solving the integral transport equation', Annals of Nuclear Energy 14, 463 (1987).

150. Mohanakrishnan P. Annals of Nuclear Energy 9, 261, 1982.

151. S. V. G. Menon, D. C. Khandekar, 'Convergence of the inner-outer iteration scheme', Journal of Applied Mathematics and Physics, ZAMP-35(3), 321-333(1984).

152. Carlvik., 'A Method for Calculating Collision Probabilities in General Cylindrical Geometry and Applications to Flux Distribution and Dancoff Factors', International Conference on the Peaceful Use of Atomic Energy 3, P/681 (1964).

153. J. R. Roy, G. Marleau, 'Normalisation Techniques for Collision Probability Matrices', PHYSOR-90, Marseille, April 23-27 (1990).

154. E. M. Gelbard, 'Refinements in the Computation of Collision Probabilities', Argonne National Laboratory, CONF-850411--8, DE85 006118, 1989.

155. E. A. Villarino, R. J. J. Stamm'ler, A. A. Ferri and J. J. Casal, 'HELIOS: Angularly Dependent Collision Probabilities', Nuclear Science and Engineering, 112, 16–31 (1992).

156. C. W. Gear, ‘Initial Value Problems in Ordinary Differential Equations’, Prentice Hall, 1971.

157. A. Sood, R. A. Forster, D. Kent Parsons, ‘Analytical benchmark test set for criticality code verification’, Progress in Nuclear Energy 42 (1), 55–106 (2003).

158. X. Yang, N. Satvat, ‘MOCUM: a two-dimensional method of characteristics code based on constructive solid geometry and unstructured meshing for general geometries’, Annals of Nuclear Energy 46, 20–28 (2012).

159. S. Akimushkin, A. Avvakumov, V. Malofeev, A. Roslyakov, ‘LWR MOX Benchmark Calculations Using the BARS Code Package’, Report NSI RRC KI 90-12/ 1-12-01 (2011).

160. A. Godfrey, ‘VERA Core Physics Benchmark Progression Problem Specifications’, CASL Technical Report, CASL-U-2012-0131-002 (2011).

161. A. Yamamoto et al., ‘Benchmark Problem Suite for Reactor Physics Study of LWR Next Generation Fuels’, Journal of Nuclear Science and Technology, Vol. 39, No. 8, p. 900–912 (2002).

162. K. Okumura et al., ‘Benchmark Results of Burnup Calculation for LWR Next Generation Fuels’, PHYSOR 2002, Seoul, Korea, October 7-10, 2002.

163. D. Knott, E. Wehlage, ‘Description of the LANCER02-Lattice Physics Code for Single Assembly and Multibundle Analysis’, Nuclear Science and Engineering, 155, 331 (2007).

164. Samuel Glasstone, M. C. Edlund, 1952. ‘The elements of nuclear reactor theory’, Van Nostrand, 1952.

165. Sherly Ray, S.B. Degweker, Umasankari Kannan, ‘New homogenised axial diffusion coefficients from lattice calculations’. Annals of Nuclear Energy, 137(2020) 107029. https://doi.org/10.1016/j.anucene.2019.107029.

166. Sherly Ray, S.B. Degweker, Umasankari Kannan, 'Few-Group Diffusion Theory Parameters from Lattice Calculations using Leakage Corrected Collision Probabilities'. Annals of Nuclear Energy, 145 (2020) 107492. https://doi.org/10.1016/j.anucene.2020.107492.

167. K. R. Rempe and K. S. Smith, 'SIMULATE-3 Pin Power Reconstruction: Methodology and Benchmarking', Nuclear Science and Engineering: 103, 334-342 (1989).

168. M. R. Wagner, 'Three-dimensional Nodal Diffusion and Transport Theory Methods for Hexagonal-z geometry', Nuclear Science and Engineering: Volume 103, 1989.

169. Noh, J., Cho, N., 'A new Diffusion Nodal Method Based on Analytical Function Expansion', Transactions of the American Nuclear Society, Volume 69, 1993.

170. N. Poursalehi, A. Zolfaghari and A. Minuchehr, 'Three-dimensional high order nodal code, ACNECH, for the neutronic modelling of hexagonal-z geometry', Annals of Nuclear Energy, vol. 68, pp. 172–182, 2014.

171. Daogang Lu, Chao Guo, 'Development and Validation of a Three-Dimensional Diffusion Code Based on a High Order Nodal Expansion Method for Hexagonal-*z* Geometry', http://dx.doi.org/10.1155/2016/6340652, 2016.

172. K. S. Smith, 'Nodal diffusion methods and lattice physics data in LWR analyses: Understanding numerous subtle details', Progress in Nuclear Energy xxx (2017) 1-10. 2017,

173. Deok Jung Lee, YongHee Kim, YongBae Kim, 'A Consistent Coupling of Nodal Expansion Method, Analytic Nodal Method, and Finite Difference Method for Three-Dimensional Reactor Core Analysis', Proc. Int. Topl. Mtg. Advances in Reactor Physics

and Mathematics and Computation into the Next Millennium (PHYSOR 2000), Pittsburgh, Pennsylvania, May 7–12, 2000, (American Nuclear Society) 2000.

174. S. S. Bajaj and A. R. Gore, 'The Indian PHWR', Nuclear Engineering Design, 236, 701, 2006.

175. S. A. Bhardwaj, 'The Future 700 MWe Pressurized Heavy Water Reactor', Nuclear Engineering Design, 236, 861, 2006.

176. IAEA3DPWR,https://engineering.purdue.edu/PARCS/Code/TestSuite/CalculationMode/StandAloneMode/Eigenvalue/IAEA3DPWR, 2014.